CHARACTERIZING WATER-SOLUBLE ORGANIC AEROSOL AND THEIR EFFECTS ON CLOUD DROPLET FORMATION: INTERACTIONS OF CARBONACEOUS MATTER WITH WATER VAPOR

A Thesis
Presented to
The Academic Faculty

by

Akua A. Asa-Awuku

In Partial Fulfillment
of the Requirements for the Degree
Doctor of Philosophy in the
School of Chemical and Biomolecular Engineering

Georgia Institute of Technology
April 2008

CHARACTERIZING WATER-SOLUBLE ORGANIC AEROSOL AND THEIR EFFECTS ON CLOUD DROPLET FORMATION: INTERACTIONS OF CARBONACEOUS MATTER WITH WATER VAPOR

Approved by:

Dr. Athanasios Nenes,
Committee Chair
School of Chemical and Biomolecular Engineering
Georgia Institute of Technology

Dr. Athanasios Nenes, Advisor
School of Chemical and Biomolecular Engineering
Georgia Institute of Technology

Dr. Athanasios Nenes
School of Chemical and Biomolecular Engineering and Department of Earth and Atmospheric Science
Georgia Institute of Technology

Dr. Michael Bergin
School of Civil and Environmental Engineering
Georgia Institute of Technology

Dr. Carson Meredith
School of Chemical and Biomolecular Engineering
Georgia Institute of Technology

Dr. Amyn Teja
School of Chemical and Biomolecular Engineering
Georgia Institute of Technology

Dr. Rodney Weber
Department of Earth and Atmospheric Science
Georgia Institute of Technology

Date Approved: March 21 2008

To my ancestors,

those who came before me

and paved the way for me today

ACKNOWLEDGEMENTS

I would like to thank He who makes all things possible – my life has been a series of fortunate events by his design. I would like thank my family whom has provided support, inspiration, and unconditional love in all my pursuits. To my my mother and father who showed me how to work hard and enjoy life, who let me believe that anything is possible, and to always remember the important things in life; to my sister who has looked out for me my entire life and continues to do so; to my roommate, who always had a willing ear and sound advice; to all my friends who celebrated with me during the highs and continued to celebrate with me through the lows and to my research group that has grown with me during this process, I thank you from the bottom of my heart. I would especially like to thank my advisor, Dr. Athanasios Nenes, for the countless times he has provided advice and given direction in support of my academic endeavors. Over the past years, I have experienced numerous opportunities in travel, research, and life and they have all been with the help of his guidance. I have had the fortune in life to be surrounded by a network of people who have fortified my dedication to pursue my ambitions, and for that I am truly grateful. I cannot say it enough. Thank you. Thank you. Thank you.

TABLE OF CONTENTS

LIST OF TABLES

LIST OF FIGURES

LIST OF SYMBOLS AND ABBREVIATIONS

CCN – Cloud Condensation Nuclei

D_p -- the droplet diameter [m], diameter corresponding radial distance R_p

D_s -- diameter corresponding radial distance R_s

D_v' -- mass transfer coefficient of water vapor from the gas to the droplet.

FICA – Fitted CCN Activity

$M_{w,}$ -- the molecular weight,

n_s -- the moles of solute dissolved in the droplet,

ρ_w -- density of water

r -- radial distance from core droplet center

R -- the universal gas constant

R_c, -- radial distance at the core surface,

R_s -- the distance where the dilution effect of water condensation on the droplet surface (dilution) balances diffusional supply of solute from the core

R_p --radial distance at droplet surface

S -- ambient water vapor saturation ratio

S_c -- critical supersaturations

S_{eq} -- equilibrium saturation ratio of the growing droplet,

σ_w -- Surface tension of water,

t – time in seconds

V , droplet Volume

ν -- Van't Hoff factor,

SUMMARY

Aerosols have significant impacts on earth's climate and hydrological cycle. They can directly reflect the amount of incoming solar radiation into space; by acting as cloud condensation nuclei (CCN), they can indirectly impact climate by affecting cloud albedo. Our current assessment of the interactions of aerosols and clouds is uncertain and parameters used to estimate cloud droplet formation in global climate models are not well constrained. Organic aerosols contribute much of the uncertainty in these estimates and are known to affect the ability of aerosol to form cloud droplets (CCN Activity) by i) providing solute, thus reducing the equilibrium water vapor pressure of the droplet and ii) acting as surfactants capable of depressing surface tension, and potentially, growth kinetics. This thesis investigates various organic aerosol species (e.g., marine, urban, biomass burning, Humic-like Substances). An emphasis is placed on the water soluble components and secondary organic aerosols (SOA). In addition the sampled organic aerosols are acquired via different media; directly from in-situ ambient studies (TEXAQS 2006) environmental chamber experiments, regenerated from filters, and cloud water samples. Novel experimental methods and analyses to determine surface tension, molar volumes, and droplet growth rates are presented from nominal volumes of sample. These key parameters for cloud droplet formation incorporated into climate models will constrain aerosol-cloud interactions and provide a more accurate assessment for climate prediction.

CHAPTER I

INTRODUCTION

Changes in climate can affect health, air quality, energy, food and water resources and subsequently human sustainability. As a result, understanding changes in cloud formation that alter the hydrological cycle and climate is an important issue that must be addressed in engineering research. Aerosol provide the nuclei for which water can condense and form cloud droplets; the link between particulate matter and cloud formation is often referred to as the aerosol-indirect effect and is a major source of uncertainty in global climate models [99, 205, 130](Fig. 1).

Much of the uncertainty is due to the lack of understanding of the organic aerosol interactions with water vapor. Constraining the interactions and feedbacks of water vapor, aerosols, and clouds are complex. As a result, the global annual influence of the anthropogenic indirect aerosol effect is subject to large uncertainties [130, 34, 158, 90, 99]. Understanding the ability of aerosol to form droplets and act as cloud condensation nuclei (CCN) is a strong function of their size, composition and physical state; hence the following work provides novel experimental and analytical techniques to assess these thermodynamic and droplet kinetic parameters necessary to constrain model parametrizations for organic droplet formation.

1.1 The importance of the water-soluble organic fraction

Water-soluble organic compounds (WSOC) are ubiquitous in the atmosphere; their interactions with water are intricate for they can significantly affect particle hygroscopicity, reduce the equilibrium water vapor pressure, affect growth kinetics and decrease surface tension at the droplet interface [45, 56, 60, 175, 176]. As a consequence, these organics may enhance or suppress CCN activity, hence significantly

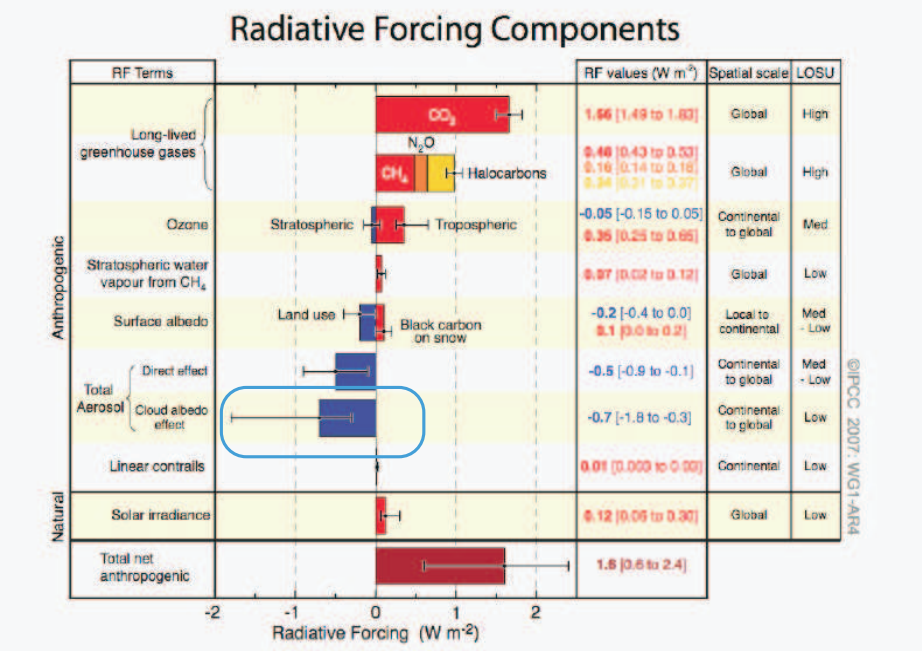

Figure 1: Anthropogenic Radiative Forcing Assessment. The aerosol-indirect is classified with a low level of scientific understanding (LOSU) and is subject to the greatest uncertainty.

impact cloud droplet number and the aerosol indirect effect [58, 61, 140, 184].

Roughly half of global CCN contain carbonaceous compounds [145]. Carbonaceous material (organic carbon, OC) can comprise up to 70-90% of aerosol mass [7, 27, 214], 10-70% of which may be water-soluble organic carbon (WSOC) [59, 201, 218]. WSOC are present in primary organic carbon but also formed during the oxidation of volatile organic carbon (VOC) to secondary organic aerosol (SOA) [109, 166, 175].

WSOC is believed to be a mixture of neutral and acidic polar organic compounds [44]. They are important contributors to the aerosol indirect effect for WSOC can affect CCN activity by *i*) providing solute, thus reducing the equilibrium water vapor pressure of the droplet, and, *ii)* acting as surfactants capable of depressing surface tension, and potentially, growth kinetics [45, 61, 64, 109, 123, 140, 184]. Yet owing to its complexity, WSOC cannot be completely speciated using standard analytical methods, but instead is often characterized using "functional group analysis", using either chromatographic techniques or nuclear magnetic resonance [43, 174, 197, 198].

WSOC can be classified broadly into hydrophilic and hydrophobic fractions; these are usually operationally defined but correlate with carbon chain length and number of functional groups per molecule. Hydrophilic compounds are typically highly oxygenated low molecular weight compounds (with potentially numerous carbonyls and carboxyl groups per molecule) and tend to be highly soluble in water and exhibit limited surfactant behavior; hydrophobics can be longer in length, less hygroscopic, and strongly depress surface tension [109].

An important class of hydrophobic WSOC are Humic-like Substances (HULIS); these are a mixture of high molecular weight compounds that are strong surfactants [44, 111, 173]. Surfactants have been known for a long time to be ubiquitous, e.g.,[74]. According to [59], HULIS depressed surface tension in fog water samples by 15-20% at a 100 mg C L^{-1} WSOC concentration; [111] showed that HULIS dissolved in water at a concentration of 1000 mg L^{-1} could decrease surface tension by 25-42% or even more if salts like $(NH_4)_2SO_4$ are present in solution. HULIS are present in continental aerosol, urban, rural and smog samples [44, 59, 77, 89, 111, 119]. Despite their importance, the thermodynamic properties of HULIS (e.g., average molecular weight, molar volume, solubility) are poorly known. This is largely due to the complexity of HULIS, which do not have a definite chemical structure, but are often described as a "network" of compounds binding together in solution, potentially forming oligomers and macromolecules [76, 106, 107, 112].

Aerosol formed during biomass burning episodes are a major source of WSOC [109, 197]; for VOC emissions and SOA occur in abundance. In pyrogenic air masses, WSOC can account for 45-75% of the total carbon mass [62, 77, 134]. Natural VOC emissions (e.g., monoterpernes, sesquiterpenes), estimated to be 1150 Tg yr^{-1} [84], are a major source of SOA. Alkene ozonolysis is well established as a source of SOA [1, 17, 19, 49, 67, 72, 86, 109, 120, 182, 208]. Attempts to speciate SOA [1, 17, 49, 72, 106] have been met with limited success, as 80 to 90% of the aerosol mass can remain

uncharacterized [106, 167, 179]. The potential for forming oligomeric or polymeric structures [19, 72, 73, 107] has been suggested to explain the uncharacterized SOA fraction. Oligomers have the potential to exhibit characteristics similar to humic-like substances (HULIS) [19], which strongly depress surface tension [14, 47, 76, 111, 173] and potentially, droplet growth kinetics. All of these can have important impacts on CCN activity. Nevertheless, a complete thermodynamic characterization of the secondary aerosol, and its water-soluble components (required to constrain cloud droplet formation) have remained elusive [109].

For marine conditions, CCN number concentration and cloud droplet number may increase 10 to 15% in the presence of WSOC [2, 138, 147, 220]. The sources and chemical composition of marine organics vary; primary organic marine aerosols (POMA) generated during bubble bursting may be insoluble high molecular weight organic matter [147]. POMA concentrations vary with season [216] and are attributed to emissions during phytoplankton blooms [109, 147, 216]. The production of secondary organic marine aerosols (SOMA) during cloud processing (mostly WSOC and carboxylic acids such as oxalate) is persistent in marine cloud regions [190]. SOMA can be produced through glyoxylic acid oxidation pathways [192] via several aqueous phase intermediates [31, 57, 128].

1.2 Describing cloud droplet formation

The theory traditionally used to describe the formation of cloud droplets from CCN was first developed by Köhler and is a simple thermodynamic model that describes cloud droplet activation under ideal conditions [115]. Traditional Köhler theory has successfully been applied to CCN composed of deliquescent inorganic salt aerosols (e.g., ammonium sulfate and sodium chloride) and low molecular weight organic species that exhibit hygroscopic behavior (e.g., adipic acid and glutaric acid) [41, 159].

Unfortunately, the theory is less successful in describing the behavior of less hygroscopic non-ideal organic compounds [41, 159]. Analysis of ambient CCN measurements [35, 207] can show large deviations (often attributed to the complex interaction of organics with water) between predicted and measured CCN concentration under polluted conditions. Organics, depending on their solubility, can contribute solute [184, 121]. Hydrophobic compounds, such as HULIS, with multiple functional groups may act as strong surfactants and considerably depress surface tension [184, 61, 140]; compressed surfactant layers may act as "film-forming compounds," and may influence droplet growth kinetics enough to affect droplet number and spectral dispersion [22, 74, 64, 141, 35]. Polymerization reactions, thought to occur in secondary organic aerosol [129], may also have a considerable impact on their CCN properties [206]. All the effects combined give a wide and complex range of effects on CCN and cloud droplet formation [141].

A common assumption for partially soluble compounds is that solute instantaneously dissolves and distributes uniformly throughout the drop [121, 159, 181]. Compared to electrolytes, the majority of organic compounds are not very soluble in water, do not readily deliquesce, have a higher molar mass and thus diffuse more slowly in aqueous solutions. The implication for a growing droplet is that mass transfer of the dissolving organics may not be fast enough to assure uniform distribution of solute through the droplet volume; this kinetic limitation may decrease the solute concentration at the droplet surface and increase the droplet equilibrium vapor pressure.

[12] showed that if sufficient, the latter may delay or even hinder droplet formation. Thus, assuming instantaneous dissolution and distribution of solute throughout the droplet volume could slightly overestimate the effect of partially soluble compounds on CCN activation. A numerical model of the process was developed. Simulations of cloud droplet growth were performed for solute diffusivity, droplet growth rates, dry

particle and droplet diameters relevant for ambient conditions. Simulations suggest that high ambient supersaturations and low solute diffusivity are major contributors to significant decreases in effective solute surface concentrations during droplet growth. The numerical simulations were incorporated into Köhler theory to assess the impact of dissolution kinetics on the droplet equilibrium vapor pressure. The modified Köhler theory implies that only CCN, most likely composed of WSOC, with slowly dissolving solute could have a "dynamical" equilibrium saturation ratio that is appreciably different from that obtained using thermodynamic equilibrium arguments alone.

1.3 Thesis outline

As previously mentioned, experimental emphasis is placed on probing the characteristics of the water-soluble organic aerosol component. The aerosol studied are from various sources; laboratory studies focus on water-soluble properties of biomass burning extract (Chapter 2), secondary aerosol (SOA) from the ozonloysis of terpenes (Chapters 3 and 4) and marine and urban cloud water (Chapter 5 and 6) . In the chapters 2 and 3 analytical methods are developed and presented to infer thermodynamic properties (molar mass and surface tension) of the organic system. These methods are then applied to in-situ measurements and off-line measurements of SOA generated from the ozonloysis of sesquiterpenes (Chapter 4). In chapters 5 and 6 we apply these novel characterization methods to a unique sampling technique and infer properties of already activated CCN from cloud water samples; the water-soluble properties inferred from these cloud water samples are of particular importance for CCN predictions and closure studies. Lastly, airborne CCN measurements from the TEXAS Air Quality Study of 2006 explore the behavior and evoloution of ambient CCN in urban plumes. This wide array of measurements, experimental techniques and analysis are designed to move toward a better understanding of organic cloud

droplet formation and terminally, aerosol-cloud climate interactions.

CHAPTER II

WSOC PROPERTIES OF BIOMASS BURNING CCN

In this study, a biomass burning sample acquired during a prescribed burning event in Georgia [200], is fractionated into hydrophilic and hydrophobic components to assess their individual contribution to surface tension depression and CCN Activity. Average molar volumes are inferred from Köhler Theory Analysis KTA the surfactant characteristics are determined and the relative amount of hydrophobic and hydrophilic compounds are determined. Note: This chapter appears as reference [16].

2.1 Experimental methods

Fine Biomass Burning (BB) particulate matter ($PM_{2.5}$) was collected on pre-baked quartz fiber filters with a Thermo Anderson Hi-Volume Air Sampler during a prescribed burning in Augusta, Georgia at Fort Gordon and in Columbus, Georgia at Fort Benning, which are both located in heavily wooded areas, in April 2004 [126, 200]. Sampling and Filter collection methods can be found in [126]. The freshly burned biomass aerosol is subsequently extracted in water and fractionated into hydrophobic and hydrophilic fractions. Figure 2 outlines the procedure adopted to characterize the original and fractionated samples. Each step is described in subsequent sections.

2.1.1 Extraction and fractionation of biomass burning sample

WSOC is extracted with 125 ml of pure water from the filter by sonication in a heated water bath ($\sim 60\,^{\circ}$C) [20, 198] for 1.25 hours. A portion of this sample (BB) was then fractionated into hydrophilic (HPHIL) and hydrophobic (HPHOB) components using a macro-porous nonionic resin (XAD-8) Solid Phase Extraction (SPE) column [51, 198]. With the WSOC solution adjusted to pH=2 using HCl, the resin does not

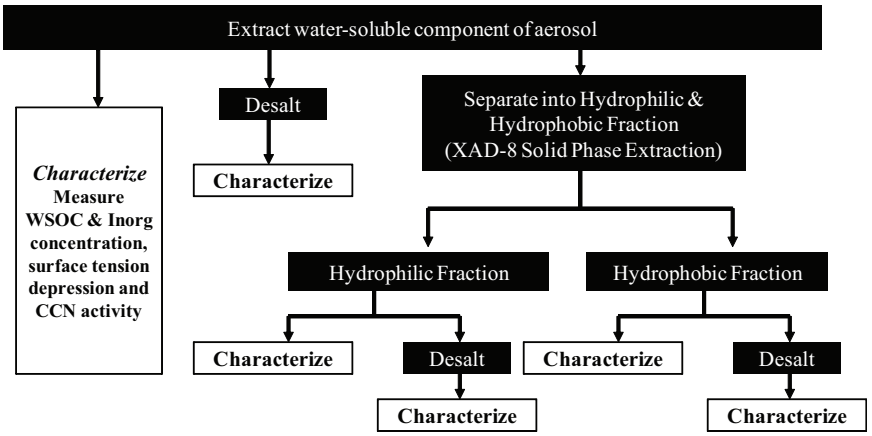

Figure 2: Procedure used for biomass burning sample analysis. The water-soluble component of the aerosol sample is extracted and characterized for carbon and inorganic content, surface tension and CCN properties. The sample is then desalted, fractionated into hydrophilic (HPHIL), hydrophobic (HPHOB), desalted hydrophilic (D-HPHIL) and desalted hydrophobic (D-HPHOB) components, all of which are characterized.

retain hydrophilic compounds. Calibrations suggest this includes saccharides, amines, and carbonyls and aliphatic monocarboxylic/dicarboxylic/oxocarboxylic acids with less than 4 or 5 carbons, or hydrophobic compounds with pKa less than 2. The column retains the long and short-chained hydrophobic compounds, which calibrations suggest may be aromatic acids, phenols, organic nitrates, cyclic acids, carbonyls and monocarboxylic and dicarboxylic chains greater than 3 to 4 carbons [198]. The column is then eluted to pH 13 and a large amount of the adsorbed hydrophobic fraction is removed. The recovered hydrophobic fraction is adjusted to pH 2 with HCl to avoid the oxidation of organic compounds. Of the compounds tested, aromatic acids and phenols had the largest recoveries. The hydrophobic compounds retained on the column at pH 2 and recovered at pH 13 exhibit a dark brown color, suggestive of HULIS [76]. Speciation methods have shown that HULIS in WSOC can be found within the hydrophobic fraction [44, 114, 118, 198].

Part of the BB, HPHOB and HPHIL components are subsequently de-salted with single-use Oasis® HLB Extraction Cartridges (Waters, Milford, Massachusetts), to

reduce the concentration of electrolytes in the samples. Most organics are retained on the resin while inorganic ions pass through. The organics are subsequently eluted with 100% high-purity methanol (Romil, Cambridge, UK). This eluate is dried under a gentle stream of nitrogen gas to remove the methanol and re-dissolved with 18 Mohm ultrapue water. The desalted samples will be referred to as D-HPHOB, D-HPHIL and D-BB (Table 1).

Table 1: Composition of each sample considered in this study.

Sample	[a]WSOC (mg C L^{-1})	[b]Cl^- (μg L^{-1})	[b]SO_4^{2-} (μg L^{-1})	[b]NO_3^- (μg L^{-1})
BB	850	17510	19698	20834
HPHIL	40	399031	7700	0
HPHOB	375	4058	27	0
D-BB	600	2438	4056	3310
D-HPHIL	130	7.5	15.3	0
D-HPHOB	450	15.6	53.8	0

[a] The uncertainty of WSOC measurements is 3-5%
[b] The uncertainty is 40, 200, and 133 μg L^{-1} for Cl^-, SO_4^{2-}, and NO_3^- measurements, respectively.

It should be noted that there can be a potential for artifacts in the fractionation process. During the desalting process low molecular weight organic compounds (i.e acetic and formic acid) that do not strongly adsorb on the resin may pass through the chromatography column. Hence only when comparing the hydrophilics will the D-HPHIL sample, compared to HPHIL, be somewhat enriched in higher molecular weight organics. In addition, not all hydrophobic compounds are recovered from the column. Based on calibrations [198], carbonyls and carboxylic acids greater than roughly C_5 and organic nitrates are thus most likely to be under-represented in this analysis.

2.1.2 Measurement of chemical composition

The WSOC content of the original, fractionated and desalted samples (Table 1) were measured with a Total Organic Carbon (TOC) Analyzer (Sievers Model 800 Turbo, Boulder, CO). A detailed description of the method can be found in [198]. We also measure anions (SO_4^{2-}, $Cl^-$and NO_3^-) and cations (Na^+, NH_4^+, Mg^+, Ca^{2+}, K^+) with a Dionex DX-500 ion chromatograph with Na_2CO_3/$NaHCO_3$ eluent and a Metrosep A Supp 5-100 analytical column (Metrohm, Switzerland). In the original and fractionated samples, ammonium was in excess, suggesting that all the organic and inorganic acids were neutralized.

2.1.3 Surface tension measurements

All surface tension measurements were performed using the pendant drop method with a KSV CAM 200 optical contact angle and surface tension goniometer. The surface tension at the liquid-air interface, σ, depends on the density jump across the interface, the gravitational constant, the radius of the droplet and the contact angle between the droplet and needle used for forming the pendant drop. The drop is allowed to equilibrate for 30-100 seconds, providing enough time so that large molecules (i.e., HUMIC-like substances) are fast enough to diffuse to the surface layer of activated CCN [202, 12]. Fifty pendant drops were used for each surface tension measurement, requiring in total less than 200 μL of sample; the σ for commercial ultrafine de-ionized ultra-filtered water (Fischer-Scientific, W-2) was measured in between organic samples and were found to agree consistently within 2% of reported literature values at room temperature. This en sures that cross-contamination between samples did not occur. The temperature was measured with a 50 K Ohm Thermoresistor (Digikey ERT-D2FHL503S) thermocouple.

The surfactant characteristics for each sample (Table 2) were characterized by measuring surface tension as a function of dissolved carbon concentration (at the

Table 2: Average α and β parameters of the Szyszkowski-Langmuir model for all samples considered.

Sample	α(mN m^{-1} K^{-1})	β^c (L mg^{-1})
BB	2.78	1.72×10^{-6}
HPHIL	1.00	5.78×10^{-7}
HPHOB	9.18	6.02×10^{-6}
D-HPHIL	1.54×10^{-1}	8.23×10^{-6}
D-HPHOB	6.98	4.62×10^{-6}

[c]Measurements obtained between 296 and 299 ° K.

original sample concentration, then at 1:1, 1:2, 1:3 and 1:4 dilution with 18-Mohm ultrapure water). The measurements were then fit to a Szyszkowski-Langmuir [124] adsorption isotherm which expresses σ as a function of the soluble carbon,

$$\sigma = \sigma_w - \alpha T \ln(1 - \beta c) \tag{1}$$

where c is the concentration of soluble carbon (mg C L^1), α and β are empirical constants, obtained from least square fitting to σ measurements, and σ_w is the surface tension of 18-Mohm ultrapure water at the experiment temperature. If the surfactant is composed of a single compound, Eq.(1) describes a Gibbs adsorption isotherm of the partitioning of surfactant between the bulk and droplet surface layer, α and β are related to the orientation of dissolved molecules and their interactions at the surface interface [124]. Even though WSOC is a complex mixture of compounds, Eq.(1) still reproduces the measurements very well (Fig. 5). Table 2 is a summary of α and β parameters obtained from fitted σ data for the original biomass burning and fractionated samples.

In addition to measurements of the original and extracted samples, we also measured the effect of adding electrolytes on surface tension; limited by the amount of fractionates available, we performed this exercise on the original BB sample. The concentration of carbon was kept constant at 850 mg L^{-1} and premeasured amounts

of electrolytes were dissolved. $(NH_4)_2SO_4$ and NaCl were used in these experiments, typical of ionic species found in the atmosphere.

2.1.4 CCN activity measurements

Aerosol generated from the original BB sample and fractions were activated into cloud droplets to determine their CCN activity. 80 to 100 μL of organic sample were placed in 3-5 ml of commercial ultrafine de-ionized ultra-filtered water (Fischer-Scientific, W-2) and atomized with a collision-type (University of Minnesota) atomizer (Fig. 3) operated at 3.5 psig pressure. The polydisperse droplets are subsequently dried (to $\sim$10% relative humidity) by passing them through two silica gel dryers (Fig. 3), neutralized by a Kr-85 bipolar ion source and classified using a Differential Mobility Analyzed (DMA 3081) (Fig. 3). The classified aerosol is then split and passed though a TSI 3010 Condensation Particle Counter (CPC) for measuring aerosol number concentration, (CN). CCN concentrations were measured in the other stream by a Droplet Measurement Technologies Continuous-Flow Streamwise Thermal Gradient CCN Counter (STGC) [122, 164].

CCN activity of the aerosol was characterized as follows. For a fixed supersaturation the "activation curves" (i.e., ratio of CCN to CN) was measured between 10 and 250 nm dry mobility diameter. Activation ratios are then determined from 0.2% to 1.0% supersaturation. Figure 4 shows an example of activation curves obtained for D-HPHIL activation. The activation curves are then fit to a sigmoidal curve, neglecting the impact of doubly charged particles which appear as a characteristic secondary peak to the left of the main sigmoid (Fig. 4). The particle dry diameter size, d, at which 50% of the particles were CCN represent the dry diameter of the particle with critical supersaturation equal to the instrument supersaturation. The dependence of d with respect to supersaturation can be used to infer solute molar volume and the presence of surfactants using KTA (Section 2.2) [150].

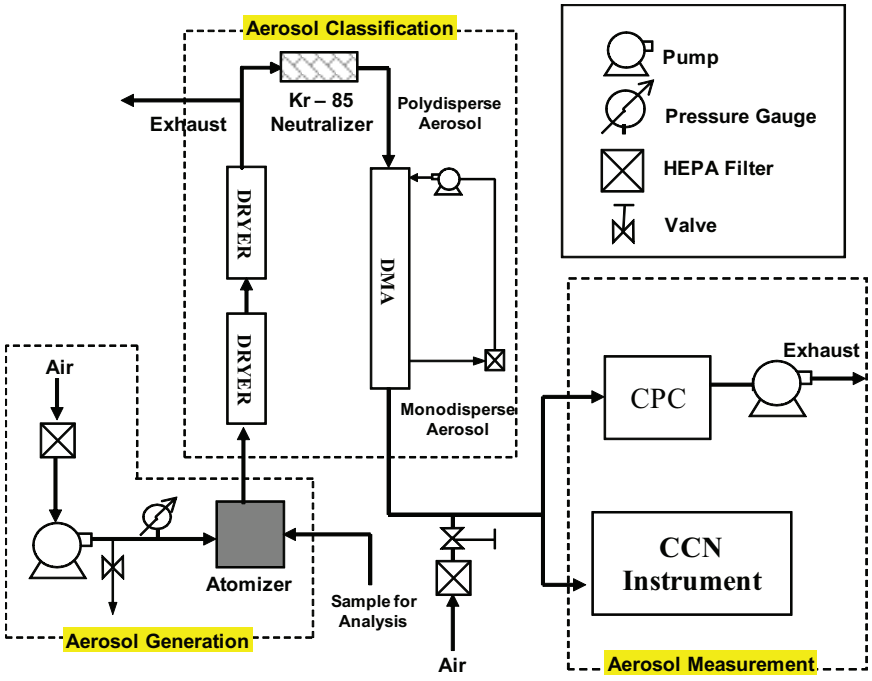

Figure 3: Experimental setup for measuring CCN activity of biomass burning samples. Atomized sample is dried, charged and classified with a DMA. The classified aerosol stream is split into the CPC and the CCN instrument.

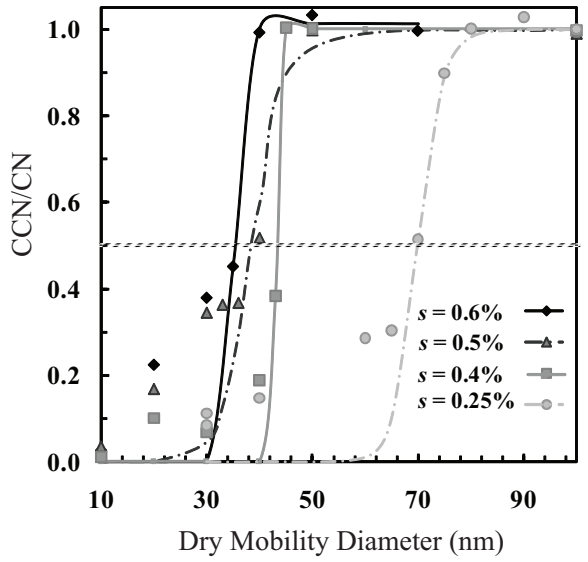

Figure 4: Example of CCN/CN data (D-HPHIL) with their corresponding sigmoidal fits.

2.2 Description of Köhler theory analysis

2.2.1 Single component CCN theory

Each particle requires a discrete amount of water vapor supersaturation to activate into cloud droplets. This "critical supersaturation", s_c, for simple (water-soluble) single-component aerosol is given by [115, 179]

$$s_c = \left(\frac{4A^3}{27B}\right)^{\frac{1}{2}}, A = \left(\frac{4M_w\sigma}{RT\rho_w}\right), B = \left(\frac{6n_sM_w\nu}{\pi\rho_w}\right) \tag{2}$$

where M_w, ρ_w are the molecular weight and density of water, respectively, R is the universal gas constant, n_s are the moles of solute dissolved in the droplet, ν is the effective van't Hoff factor of the solute, T is the ambient temperature and σ is the droplet surface tension at the point of activation. Single-component Köhler theory can be aptly applied to soluble inorganic salts and has been successfully applied to soluble low molecular weight organics as well [42, 60, 159]

2.2.2 Multi-component CCN theory

For multi-component CCN, the contribution of solute from each organic and inorganic component can be accounted for as a modification of the Raoult term (B term in Eq.(2) as:

$$B = \sum_i B_i = \sum_i \left(\frac{\rho_i}{\rho_w}\right)\left(\frac{M_w}{M_i}\right)\varepsilon_i\nu_i d^3 = d^3\left(\frac{M_w}{\rho_w}\right)\sum_i\left(\frac{\rho_i}{M_i}\right)\varepsilon_i\nu_i \tag{3}$$

where d is the dry diameter of the CCN, and ρ, ε, ν, M_i are the density, volume fraction, effective van't Hoff factor and molar mass of the solute i, respectively. ε_i is related to the mass fraction of i, m_i, as

$$\varepsilon_i = \frac{m_i/\rho_i}{\sum_i m_i/\rho_i} \tag{4}$$

m_i are obtained from measurements of chemical composition. For a single component ε_i= 1 and Eq.(3) reduces to Eq. (2).

2.2.3 Köhler theory analysis of ambient CCN

Assuming that all solute dissolves, Eq. (2) can be written as

$$s_c = \left(\frac{256M_w^3\sigma^3}{27R^3T^3\rho_w^3}\right)^{1/2}\left[\sum_i\left(\frac{M_w}{\rho_w}\right)\left(\frac{\rho_i}{M_i}\right)\varepsilon_i\nu_i\right]^{-1/2} d^{-3/2} = \omega d^{-3/2} \tag{5}$$

where

$$\omega = \left(\frac{256M_w^3\sigma^3}{27R^3T^3\rho_w^3}\right)^{\frac{1}{2}}\left[\sum_i\left(\frac{M_w}{\rho_w}\right)\left(\frac{\rho_i}{M_i}\right)\varepsilon_i\nu_i\right]^{-\frac{1}{2}} \tag{6}$$

The molar volume of the organic component, $\frac{M_j}{\rho_j}$, is explicitly solved for by rearranging Eq.(6) as follows:

$$\frac{M_j}{\rho_j} = \frac{\varepsilon_j\upsilon_j}{\frac{256}{27}\left(\frac{M_w}{\rho_w}\right)^2\left(\frac{1}{RT}\right)^3\sigma^3\omega^{-2} - \sum\limits_{i\neq o}\frac{\rho_i}{M_i}\varepsilon_i\nu_i} \tag{7}$$

where j is used to denote the organic constituent and all other components i refer to the inorganic components present in the aerosol. Equation (7) is the basis of KTA [150]. In this study, KTA is applied as follows:

1. *If there are no strong surfactants present* (i.e., the surface tension of the CCN does not depend on the concentration of solute at the point of activation), ω does not depend on d and its value can be determined from a power law fit between measured s_c and d (Table 3). Application of Eq.(7) then infers the average molar volume of the water-soluble organics, provided that the volume fractions of all constituents are measured (from WSOC for organics and IC for inorganics) and the composition of the inorganics are known.

2. *If there are strong surfactants present* (i.e., the surface tension of the CCN does depend on the concentration of solute at the point of activation), ω depends on d, so method "a" cannot be used to infer the molar volume. Instead, two alternate methods can be used:

Table 3: Properties used for Köhler Theory Analysis of all samples.

Property (units)	BB	D-HPHIL	D-HPHOB
σ(N m^{-1})	6.83×10^{-2}	6.85×10^{-2}	3.53×10^{-2}
ω(m1.5)^d	7.78×10^{-14}	3.86×10^{-14}	6.26×10^{-14}

^{d} obtained only for the data with $s_c \leq 0.6\%$

Method b_1. Since ω depends weakly on d at low supersaturation (because the CCN are dilute enough at the point of activation so that surface tension is approximately constant) method "a" can be used for a subset of the activation experiments. The appropriate supersaturation range can be determined from the experimental data, by examining the slope of s_c vs. d.

Method b_2. For each supersaturation, directly apply Eq. (7) and an estimate of surface tension at the point of activation (obtained by using Köhler theory to estimate water volume and from there, WSOC concentration) to infer molar volume. Then compute the average molar volume over the range of supersaturations examined.

2.2.4 Molar volume sensitivity analysis

The uncertainty in inferred organic molar volume, $\Delta\left(\frac{M_j}{\rho_j}\right)$, is quantified as

$$\Delta\left(\frac{M_j}{\rho_j}\right) = \sqrt{\sum_{\text{for all x}} \Phi_x \Delta x^2} \tag{8}$$

where Φx is the sensitivity of molar volume to each of the measured parameters x (i.e., any of σ, ω, ε_i, ε_j, ν_i,and ν_j)

$$\Phi_x = \frac{\partial}{\partial x}\left(\frac{M_j}{\rho_j}\right) \tag{9}$$

and Δx is the uncertainty in x. The Φ_x for Eq. (9) is obtained by differentiating Eq. (7) and are shown in Table 4.

Table 4: Sensitivity of Molar Volume to its dependant parameters.

x	$\Phi_x,\ \frac{\partial}{\partial x}\left(\frac{M_j}{\rho_j}\right)$
σ	$\left(\frac{3\times256}{27}\left(\frac{M_w}{\rho_w}\right)^2\left(\frac{1}{RT}\right)^3\frac{\sigma^2\omega^{-2}}{\varepsilon_j\nu_j}\right)\left(\frac{M_j}{\rho_j}\right)^2$
ω	$\left(\frac{2\times256}{27}\left(\frac{M_w}{\rho_w}\right)^2\left(\frac{1}{RT}\right)^3\frac{\sigma^3\omega^{-3}}{\varepsilon_j\nu_j}\right)\left(\frac{M_j}{\rho_j}\right)^2$
ν_{NH_4Cl}	$\left(\frac{\frac{\rho_{NH_4Cl}}{M_{NH_4Cl}}\varepsilon_{NH_4Cl}}{\varepsilon_j\nu_j}\right)\left(\frac{M_j}{\rho_j}\right)^2$
$\nu_{(NH_4)_2SO_4}$	$\left(\frac{\frac{\rho_{(NH_4)_2SO_4}}{M_{(NH_4)_2SO_4}}\varepsilon_{(NH_4)_2SO_4}}{\varepsilon_j\nu_j}\right)\left(\frac{M_j}{\rho_j}\right)^2$
$\nu_{NH_4NO_3}$	$\left(\frac{\frac{\rho_{(NH_4)_2SO_4}}{M_{(NH_4)_2SO_4}}\varepsilon_{NH_4NO_3}}{\varepsilon_j\nu_j}\right)\left(\frac{M_j}{\rho_j}\right)^2$
ε_{NH_4Cl}	$\frac{1}{\varepsilon_j\nu_j}\left(\frac{\rho_{NH_4Cl}}{M_{NH_4Cl}}\varepsilon_{NH_4Cl}\nu_{NH_4Cl}+\frac{\rho_{NH_4NO_3}}{M_{NH_4NO_3}}\nu_{NH_4NO_3}\right)\left(\frac{M_j}{\rho_j}\right)^2$
$\varepsilon_{(NH_4)_2SO_4}$	$\frac{1}{\varepsilon_j\nu_j}\left(\frac{\rho_{(NH_4)_2SO_4}}{M_{(NH_4)_2SO_4}}\varepsilon_{(NH_4)_2SO_4}\nu_{(NH_4)_2SO_4}+\frac{\rho_{NH_4NO_3}}{M_{NH_4NO_3}}\nu_{NH_4NO_3}\right)\left(\frac{M_j}{\rho_j}\right)^2$
ν_j	$\frac{256}{27}\left(\frac{M_w}{\rho_w}\right)^2\left(\frac{1}{RT}\right)^3\frac{-\sigma^3\omega^{-2}\nu_j^{-2}}{\varepsilon_j}\left(\frac{M_j}{\rho_j}\right)^2+\left(\sum_{i\neq j}\frac{\frac{\rho_i}{M_i}\varepsilon_i\nu_i}{\varepsilon_j}\right)\nu_j^{-2}\left(\frac{M_j}{\rho_j}\right)^2$
ε_j	$\frac{256}{27}\left(\frac{M_w}{\rho_w}\right)^2\left(\frac{1}{RT}\right)^3\frac{-\sigma^3\omega^{-2}\varepsilon_j^{-2}}{\nu_j}\left(\frac{M_j}{\rho_j}\right)^2-\left(\begin{array}{l}\frac{\rho_{NH_4Cl}}{M_{NH_4Cl}}\frac{\varepsilon_{NH_4Cl}\nu_{NH_4Cl}}{\nu_j}\left(-\varepsilon_j^{-2}\right)\\+\frac{\rho_{(NH_4)_2SO_4}}{M_{(NH_4)_2SO_4}}\frac{\varepsilon_{(NH_4)_2SO_4}\nu_{(NH_4)_2SO_4}}{\nu_j}\left(-\varepsilon_j^{-2}\right)\\+\frac{\rho_{NH_4NO_3}}{M_{NH_4NO_3}}\frac{\nu_{NH_4NO_3}}{\varepsilon_j\nu_j}\\+\frac{\rho_{NH_4NO_3}}{M_{NH_4NO_3}}\frac{\left(1-\varepsilon_{NH_4Cl}-\varepsilon_{(NH_4)_2SO_4}-\varepsilon_j\right)\nu_{NH_4NO_3}}{\upsilon_j}\left(-\varepsilon_j^{-2}\right)\end{array}\right)$

2.3 Experimental results

2.3.1 WSOC and inorganic composition

Table 1 is a summary of the composition for all samples analyzed in this study. The original 850 mg C L^{-1} BB sample had to be fractionated twice to yield enough carbon mass in samples for surface tension and KTA. The HPHOB, D-HPHIL, and D-HPHOB fractions shown in Table 1 are from this later fractionation. The desalted original sample contained significant amounts of ions after the desalting process (17% of the original anion fraction) (Table 1) and thus is not considered in our analysis, as it does not truly reflect a "desalted" sample.

2.3.2 Surface tension depression

The WSOC of the original BB sample contains large amounts of surfactants; at a concentration of 850 mg C L^{-1}, σ was measured to be 59 mN m^{-1} (25^{o}C), 18 % lower than the surface tension at infinite dilution with 18-Mohm ultrapure water (71.24 $\pm$ 0.53 mN m^{-1}). The σ value of the infinitely diluted solution is very close to pure water, $\sim$ 2% different from reported literature values for water at room temperature [215]. The σ value for BB is similar in magnitude to the surface tension depression reported by [59] for fog water samples and [111] for HULIS dissolved in water.

From our speciated activated aerosol study, the original sample and hydrophobic component can significantly depress surface tension with increasing carbon concentration; the hydrophilic components do not (Fig. 5). The desalted hydrophobic and desalted hydrophilic components do not depress surface tension as much as their salted counterparts. Of the three salted samples, the HPHOB sample exhibits the largest sensitivity to the presence of salts. The behavior of the HPHOB fraction suggests it is composed of HULIS [198]. The D-HPHIL and HPHIL fractions effectively have the same σ as water, even at very large carbon concentrations (Fig. 5).

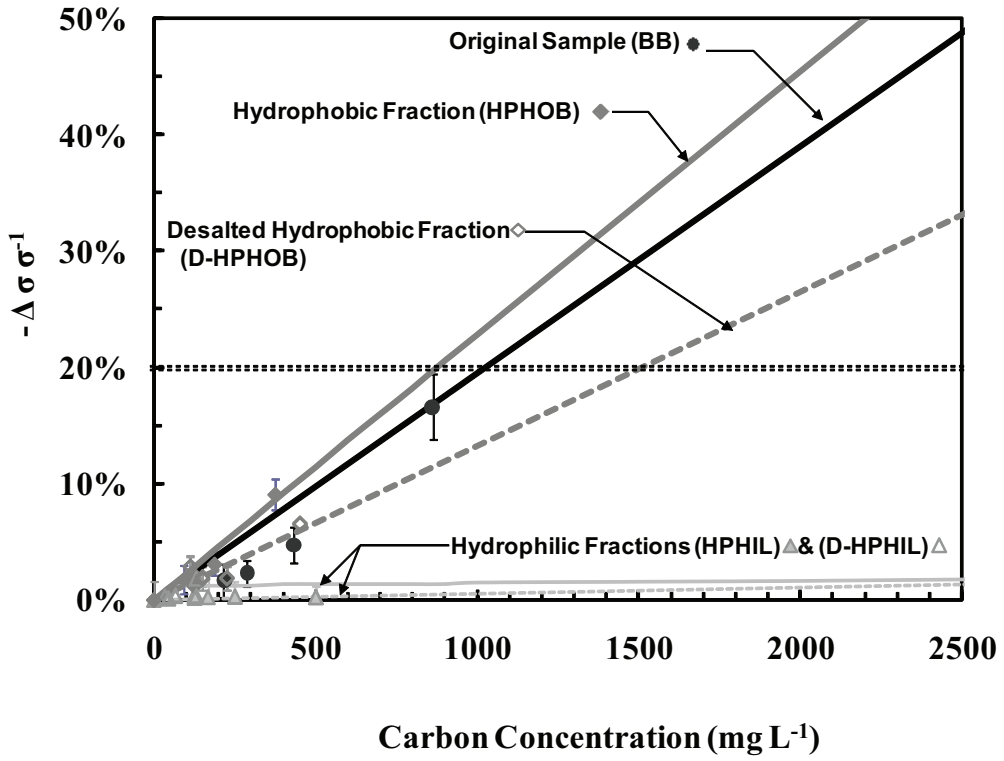

Figure 5: Surface tension of fractionated biomass burning samples. Effective surface tension curves are based on Szyszkowski-Langmuir fit to data at room temperatures. The original sample (solid black), hydrophobic (dark grey), and hydrophilic fractions (light grey) are shown. The desalted components are represented by dashed lines. The double dashed line indicates a surface tension depression of 20%.

Addition of electrolytes to the BB sample (where WSOC concentration is maintained constant at 850 mg L^{-1}) further depresses droplet σ (Fig. 6). This is consistent with behavior seen by [111] for HULIS with salts. Greater amounts of NaCl than $(NH_4)_2SO_4$ are required to reduce surface tension by the same amount, as the bivalent SO_4^{2-} is more effective than Cl^- in partitioning the hydrophobic organics (which are anionic surfactants) to the surface layer [95, 98]. Nonetheless, the increasing presence of an inorganic salt in the BB sample (which could happen e.g., in cloud processing of the aerosol) can further decrease surface tension by more than 20% and hence can have an important impact on CCN activity.

2.3.3 CCN activity

Figure 7 shows the critical supersaturation, s_c, of particles generated from the BB and fractionated samples, as a function of their d. $(NH_4)_2SO_4$has been added as a basis of comparison, and based on its van't Hoff factor and molar volume, is expected to be more CCN active than all samples of Table 1 (i.e., its activation spectrum should lie to the left of the samples). Indeed, this is mostly the case; the activation spectra for HPHIL and D-HPHIL are closest to $(NH_4)_2SO_4$. Strong surfactants are not present in the HPHIL, D-HPHIL, as their surface tension is not substantially different from water, even at very high carbon concentrations (Fig. 6). This suggests that the hydrophilic components are composed of soluble, low molecular weight compounds which is consistent with the functional group calibration analysis of [198, 200] done for similar samples.

Surprisingly, HPHOB (which contains the least hydrophilic component of WSOC) was the most CCN active of all samples, surpassing even $(NH_4)_2SO_4$ (Fig. 7). This seemingly counterintuitive finding can be reconciled when considering the synergism between the salts and organics. HPHOB contains large amounts of salts, so based on that alone, one would expect CCN activity close to pure $(NH_4)_2SO_4$. However, the

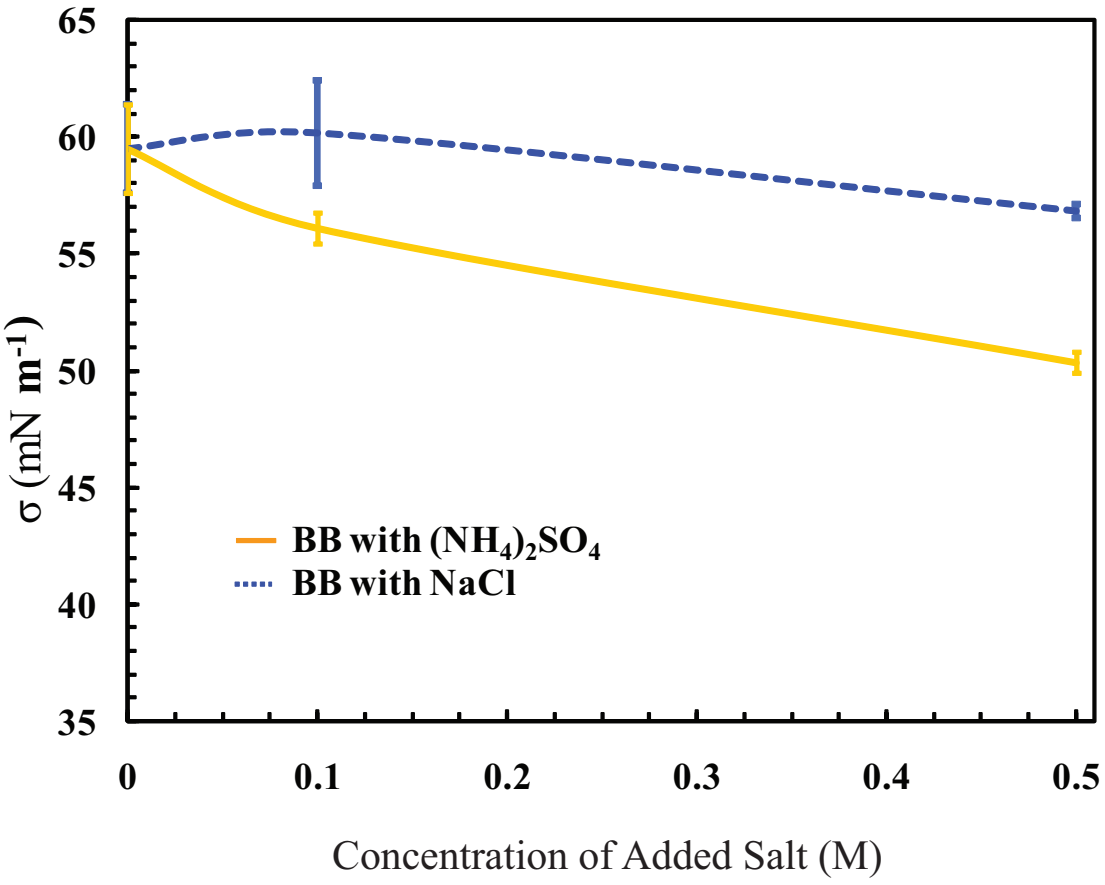

Figure 6: Surface Tension of BB sample with the addition of $(NH_4)_2SO_4$ and NaCl. WSOC concentration is constant at 850 mg L^{-1}

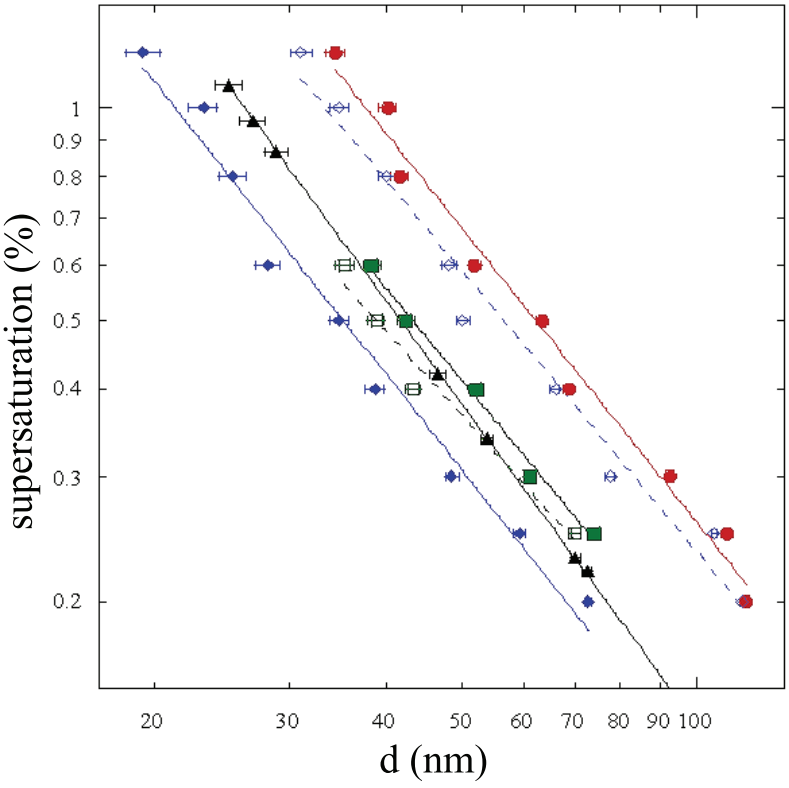

Figure 7: Critical supersaturation vs. dry particle diameter for BB Fractions and $(NH_4)_2SO_4$. The original sample (solid red circles), hydrophobic (blue diamonds), hydrophilic (green squares) and $(NH_4)_2SO_4$ (black triangles) are shown. The desalted samples are represented by dashed lines and open symbols.

of surfactants present in HPHOB, because of the concentrated salts present in the CCN, tend to partition on the CCN surface and depress surface tension, as was seen in Fig. 6. This "salting out" effect of the organics would then decrease the CCN critical supersaturation, making the HPHOB better CCN than pure $(NH_4)_2SO_4$. "Salting out" of organics can also explain why HPHOB becomes even more CCN active (compared to $(NH_4)_2SO_4$) as the dry CCN diameter decreases (Fig. 7); according to Köhler theory, the concentration of solute (organic and inorganic) increases at the point of activation as dry particle size decreases. Both decrease surface tension as dry size decreases, which implies that the CCN activity of HPHOB and $(NH_4)_2SO_4$ diverge more at small diameters. Conversely, at large d, the concentrations of solute at the point of activation are lower, the surface depression of HPHOB is relatively small, and the CCN activity curve of HPHOB and $(NH_4)_2SO_4$ tend to converge (Fig. 7).

The D-HPHOB fraction has lower CCN activity than $(NH_4)_2SO_4$ and HPHOB. In comparison to $(NH_4)_2SO_4$,lowering of surface tension in D-HPHOB is not compensated by the lack of solute during the desalting. D-HPHOB and BB have similarly low CCN activity and the BB sample is the least active of all samples. As illustrated in Fig. 7, one cannot assume the CCN activity of BB should reside somewhere between HPHOB and HPHIL. Even though the BB sample contains more soluble material (mostly inorganics and some unknown amount of hydrophilics) and did depress surface tension (attributed the presence of electrolytes and hydrophobics) the contribution and interactions with water vapor of all three speciated components: hydrophilics, hydrophobics and inorganics is not additive. Regardless, KTA on all samples should give molar volume estimates that are consistent, i.e., lowest for HPHIL, then BB, and finally, HPHOB.

Table 5: Results of Köhler Theory Analysis.

Sample	$(\frac{M_j}{\rho_j})$ (m^3 mol^{-1})	M_j (g mol^{-1})[e]
BB	1.6×10^{-4}	248
D-HPHIL	6.2×10^{-5}	87
D-HPHOB	5.6×10^{-4} (method b_1)[f]	780 (method b_1)[f]
	6.1×10^{-4}(method b_2)	859 (method b_2)

[e] Assuming an average density of 1400 kg m^{-3} [204]
[f] Determined from data with s_c between 0.4% and 0.6%.

2.4 Köhler theory analysis of samples

2.4.1 Molar volume estimations

We compute average organic molar volumes for the original and desalted hydrophobic and hydrophilic samples (i.e., BB, D-HPHIL, D-HPHOB), where the organic volume fraction dominates (Table 5) hence KTA is subject to less uncertainty [150]. The inorganic compounds present in the sample are assumed to be a mixture of ammonium sulfate, ammonium chloride, and ammonium nitrate in proportion to their ionic concentrations (Table 1).

In computing the volume fraction of each constituent in the dry aerosol, Eq. (4), we multiplied the WSOC concentration with 1.4 to obtain the total dissolved organic carbon mass concentration [204]; the relative amount of each component (OC and inorganic salts) in solution is then used to determine their mass fraction, m_i, in the dry aerosol (Table 1). Because it can be assumed that our hydrophobic sample is much like the extracted F5 sample of [46] with a density of 1.5 g cm^{-3}, we estimate a conservative molecular weight and account for changes in density in our molar volume sensitivity analysis by varying density from 1.4 to 1.6 g cm^{-3}. In applying Eq. (4), the density of $(NH_4)_2SO_4$, NH_4Cl, NH_4NO_3 was taken to be 1760, 1800, and 1500 kg m^{-3} respectively [153]. OC density was the most uncertain, and here is assumed to be 1400 kg m^{-3} [204]. In the case of hydrophobic molar volume analysis, surface tension becomes negative when the Szyszkowski-Langmuir fit of our data is applied. This

implies that the critical micelle concentration is reached at the point of activation beyond which surface tension depression asymptotes. Because of this, the surface tension of hydrophobics is set to 50% of pure water, corresponding to the lower limit observed for HULIS [111].

The effective van't Hoff factor, ν_i, (defined as the number of ions released into the solution times the osmotic coefficient) expresses the impact of dissociation on water activity. For multicomponent electrolyte solutions, ν_i can be accurately computed with existing thermodynamic models [143] and has been successfully applied for activation of inorganic CCN, e.g.,[159]. However, in solutions of WSOC with electrolytes (which characterize all the samples of this study), ν is quite uncertain as speciation in solution is not known, and modeling complex organic-water-inorganic interactions is challenging. For this reason, we approximate ν as follows: *i)*$\nu = 2$ for NH_4Cl and NH_4NO_3, *ii)*$\nu = 3$ for $(NH_4)_2SO_4$, *iii)* $\nu = 1$ for organics in the BB sample, as the sample is acidic and organics are not expected to substantially dissociate, *iv)* $\nu = 1$ for organics in the HPHOB and D-HPHOB samples, as they are very weakly dissociating and *iv)* $\nu = 2.5$ for D-HPHIL, as we assume the sample to be composed of dicarboxylic acids neutralized with ammonium during the extraction process; the ammonium salts are then assumed to dissociate as effectively as $(NH_4)_2SO_4$. The error in organic van't hoff factor can be as large as 20% (as titration experiments suggest; [48]) and is considered our sensitivity analysis.

The molar volumes of the organic aerosol components are estimated employing KTA (presented in Section 2.1) and the above effective van't Hoff assumptions, the results of which are shown in Table 5. The molar volume of the hydrophilic organic (6.2×10^{-5} m^3 mol^{-1}) is comparable to that of inorganic salts (7.46×10^{-5} m^3 $mol^{-1}$and 2.97×10^{-5} m^3 $mol^{-1}$for $(NH_4)_2SO_4$ and $(NH_4)Cl$, respectively) and low molecular weight mono- and di-carboxylic chains (e.g., formic and acetic acid, and succinic, glutaric, and oxalic acid with 7.54×10^{-5} m^3 mol^{-1}, 9.34×10^{-5} m^3 mol^{-1},and 6.4

$\times 10^{-5}$ m^3 mol^{-1} respectively) typical of those identified in the XAD-8 calibration studies [198]. The significantly larger estimated molar volume of the hydrophobic fraction (5.6×10^{-4} m^3 mol^{-1} using method $\mathbf{b}_1$), 6.1×10^{-4} m^3 mol^{-1} using method $\mathbf{b}_2$) is consistent with the existence of HULIS in the sample which has been previously shown by mass spectrometery methods to have molecular weights up to 1000 amu [76]. Nevertheless, we speculate that the average organic molar mass inferred from KTA could be smaller for several reasons: *i*) the KTA value is a number averaged property, which weighs the average towards a smaller number, when compared to mass-based averaging, and, *ii*) HULIS may have a higher ν than unity, as they are comprised of several polyfunctional groups that may contain polar groups like carbonyls, carboxyls, and hydroxls [76, 113]. Therefore, when KTA is applied assuming $\nu = 1$, the inferred molar volume decreases to compensate.

The average molar mass for the orginal BB samples was found to be 248 g mol^{-1}. Assuming that the organics in the original BB sample is a mixture of D-HPHIL and D-HPOB, we can infer the relative proportion of HPHIL and HPOB via the following equation

$$M_{BB} = \chi M_{HPHIL} + (1 - \chi) M_{HPHOB} \tag{10}$$

where χ is the mol fraction of hydrophilics in the original BB sample and M_{BB}, M_{HPHIL}, M_{HPHOB} are the inferred molar masses from the BB, HPHIL and HPHOB samples. Eq. (10) can be solved for χ to yield

$$\chi = \left(\frac{M_{BB} - M_{HPHIL}}{M_{HPHOB} - M_{HPHIL}} \right) \tag{11}$$

We determine that $\chi \sim 0.25$, i.e., there are approximately 3 hydrophilic compounds for every 1 hydrophobic macromolecule in the original WSOC mixture.

Table 6: Molar Volume Sensitivity Analysis for BB Sample.

Property (units)	Δx	Φ_x ($m^3 mol^{-1} x^{-1}$)	Molar Volume uncertainty %
σ (N m^{-1})	1.37×10^{-3}	1.06×10^{-2}	9.7
ω ($m^{1.5}$)	9.49×10^{-15}	6.25×10^{9}	39.3
ν_{NH_4Cl}	0.5	1.49×10^{-5}	4.9
$\nu_{(NH_4)_2SO_4}$	0.5	7.43×10^{-6}	2.5
$\nu_{NH_4NO_3}$	0.5	6.08×10^{-6}	2.0
ε_{NH_4Cl}	1.95×10^{-3}	9.34×10^{-4}	1.2
$\varepsilon_{(NH_4)_2SO_4}$	2.03×10^{-3}	9.22×10^{-4}	1.2
$\varepsilon_{organic}$	6.36 × 10-3	1.09×10^{-3}	4.6
$\nu_{organic}$	0.20#	1.78×10^{-4}	23.6
Total Uncertainty			47.5

error based on observations of 20% dissociation of organic HULIS in titration experiments [48].

2.4.2 Molar volume sensitivity and uncertainty analysis

Application of the sensitivity analysis requires quantification of the uncertainty for all parameters that affect $\frac{M_j}{\rho_j}$. $\frac{\Delta\sigma}{\sigma}$ is 2% (Section 2.3.2), $\Delta\,\omega$ is the standard deviation derived from the fit of s and d experimental data to the Köhler curve, $\Delta\nu_i$ is 0.5, $\Delta\nu_j$ is 0.2, and $\Delta\varepsilon_i$ and $\Delta\varepsilon_j$ are uncertainties associated with assuming organic aerosol density of 1.4 to 1.6 g mol^{-1} [204].

The sensitivity analysis for methods b_1 and b_2 suggests that one of the largest sources of uncertainty for molar volume estimates arises from ω (Tables 6, 7, 8 and 9), which is not surprising, given that it cumulatively expresses CCN activity. Furthermore, ω may vary significantly in the presence of strong surfactants, as the concentration of solute at the critical diameter (which varies considerably over a range of s_c) controls σ. CCN with low s_c (large d) tend to have low WSOC concentration at activation and do not affect σ depression at the droplet layer as much as CCN of smaller d and higher s_c. For these reasons, σ may contribute considerable uncertainty in organic molar volume estimates (up to 10% as shown) but can be the second largest source of uncertainty for samples containing strong surfactants (e.g., hydrophobics). In the case of hydrophobics, uncertainty from exact knowledge of σ

Table 7: Molar Volume Sensitivity Analysis for D-HPHIL Sample.

Property (units)	Δx	Φ_x ($m^3 mol^{-1} x^{-1}$)	Molar Volume uncertainty %
σ (N m^{-1})	1.37×10^{-3}	3.90×10^{-3}	7.2
ω ($m^{1.5}$)	4.43×10^{-15}	4.62×10^{9}	27.6
ν_{NH_4Cl}	0.5	3.58 × 10-8	0.0
$\nu_{(NH_4)_2SO_4}$	0.5	2.70 × 10-9	0.0
ε_{NH_4Cl}	6.89×10^{-5}	8.27×10^{-5}	0.0
$\varepsilon_{(NH_4)_2SO_4}$	1.31×10^{-5}	8.26×10^{-5}	0.0
$\varepsilon_{organic}$	8.2×10^{-5}	1.72×10^{-4}	0.0
$\nu_{organic}$	0.20#	3.56 × 10-5	9.6
Total Uncertainty			30.1

error based on observations of 20% dissociation of organic HULIS in titration experiments [48].

Table 8: Molar Volume Sensitivity Analysis for D-HPHOB Sample.

Property (units)	Δx	Φ_x ($m^3 mol^{-1} x^{-1}$)	Molar Volume uncertainty %
σ (N m^{-1})	7.06×10^{-4}	5.53×10^{-2}	7.0
ω ($m^{1.5}$)	4.43×10^{-15}	2.08×10^{10}	16.5
ν_{NH_4Cl}	0.5	2.65×10^{-7}	0.0
$\nu_{(NH_4)_2SO_4}$	0.5	3.38×10^{-7}	0.0
ε_{NH_4Cl}	3.63×10^{-6}	1.16×10^{-2}	0.0
$\varepsilon_{(NH_4)_2SO_4}$	0	1.16×10^{-2}	0.0
$\varepsilon_{organic}$	1.16×10^{-5}	1.23×10^{-2}	0.0
$\nu_{organic}$	0.20#	6.50×10^{-4}	23.3
Total Uncertainty			29.5

error based on observations of 20% dissociation of organic HULIS in titration experiments [48].

may introduce even larger uncertainty in molar volume estimates. The uncertainty in the van't Hoff factor may also be an important source of uncertainty in estimated organic molar volume ($\sim 24\%$) even though inorganic fractions and uncertainties are small (especially for the BB and D-HPHOB samples).

Using an average organic mass density of 1.4 g cm^{-3} [204] we find the organic component in the original sample (BB) to have an average molar mass of 248 ± 117 g mol^{-1}, the hydrophobics in D-HPHOB to be on average 780 ± 231 g mol $^{-1}$ and the hydrophilic component of D-HPHIL to be the lightest, with an average of 87 ±

Table 9: Molar Volume Sensitivity Analysis for D-HPHOB at each supersaturation measured.

Quantity (units)	s=1.00%	0.80%	0.60%	0.50%	0.40%	0.30%	0.20%
$\left(\frac{M_j}{\rho_j}\right)$ (m^3 mol^{-1})	5.97×10^{-4}	5.80×10^{-4}	5.57×10^{-4}	4.45×10^{-4}	6.51×10^{-4}	5.98×10^{-4}	8.68×10^{-4}
σ (N m^{-1})	3.53×10^{-2}	3.53×10^{-2}	3.53×10^{-2}	3.53×10^{-2}	3.53×10^{-2}	3.53×10^{-2}	3.53×10^{-2}
$\Delta\sigma$	7.06×10^{-4}	7.06×10^{-4}	7.06×10^{-4}	7.06×10^{-4}	7.06×10^{-4}	7.06×10^{-4}	7.06×10^{-4}
Φ_σ (m^4 mol^{-1} N^{-1})	5.93×10^{-2}	5.76×10^{-2}	5.42×10^{-2}	4.43×10^{-2}	6.47×10^{-2}	5.96×10^{-2}	8.65×10^{-2}
$\Phi_\sigma\Delta\sigma$	7.01%	7.02%	6.87%	7.02%	7.02%	7.03%	7.03%
$\omega(m^{1.5})$	6.48×10^{-14}	6.39×10^{-14}	6.32×10^{-14}	5.60×10^{-14}	6.77×10^{-14}	6.48×10^{-14}	7.81×10^{-14}
$\Delta\omega$	4.43×10^{-15}	4.43×10^{-15}	4.43×10^{-15}	4.43×10^{-15}	4.43×10^{-15}	4.43×10^{-15}	4.43×10^{-15}
Φ_ω	$2.15\times10^{1}0$	$2.12\times10^{1}0$	$2.02\times10^{1}0$	$1.86\times10^{1}0$	$2.25\times10^{1}0$	$2.16\times10^{1}0$	$2.60\times10^{1}0$
$\Phi_\omega\Delta\omega$	15.96%	16.21%	16.04%	18.50%	15.31%	16.00%	13.28%
$\varepsilon_{organic}$	1.00	1.00	1.00	1.00	1.00	1.00	1.00
$\Delta\varepsilon_{organic}$	8.47×10^{-4}	8.47×10^{-4}	8.47×10^{-4}	8.47×10^{-4}	8.47×10^{-4}	8.47×10^{-4}	8.03×10^{-19}
$\Phi_{\varepsilon_{organic}}$ (m^3 mol^{-1})	0 1.33×10^{-2}	1.22×10^{-2}	7.83×10^{-3}	1.70×10^{-2}	1.41×10^{-2}	2.91×10^{-2}	
$\Phi_{\varepsilon_{organic}}\Delta\varepsilon_{organic}$	0.00%	1.94%	1.86%	1.49%	2.21%	1.99%	0.00%
$\nu_{organic}$	1.00	1.00	1.00	1.00	1.00	1.00	1.00
$\Delta\nu_{organic}$#	0.2	0.2	0.2	0.2	0.2	0.2	0.2
$\Phi_{\nu_{organic}}$ (m^3 mol^{-1})	0 6.57×10^{-4}	6.24×10^{-4}	4.07×10^{-4}	1.11×10^{-3}	6.41×10^{-4}	8.35×10^{-4}	
$\Phi_{\nu_{organic}}\Delta\nu_{organic}$	0.00%	22.65%	22.40%	18.27%	34.14%	21.44%	19.23%

error based on observations of 20% dissociation of organic HULIS in titration experiments [48].

26 g mol^{-1} (Table 5).

2.5 Implications and summary

This study is focused on characterizing the properties of water-soluble organics found in fresh biomass burning aerosol. The aerosol, after collection upon filters, is dissolved in water and fractionated into hydrophobic and hydrophilic components using XAD-8 solid phase extraction, and subsequently desalted. The original, fractionated and desalted samples are then characterized for their surfactant properties and average thermodynamic properties relevant for CCN activation (i.e., surface tension depression, solubility and average molar volume). Characterization of solubility and molar volume is done by combining CCN activity measurements with Köhler Theory using the method of "Köhler Theory Analysis" (KTA) (first introduced by [150], and further developed here). The surface tension and CCN activity of these different samples are measured with a KSV CAM 200 goniometer and a DMT Streamwise Thermal Gradient CCN Counter, respectively.

It was found that the less hygroscopic soluble hydrophobic fractions can readily activate at high supersaturations and depending on the presence of inorganic species, can exhibit larger CCN activity than pure $(NH_4)_2SO_4$. This phenomenon can be attributed to "salting-out" of organics to the CCN surface layer from the presence of electrolytes; this would decrease surface tension and critical supersaturation. This hypothesis is supported by direct measurements of surface tension, as well as from measurements of CCN activity.

Surfactant behavior in the samples is attributed to the hydrophobic fraction that exhibit properties common to HULIS. The presence of inorganic salts may enhance surface tension depression to an extent in which insoluble hydrophobic aerosol may be better CCN than their pure inorganic counterparts. This supports the suggestion by [111], to include the interaction of inorganic and organic species effect on surface

tension, whenever appropriate, in aerosol-cloud interaction studies.

Using an average organic mass density of 1.4 g cm^{-3} we infer the hydrophobic and hydrophilic fractions to be 780 $\pm$ 231 g mol^{-1} and 87 $\pm$ 26 g mol^{-1}, respectively. From these average values, we estimate the relative molar ratio of hydrophilics to hydrophobics to be 3:1. Solubility limits, seen as an abrupt change in the scale dependence of $s_c$from$d^{-1.5}$ to d^{-a} (a >1.5), were not observed [150].

The inferred molar volumes for the samples considered in this study are on average subject to 36% uncertainty. Most of the uncertainty arises from the slope of the $s_c - d$ fit and σ [150] and ν in the case of aggregate organics. Nevertheless, the molar volume estimates are in agreement with expected ranges for these compounds and suggest that KTA can be applied effectively to characterize CCN activity of water-soluble organic aerosol.

The study shown here presents a novel method to describe the complex detailed inorganic, organic and water vapor interactions within a Köhler theory framework appropriate for GCM parameterizations of aerosol-cloud interactions. We have demonstrated that this novel method can successfully be applied to a very complex aerosol and provide aggregate properties that comprehensively characterize its CCN activity. In future work, the properties from other sources of carbonaceous aerosol should be characterized as presented here. Over time, such efforts will provide a comprehensive set of constraints for physically-based assessments of the indirect effects of carbonaceous aerosol.

CHAPTER III

WSOC PROPERTIES OF SOA FROM FILTER SAMPLES

The CCN properties, surfactant characteristics, and droplet growth kinetics of secondary organic aerosol (SOA) formed from the ozonolysis of three parent alkene hydrocarbons (terpinolene, 1-methlycycloheptene and cycloheptene) are explored. Based on measurements of CCN activity, total carbon and inorganic ion concentrations, we estimate the average molar volume of the water-soluble organic component using Köhler Theory Analysis (KTA). The results suggest that the water-soluble organics in the SOA are composed of relatively low molecular weight species, with an effective molar mass less than 200 g mol^{-1}. This finding is consistent with the speciated fraction for some of the SOA, and suggests that KTA can be applied to complex organic aerosol, such as that found in the atmosphere. From measurements of CCN activity and Köhler Theory, we apply a novel method to infer the surface tension at the point of activation; this is used to infer the presence of surface-active organics. It is found that the water-soluble carbon can be surface-active, depressing surface tension 10-15% from that of pure water at concentrations relevant for CCN activation. Although important, this level of surface tension depression is lower than expected for HULIS, which suggest that they are not likely in the SOA examined. In all cases, the CCN exhibit droplet growth kinetics similar to $(NH_4)_2SO_4$. Note: This chapter appears as reference [14].

3.1 Motivation

Natural VOC emissions (e.g., monoterpernes, sesquiterpenes), estimated to be 1150 Tg yr^{-1} [84], are a major source of SOA. Alkene ozonolysis is well established as a source of SOA [1, 17, 19, 38, 49, 67, 72, 86, 97, 108, 109, 110, 120, 129, 182, 208].

Attempts to speciate SOA [1, 17, 49, 72, 108] have been met with limited success, as 80 to 90% of the aerosol mass can remain uncharacterized [108, 167, 179]. The potential for forming oligomeric or polymeric structures [19, 72, 73, 107] has been suggested to explain the uncharacterized SOA fraction. Oligomers have the potential to exhibit characteristics similar to humic-like substances (HULIS) [19], which strongly depress surface tension [16, 47, 76, 111, 173] and potentially, droplet growth kinetics. All of these can have important impacts on CCN activity. Nevertheless, a complete thermodynamic characterization of the secondary aerosol, and of WSOC (required to constrain cloud droplet formation) have remained elusive [109].

In this study we report the experimental investigation of the CCN activity of the water soluble fraction of SOA generated in laboratory chamber ozonolysis of alkenes; these measurements are then used to obtain thermodynamic properties (e.g., molar mass and surface tension depression), which are inferred using Köhler Theory Analysis (KTA) [16, 150]. Furthermore, we characterize WSOC SOA droplet growth kinetics, relative to pure $(NH_4)_2SO_4$. Finally, we evaluate (by comparing inferred properties to direct measurements) the applications of KTA for complex organic aerosol systems.

3.2 Experimental methods and theoretical analysis

3.2.1 Filter extraction and chemical composition

Secondary organic aerosol is generated from the seedless dark ozonolysis of three parent alkenes (cycloheptene, 1-methylcycloheptene and terpinolene) and collected upon Teflon filters. The ozonolysis experiments were performed in the Caltech dual 28 m^3 teflon chambers under dry conditions ($> 5\%$ relative humidity), a detailed description of which can be found in [110]. The ozone mixing ratio was three times that of the reactant concentration (Table 10) to insure adequate oxidation [72]. SOA chemical speciation information measured by liquid chromatography/mass-spectrometry and ion trap mass spectrometry are available for the cycloheptene and 1-methylcycloheptene

precursors from [72] (Table 10). No chemical speciation data are available for SOA generated from terpinolene. The presented analysis is the first study to characterize the CCN-relevant properties of WSOC from cycloheptene and 1-methylcycloheptene ozonolysis. Table 10 presents the estimated average (mole fraction weighted) molar mass and carbon to organic carbon mass ratio for the speciated organics.

Following the protocols outlined in [200] and Weber (2006), the WSOC in the filter samples was extracted in pure water (18 M Ohms) during a 1.25 h sonication process with heat (water bath temperature $\sim$60 $^{\circ}$C). WSOC concentration was then measured with a Total Organic Carbon (TOC) Turbo Siever analyzer [197]. Anion concentrations (SO_4^{2-}, $Cl^-$and NO_3^-) of the extracted sample were measured with the Dionex DX-500 ion chromatograph with Na_2CO_3/$NaHCO_3$ eluent and Metrosep A Supp 5-100 analytical column (Metrohm, Switzerland). Table 11 provides a summary of the offline WSOC chemical composition measurements and nominal anion concentrations (less than 2.55×10^{-5} mg L^{-1}) in the extracted samples; as expected, the ion concentrations are very low and contribute negligible solute to the samples. However, it is possible that the process of aerosol collection, dissolution, atomization, and subsequent drying may affect the partitioning of CCN properties and growth kinetics of the SOA. In future studies, we will do both online and filter analysis to see whether the extraction process introduces significant artifacts.

3.2.2 CCN activity of SOA

The instruments and experimental set-up used to measure CCN activity are identical to those described in [16] and [150]. 3-5 ml of extracted sample is atomized in a collision type atomizer (University of Minnesota), dried with two diffusional driers and subsequently classified with a scanning mobility particle sizer (TSI SMPS 3080). A 0.71 cm impactor is placed on the aerosol inlet and aerosol are charged with a Kr-85 neutralizer (TSI 3077A). The sheath to flow ratio within the differential mobilility

analyzer (TSI DMA 3081) is kept at a constant 10 L min^{-1} to 1 L min^{-1}. Scanning Mobility CCN Analysis (SMCA) first introduced by [142], is used to obtain fast size-resolved CCN activity. As with stepping mode measurements the classified aerosol is split to be counted by a condensation particle counter (TSI 3010) and also activated into droplets using a DMT Continuous Flow Stream-wise Thermal Gradient Chamber [122, 164]. The total concentration (CN) of sized particles measured by the CPC is used to determine the ratio of CCN to CN. The process is repeated for different particle sizes. For each supersaturation, s, the cut-off diameter, d, (defined as the point at which CCN/CN=0.5) provides a quantitative characterization of the SOA CCN activity (i.e., for a given s, a larger d corresponds to a lower CCN activity). The experiments are repeated a minimum of four times for each supersaturation and any influence of doubly charged particles are neglected as shown in [150].

3.2.3 Addition of inorganic salts

The impact of adding electrolytes to the CCN activity of the WSOC is explored by mixing a pre-calculated amount of $(NH_4)_2SO_4$ to the dissolved SOA sample (so that the salt mass fraction in the atomized aerosol is known). The mass of organic carbon, $m_{organic}$, in the extracted sample is determined by multiplying the measured WSOC carbon concentration by an organic carbon-to-carbon ratio of 2. The factor of 2 (Table 10) is estimated from speciation information provided in [72] and its subsequent supplemental material. For each identified compound the carbon to organic carbon ratio is determined from its molecular formulae and weighted by its abundance in the speciated compounds. The inorganic mass to be added, m_i, to obtain the resulting inorganic mass fraction, α, is then computed as,

$$m_i = \frac{\alpha}{(1-\alpha)} m_{organic} \tag{12}$$

where $m_{organic} = 2 \times [WSOC]\ V_{sample}$, [WSOC] is the the WSOC concentration

(mg C L^{-1}), and V_{sample} is the sample volume (ml). The 18 Mohms of filtered water used to extract the water during sonication contributes negligible ions to the particulate matter (Table 11).

3.2.4 Measuring and inferring surface tension of the CCN

A CAM 200 pendant drop method goniometer is used to directly measure surface tension. A description of the method and procedure can be found in [16]. Since the surface tension depression strongly depends on [WSOC] [45, 92, 111], surface tension, σ, is measured at numerous concentrations. The measurements are then fit to the Szyskowski-Langmuir isotherm [16, 124],

$$\sigma = \sigma_w - \alpha T \ln(1 + \beta c) \tag{13}$$

where σ_w is the surface tension of pure water at temperature, T, (obtained by infinitely diluting our sample with deionized ultra-filtered water), and α, β are empirical constants obtained from the fit. Unfortunately, direct measurement of σ of WSOC solutions at concentrations relevant for CCN activation (10^3 ppm and above) requires significant amount of mass ($10^3 \mu$g and above) or usage of dilute WSOC sample. If α, β are based on using dilute samples, extrapolation of Eq.(13) to higher concentrations is often subject to substantial uncertainty because *i*) the uncertainty α and β can translate to large uncertainty in σ and *ii)* may not be applicable at concentrations close to or above the critical micelle concentration; we propose the following alternate method of inferring σ from CCN measurements.

As one approaches the critical micelle concentration for a solution containing organic surfactants and electrolytes, the surface tension of droplets would tend to vary little with carbon concentration. Adding electrolytes can enhance surfactant partitioning to the surface layer (otherwise known as "salting-out" effect) [16, 111]. A ubiquitous bivalent ion, such as SO_4^{2-}can be a very effective "salting-out" agent,

so that CCN containing surfactant and sulfate may have a constant surface tension (but lower than that of water). This partitioning of organics to the layer has been addressed in previous works [127, 187, 188]. Salting-out and its effect on surface tension and CCN activity, has been seen in $(NH_4)_2SO_4$ - HULIS mixtures [111] and hydrophobic water-soluble organics isolated from freshly collected biomass-burning aerosol [16, 111].

Furthermore, if the salt mass fraction exceeds 50%, the majority of dissolved solute, n_s, is usually from the inorganic salt, and any surface tension depression at the droplet layer could be attributed to the presence of organics. Hence, one could then infer the droplet surface tension, σ, at the point of activation using a combination of CCN activation experiments and Köhler theory, as follows. For particles composed of soluble and insoluble fractions, the critical supersaturation, s_c, is (Köhler, 1936; [179]),

$$s_c = \left(\frac{4A^3}{27B}\right)^{1/2} \tag{14}$$

where $A = \left(\frac{4M_w\sigma}{RT\rho_w}\right)$, $B = \left(\frac{6n_sM_w\nu}{\pi\rho_w}\right)$, R is the universal gas constant, T is droplet temperature, n_s are the moles of dissolved solute, with an effective van't Hoff factor ν. M_w and ρ_w are the molecular weight and density of water, respectively, and σ is the surface tension of the droplet at the point of activation. The assumption that the inorganic salt contributes the dominant solute implies it is the only component that contributes to B (otherwise known as the "Raoult term"),

$$B = \frac{M_w}{M_i}\frac{\rho_i}{\rho_w}d^3\varepsilon_i\upsilon_i \tag{15}$$

where d is the CCN dry diameter, M_i is the molecular weight of the inorganic constituent, ε_i is the volume fraction of the inorganic which relates to mass fraction, m, and density, ρ, as

$$\varepsilon_i = \frac{m_i/\rho_i}{m_i/\rho_i + m_o/\rho_o} \tag{16}$$

where "i" and "o" subscripts refer to inorganic and organic components, respectively. If the organic is not a strong surfactant, then s_c for the dry diameter $d$and volume ε_i, should be given by

$$s_c^* = \frac{2}{3}\left(\frac{4M_w\sigma_w}{RT\rho_w}\right)^{3/2}\left(3\frac{M_w}{M_i}\frac{\rho_i}{\rho_w}d^3\varepsilon_i\upsilon\right)^{-1/2} \tag{17}$$

where σ_w corresponds to the surface tension of pure water. However, if the organic depresses surface tension to σ (less thanσ_w), then the critical supersaturation is given by

$$s_c = \frac{2}{3}\left(\frac{4M_w\sigma}{RT\rho_w}\right)^{3/2}\left(3\frac{M_w}{M_i}\frac{\rho_i}{\rho_w}d^3\varepsilon_i\upsilon\right)^{-1/2} \tag{18}$$

If s_c and d are known from the CCN activity measurements, Eqs. (17) and (18) can be combined to give σ:

$$\sigma = \sigma_w\left(\frac{s_c}{s_c*}\right)^{2/3} \tag{19}$$

where s_c^* is given by Eq. (17); Eq.(19) represents the extension of Köhler Theory Analysis to infer surface tension SOAf1from activation experiments. If the organic contribution to the Raoult term (Eq. 15) is not negligible, then it must be accounted for in Eqs. (17-19). Thus a molar volume must be calculated to estimate the organic contribution and the inferred surface tension is determined in conjunction with KTA (Section 3.2.5).

3.2.5 Köhler theory analysis (KTA) and molar volume uncertainty

Recently several single parameter equations have been employed to characterize CCN activity [154, 162, 212]. KTA [16, 150] is used in this work to infer average molar volume (molecular weight, M, over density ρ) of the water-soluble organic fraction

of the SOA. KTA (method b_1, [150]) employs measurements of dry diameter versus critical supersaturation, $s_{c,}$ which are then fit to the expression, $s_c{}^{\frac{-3}{2}}$, also previously derived by [65, 185]. From the Fitted CCN activity (FICA) parameter, ω, estimates of σ and measurements of ionic and WSOC concentrations, $\frac{M_o}{\rho_o}$ is obtained as,

$$\frac{M_o}{\rho_o} = \frac{\varepsilon_o \upsilon_o}{\frac{256}{27}\left(\frac{M_w}{\rho_w}\right)^2 \left(\frac{1}{RT}\right)^3 \sigma^3 \omega^{-2} - \sum\limits_{i \neq o} \frac{\rho_i}{M_i} \varepsilon_i \nu_i} \tag{20}$$

KTA has been shown to constrain molecular weight estimates of known inorganic and organic mixtures to within 20% [150] and has also been applied to complex biomass burning WSOC with an estimated 40% uncertainty [16].

The measured variables employed in the KTA analysis are summarized in Table 12. In applying KTA, we assume that the effective organic van't Hoff factor, $v_{organic} = 1$. Molecular weights are presented assuming an average organic density of 1.4 g cm^{-3} [204]. The uncertainty in inferred molar volume can be computed as $\Delta\left(\frac{M_o}{\rho_o}\right) = FIX$ where Δx is the uncertainty in of each of the measured parameters x,(i.e., any of σ, ω, and υ) and is the sensitivity of molar volume to x, $\Phi_x = \frac{\partial}{\partial x}\left(\frac{M_o}{\rho_o}\right)$, derived from Eq. (20). Table 13 provides a list of Φ_x.

3.2.6 Droplet growth kinetics

When exposed to the same s profile, an activated CCN will grow to cloud droplets of similar diameter, D_p, provided that the mass transfer coefficient of water vapor to the growing droplet and the critical supersaturation is the same. The DMT CCN counter measures droplet sizes by an optical particle counter and therefore can be used to explore the impact of organics on the droplet growth kinetics. By comparing the droplet sizes of activated SOA particles against $(NH_4)_2SO_4$ particles at identical s_c, we directly assess the impact of organics on CCN growth kinetics. This is done by observing the wet diameter, D_p, that corresponds to particles with s_c equal to the instrument saturation, s, (i.e., CCN with a dry diameter equal to the cutoff diameter,

d) and subsequently evaluating D_p versus s.

3.3 Results and discussion

3.3.1 CCN activity

The cut-off diameter, d, as a function of supersaturation and $(NH_4)_2SO_4$ mass fraction are shown for all SOA samples in Figs. 8-10. WSOC from the SOA for the three parent alkenes studied (Figs. 8, 9 , and 10) indicate that as the mass fraction of $(NH_4)_2SO_4$ increases, the aerosol smoothly transitions to pure $(NH_4)_2SO_4$ behavior with roughly a $m_i^{-1/2}$ dependence. This suggests that the SOA are soluble hygroscopic relatively low molecular weight compounds that are not strong surfactants. For all three parent hydrocarbons, the original SOA samples activate at diameters larger than that of $(NH_4)_2SO_4$; this is expected as organics are, in general, less CCN active than $(NH_4)_2SO_4$. The activation curves are well represented with a power law consistent with a $d^{\frac{-3}{2}}$ dependence; this implies that the water-soluble SOA do not exhibit limited solubility [150].

3.3.2 Surface tension

11 shows the direct measurements of surface tension for all SOA samples and the Szyskowski-Langmuir fits to the data (α and β parameters of the fits are given in Table 11). None of the samples demonstrate significant surface tension depression at measured concentrations, even when extrapolated to concentrations relevant for CCN activation (100 mg C L^{-1} and above) (Fig. 11). If surfactants do exist in the SOA, it is likely they are not concentrated enough in the extracted samples to have a notable impact on surface tension; even for strong surfactants extracted from a biomass burning sample [16], the depression for concentrations up to 100 mg C L^{-1} is within the measurement uncertainty (Fig. 11).

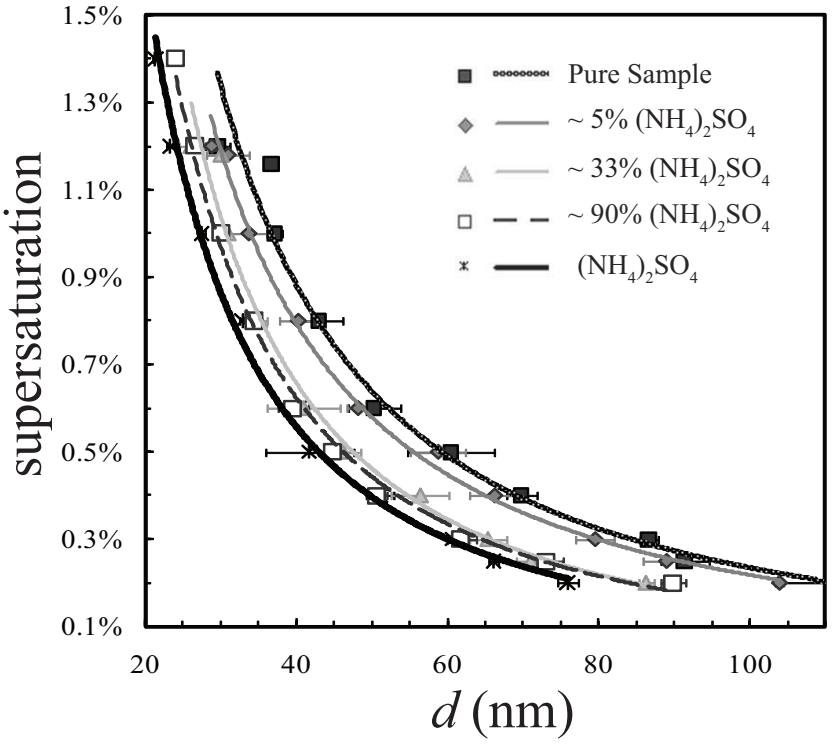

Figure 8: CCN activity of WSOC generated from ozonolysis of cycloheptene. Results are shown for pure WSOC and mixtures of $(NH_4)_2SO_4$. The cut-off diameter, d, is the point at which CCN/CN=0.5 is plotted versus supersaturation. Lines are fit of experimental data points.

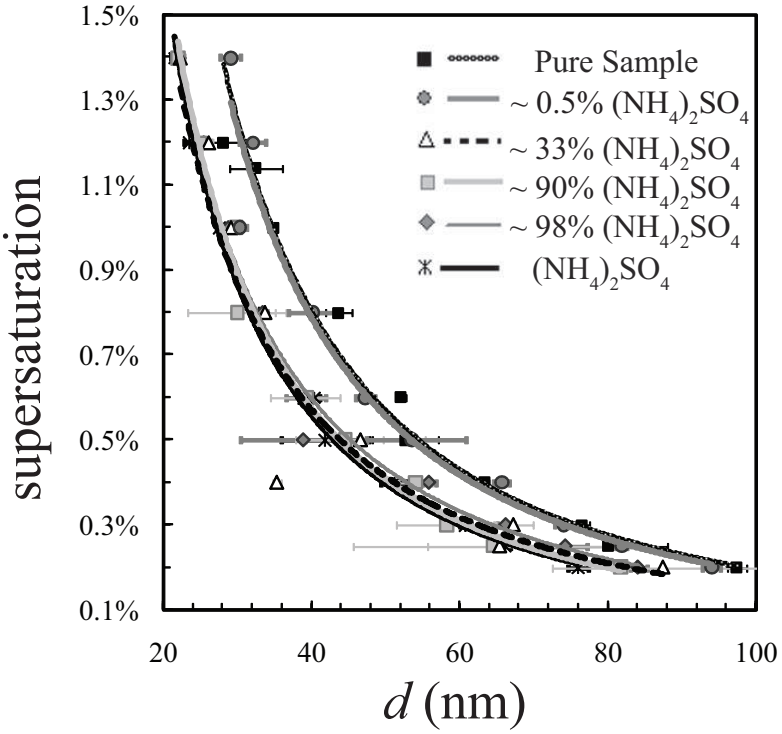

Figure 9: CCN activity of WSOC generated from ozonolysis of terpinolene. Results are shown for pure WSOC and mixtures of $(NH_4)_2SO_4$. The cut-off diameter, d, is the point at which CCN/CN=0.5) is plotted versus supersaturation. Lines are fit of experimental data points.

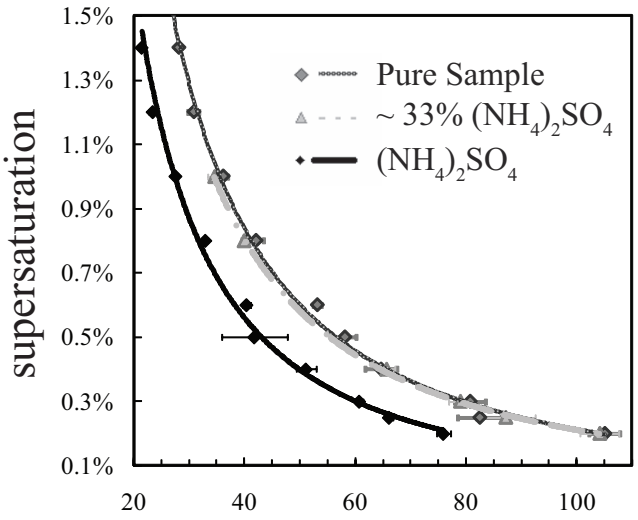

Figure 10: CCN activity of WSOC generated from ozonolysis of 1-methylcycloheptene. Results are shown for pure WSOC and mixtures of $(NH_4)_2SO_4$. The cut-off diameter, d, is the point at which CCN/CN=0.5) is plotted versus supersaturation. Lines are fit of experimental data points.

Thus, direct surface tension measurements for dilute samples would not conclusively reveal the presence of surfactants. Acquiring sufficient sample for σ measurement is challenging, so we infer surface tension using the method described in Section 3.2.4. For large mass fractions of salt (>90%), the inferred surface tension approaches that of water used to extract the WSOC from the SOA filter samples ($\sim$71 mN m^{-1}) (Table 5). However, for the 33% mixture of sulfate with cycloheptene and terpinolene, the inferred σ is $\sim$ 60 mN m^{-1} (Table 14), $\sim$15% depression from pure water, suggesting that surface active components do exist in the WSOC. The extent of surface tension depression suggests that the surfactants are appreciably strong, which is expected given the amphiphilic nature of the oxidation products; the presence of humic-like polymers (unless if in very small quantities) is unlikely, however given that expected surface tension depression is much higher at the point of activation [16, 111, 173].

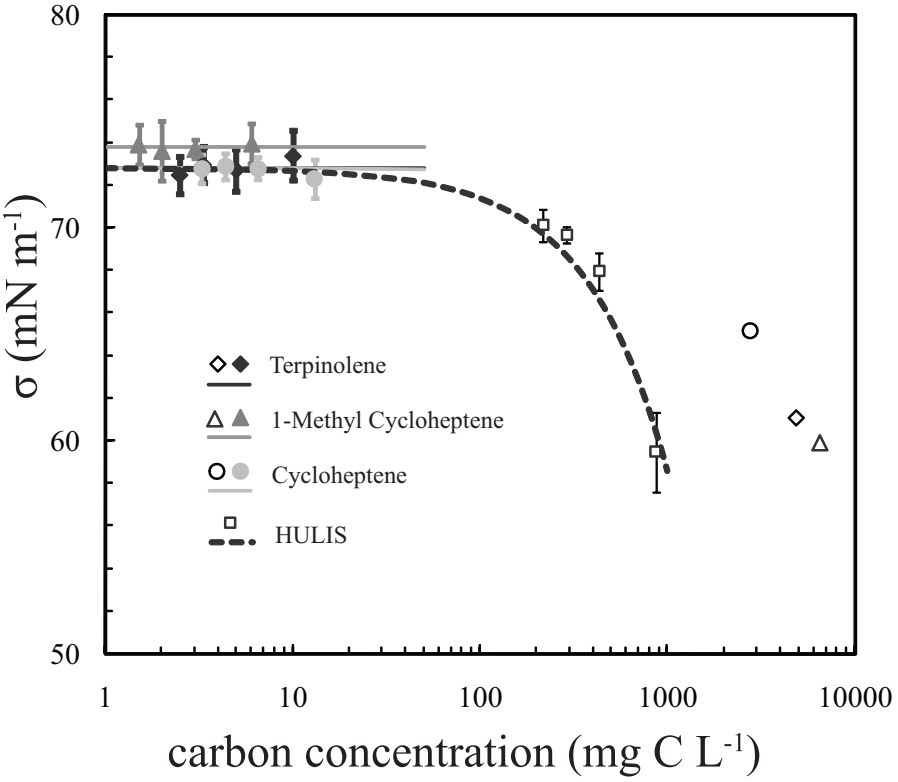

Figure 11: Direct σ measurements of SOA as a function of water-soluble carbon concentration (closed symbols) and inferred values from (Table 5) (open SOA symbols) as a function of water soluble carbon concentration at activation. Curves represent Szyskowski-Langmuir isotherm fits of experimental data. HULIS data from [16] is provided for comparison.

3.3.3 Molecular weight estimates and uncertainty

Using the inferred values of surface tension (Table 14) and assuming an aerosol density of 1.4 g mol^{-1} [204], KTA gives effective organic molecular weights of 162 $\pm$ 28 , 101 $\pm$ 20, 207 $\pm$ 54 g mol^{-1} for terpinolene, 1-methyl cycloheptene, and cycloheptene SOA, respectively (Tables 12 and 15), which are close to (that is within uncertainty of) the estimates from the [72] speciation (Table 10). If water surface tension was used to infer the molecular weight of the organics, large deviations from the [72] speciations would be found (Tables 10 and 12) which includes low molecular weight diacids, carbonyl-containing acids, diacid alkeylsters, and hydroxyl diacids (e.g., pimelic acid, 160 g mol^1; adipic acid, 146 g mol^1; glutaric acid, 132 g mol^1; succinic acid, 118 g mol^1; pimelic acid monomethyl ester, 174 g mol^1; adipic acid monomethyl ester, 160 g mol^1; 2-hydroxypimelic acid, 176 g mol^1; 2-hydroxy glutaric acid, 148 g mol^1; 6-oxohexanoic acid, 130g mol^1 and 6-oxo-7-hydroxyheptanoic acid, 158 g mol^1). This correspondence validates the use of inferred σ values in KTA and to explore the presence of surfactants.

In terms of molar volume uncertainty, the assumption that $\nu_{organic} = 1$, does not account for the partial dissociation of the organic species. The greatest source of uncertainty in the calculations arise from $\nu_{organic}$ (Table 15); $\nu_{organic}$ larger than unity suggests larger molar volumes. The potential dissociation of organics (up to 20% as measured in HULIS titration experiments; [46]), contributes roughly 23% uncertainty to the molar volume estimates. As in previous KTA studies [16, 150], the contributions of σ and ω variability to the inferred molar volume uncertainty are around 10% each. Uncertainty in molar mass (not molar volume) also arises from the value of density; varying from 1.4 g cm^{-3} to 1.6 g cm^{-3}(Turpin and Lim, 2001) increases molar masses by 14%(though relatively small compared to the uncertainty from ν). The total estimated uncertainty in molar mass is approximately 25% for all SOA samples (Table 15).

3.3.4 Droplet growth kinetics

Figure 12 presents the droplet size measurements at the instrument OPC for all supersaturations and samples considered. For all points, the flow rate within the instrument was maintained constant at 0.5 L min^{-1} and the sheath to aerosol ratio is 10:1; this ensures that all the particles were exposed to similar supersaturation profiles. From Fig. 12 we conclude that the droplet growth kinetic curves for all SOA samples are virtually indistinguishable for all s values examined; compared to $(NH_4)_2SO_4$,SOA particles grow to very similar sizes. Only in some cases, does the organic CCN appear to grow slightly larger at higher supersaturations; this is attributed to water depletion effects from the high concentrations of $(NH_4)_2SO_4$ particles within the instrument. Fewer particles of SOA ($\sim$600 cm^{-3}) do not deplete water vapor after activation, while whereas the higher concentration of $(NH_4)_2SO_4$ aerosols ($\sim$1800 cm^{-3}) after their activation deplete vapor faster than can be provided by diffusion. Although this does not affect CCN measurements, the supersaturation profile in the instrument changes slightly for the $(NH_4)_2SO_4$ calibration experiments, and D_p attained at the OPC is slightly decreased. Despite this, almost all of the growth kinetics experiments lie within the measurement uncertainty, so we conclude that the growth kinetics (or water vapor mass transfer coefficient) are uniform and equal to that of $(NH_4)_2SO_4$.

3.4 Summary and implications

In this study, we explore the CCN activity, composition, and droplet growth kinetic characteristics of SOA generated from the ozonolysis of biogenic precursors. A novel method is presented to infer surface tension depression from CCN activation experiments, which requires a much smaller aerosol sample than direct surface tension measurements at CCN-relevant concentrations. From the inferred values of surface tension we conclude that surfactants are likely present in the water-soluble fraction

of the SOA, but with a smaller effect than expected for HULIS; together with the small average molar mass inferred from KTA (100 to 200 g mol^{-1}), this suggests that HULIS are not an important component of the WSOC fraction of the SOA studied here. KTA results are consistent with available composition data when using inferred surface tensions which validate the applicability of the method for complex mixtures. Finally we find that the presence of organic surfactants does not affect droplet growth kinetics; all the SOA samples exhibit growth kinetics similar to that of $(NH_4)_2SO_4$.

Table 10: Characteristics of parent hydrocarbons and water-soluble fraction of SOA.

Hydrocarbon precursor	Cycloheptene	1-methylcycloheptene
O_3 concentration (ppb) for forming SOA	200	171
Major Type of Compounds Identified	Low Molecular Weight Compounds (<250 g mol^{-1}) diacids, carbonyl-containing acids	Low Molecular Weight Compounds (< 250 g mol^{-1})[a] diacids, carbonyl-containing acids
Classes speciated	diacid alkyl esters and hydroxy diacids	diacid alkyl esters and hydroxy diacids[a]
Major slightly soluble organic components identified (< 0.1 g/100 g H_2O)	2 Hydroxy Pimelic Acid [170 g mol^{-1}]	Adipic Acid[a] [146 g mol^{-1}]
	Pimelic Acid [160 g mol^{-1}]	Pimelic Acid[a] [160 g mol^{-1}]
	Adipic Acid [146 g mol^{-1}]	Adipic Acid Monomethyl Ester[a] [160 g mol^{-1}]
		6,7-dioxoheptanoic Acid[a] [158 g mol^{-1}]
Major Soluble Organic Component (> 0.1 g/100 g H_2O)	Glutaric Acid [132 g mol^{-1}]	Glutaric Acid [132 g mol^{-1}][a]
% Low Molecular weight species from total SOA mass derived from DMA measurements	34	44[a]
Number Averaged molecular weight of the speciated components	150	147[a]
Average mass ratio of carbon to organic carbon from speciated components	0.50	0.50[a]

Obtained from [72]

[a] Information obtained from 1-methylcyclohexene ozonolysis due to its structural similarity. Terpinolene SOA is formed in the presence of 188 ppbv O_3. Other information concerning Terpinolene SOA is not available.

Table 11: Summary of WSOC and ion concentrations, α and β parameters of the Szyszkowski -Langmuir isotherm for all SOA considered. Measured Cl-, SO2- 4 and NO-3 concentrations were all below 2.55×10^{-5} mgL^{-1}

Parent Hydrocarbon	WSOC (mg C L^{-1})	α (mN m^{-1}K^{-1})	β^b (L mg^{-1})
Cycloheptene	13	2.59	1×10^{-6}
1-methylcylcoheptene	6	4.82×10^{-5}	4.63×10^{-19}
Terpinolene	10	92.5	1×10^{-13}

Measurements are taken at room temperature between 296 and 299 °K.

Table 12: Köhler Theory Analysis Properties and Molar Volume Results

Property (units)	Cycloheptene	1-methylcylcoheptene	Terpinolene
ω (m$^{1.3}$)	7.14×10^{-14}	5.67×10^{-14}	6.53×10^{-14}
σ (N m^{-1})^c	5.99×10^{-2}	6.52×10^{-2}	6.11×10^{-2}
$\frac{M_o}{\rho_o}$ (m^3 mol^{-1})	1.44×10^{-4}	5.69×10^{-5}	7.54×10^{-5}
M_o(g mol^{-1})^d	207^c (126)^e	101^c (80)^e	162^c (106)^e

^{c} Inferred from activation experiments (Table 14).
^{d} Assuming the density of the solute is assumed to be 1400 kg m^{-3} [204].
^{e} KTA Results based on $\sigma = \sigma_{water}$ (72 mN m^{-1})

Table 13: Formulae for the Sensitivity of Molar Volume to the dependant parameters σ, ω , and ε_o

Property	Sensitivity, $\Phi_x = \frac{\partial}{\partial x}\left(\frac{M_o}{\rho_o}\right)$
σ	$\Phi_\sigma = \left(\frac{3\times256}{27}\left(\frac{M_w}{\rho_w}\right)^2\left(\frac{1}{RT}\right)^3\frac{\sigma^2\omega^{-2}}{\varepsilon_o\upsilon_o}\right)\left(\frac{M_o}{\rho_o}\right)^2$
ω	$\Phi_\omega = \left(\frac{2\times256}{27}\left(\frac{M_w}{\rho_w}\right)^2\left(\frac{1}{RT}\right)^3\frac{\sigma^3\omega^{-3}}{\varepsilon_o\upsilon_o}\right)\left(\frac{M_o}{\rho_o}\right)^2$
ε_o	$\Phi_{\upsilon_o} = \frac{256}{27}\left(\frac{M_w}{\rho_w}\right)^2\left(\frac{1}{RT}\right)^3\frac{-\sigma^3\omega^{-2}\nu_o^{-2}}{\varepsilon_o}\left(\frac{M_o}{\rho_o}\right)^2 + \left(\sum_{i\neq j}\frac{\frac{\rho_i}{M_i}\varepsilon_i\nu_i}{\varepsilon_o}\right)\nu_o^{-2}\left(\frac{M_o}{\rho_o}\right)^2$

Table 14: σ values inferred at the point of activation.

Sample	σ (mN m^{-1})	$\pm\Delta\sigma$ (mN $^{-1}$)
Cycloheptene SOA with 90 % $(NH_4)_2SO_4$	73.6	4.6
Cycloheptene SOA with 33 % $(NH_4)_2SO_4$	59.9	1.9
1-methylcycloheptene SOA with 33 % $(NH_4)_2SO_4$	65.2	2.5
Terpinolene SOA with 98 % $(NH_4)_2SO_4$	74.4	4.9
Terpinolene SOA with 90 % $(NH_4)_2SO_4$	70.5	4.0
Terpinolene SOA with 33 % $(NH_4)_2SO_4$	61.1	7.9

Table 15: Molar Volume Sensitivity Analysis for SOA.

SOA Precursor Hydrocarbon	Property x (units)	Φ_x (m^3 mol^{-1} x^{-1})	Molar volume uncertainty %
Terpinolene			
σ	1.41×10^{-3}	3.73×10^{-3}	7.0
ω	2.21×10^{-15}	2.69×10^{9}	7.9
$\varepsilon_{organic}$	0.20[f]	8.78×10^{-5}	23.3
Total Uncertainty			**26.2**
1-methylcycloheptene			
σ	1.40×10^{-3}	2.76×10^{-3}	6.8
ω	1.90×10^{-15}	2.26×10^{9}	7.5
$\varepsilon_{organic}$	0.20[f]	6.41×10^{-5}	22.5
Total Uncertainty			**25.1**
Cycloheptene			
σ	1.21×10^{-3}	8.34×10^{-3}	7.0
ω	1.58×10^{-15}	4.71×10^{9}	5.2
$\varepsilon_{organic}$	0.20[f]	1.68×10^{-4}	23.3
Total Uncertainty			**26.2**

[f] Error based on observations of 20% disassociation of organic HULIS in titration experiments [46].

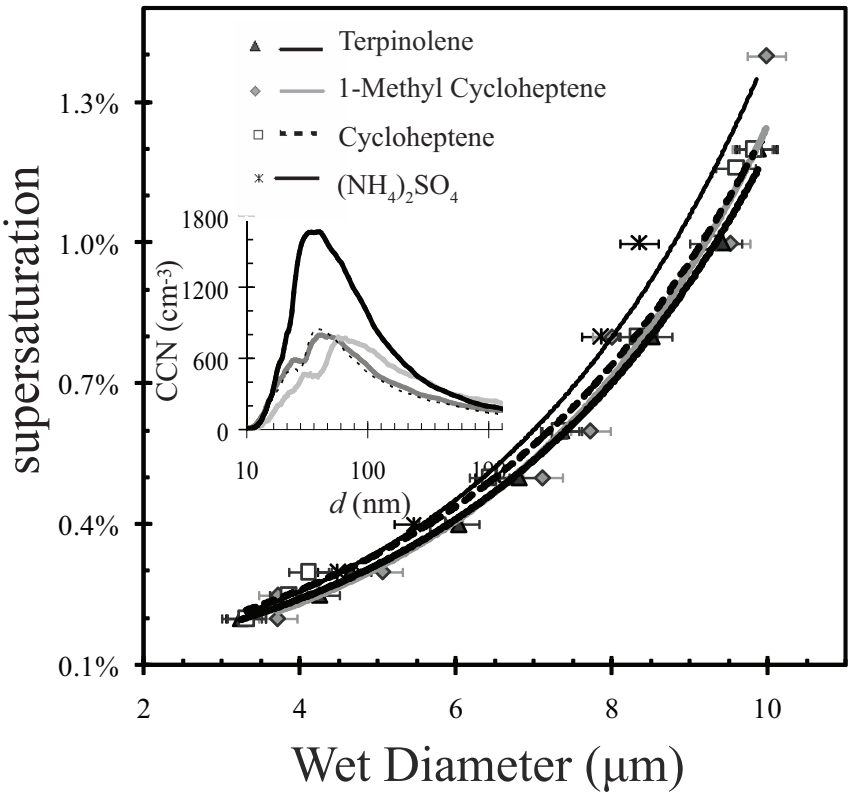

Figure 12: Growth kinetic measurements for water-soluble SOA extract and $(NH_4)_2SO_4$ CCN. Inset graph corresponds to the CCN concentration-dry diameter histogram determined at a 10:1 sheath to aerosol ratio as a function of mean dry diameter at 1% supersaturation.

CHAPTER IV

CCN PROPERTIES OF SESQUITERPENE SOA

This study investigates the droplet formation characteristics of secondary organic aerosol (SOA) formed during the ozonolysis of sesquiterpene β-caryophyllene (with and without hydroxyl radicals present). Emphasis is placed on understanding the role of semi-volatile material on Cloud Condensation Nucleus (CCN) activity and droplet growth kinetics. Results indicate that ageing of β-caryophyllene SOA significantly affects all properties measured throughout the experiments ($\sim$ 11 hours). Using a thermodenuder and two CCN instruments, we find that CCN activity is a strong function of temperature (activation diameter at 0.6%: 100$\pm$10 nm at 20 $^\circ$C and 130$\pm$10 nm at 35 $^\circ$C), suggesting that the hygroscopic fraction of the SOA is volatile. The water-soluble organic carbon (WSOC) is extracted from the SOA and characterized with Köhler Theory Analysis (KTA). The results suggest that the WSOC is composed of low molecular weight ($<$ 200 g mol^{-1}) slightly surface-active material that constitute 5-15% of the SOA mass. These properties are similar to the water-soluble fraction of monoterpene SOA, suggesting that predictive understanding of SOA CCN activity requires knowledge of the WSOC fraction but not its speciation. Droplet growth kinetics of the CCN is found to be strongly anticorrelated with WSOC fraction, suggesting that the insoluble material in the SOA forms a kinetic barrier that delays droplet growth. These results carry very important implications for the atmospheric relevance of CCN measurements and the droplet formation characteristics of SOA.

Note: This chapter appears as reference [9].

4.1 Motivation

The WSOC fraction of CCN may originate from primary emissions or form during the oxidation of volatile organic compounds (VOC) [109, 166, 175]. Natural VOC emissions (e.g., monoterpernes and sesquiterpenes) are estimated to be on the order of 1150 Tg yr^{-1} [84], and are thought to dominate anthropogenic emissions [82, 83, 109]. The resulting SOA can contribute significantly to the atmospheric organic particulate mass [50, 109, 148, 152, 166, 180, 194, 211, **?**] and become more hygroscopic during the ageing process [109, 169] hence contributing significant amounts of WSOC. Relatively little is known about the chemical composition of SOA [167, **?**, **?**]. As a consequence, the CCN-relevant thermodynamic properties (solubility, molecular weight, surfactant characteristics) and droplet growth kinetics of organic aerosol have remained elusive [109].

The hygroscopicity of SOA has been studied for numerous parent hydrocarbons and oxidation conditions [208]. SOA produced from seedless monoterpene ozonolysis, such as α-pinene, has been the focus of numerous studies [55, 97, 172, 155, 206, 210]; most find that the SOA is hygrosocopic and CCN active, but less than $(NH_4)_2SO_4$. [206] showed CCN activity dependence on the monoterpene SOA precursor, whereas [155] and [55] do not; in fact, the latter two studies show that a rather wide variety of monoterpene SOA exhibit very similar CCN properties. Ageing of aerosol is often associated with an increase in hygroscopicity (CCN activity), although this may not always be the case [208, 206]. Decreases in hygroscopicity are often attributed to the formation of oligomers that deplete the SOA from soluble monomers [208, 206]. Polymeric (i.e., high molecular weight) material tends to be less-hygroscopic and nonvolatile [19, 107, 160] and often exhibits characteristics similar to HULIS [19]. If this is the case, humic-like SOA may contain strong surfactants, depressing droplet surface tension and altering growth kinetics [16, 76, 111], both of which may impact droplet number [**?**].

Though not studied to the same extent as monoterpenes, sesquiterpenes are an important class of parent hydrocarbons because of their high aerosol yields [79, 80] and are emitted by more than fourty vegetation species in significant abundance [8, 88, 91, 93, 116, 219]. $\beta-$caryophyllene is one of the most reactive and abundant sesquiterpenes [37, 75, 88, 91, 101]. Due to the high molecular weight (low volatility) of its oxidation products, β-caryophyllene produces high aerosol yields in smog chamber experiments, as large as 70 % [125], and can be an important $PM_{2.5}$ contributor in the Southeastern United States [101]. Speciation data for the aerosol phase can be found in [29], [81], [100], [**?**], [125] and [183]. The main aerosol phase products of dark seedless β-caryophyllene ozonolysis are two semi-volatile ketoaldehydes; 3,3-dimethyl-y-methylene-2-(3-oxo-butyl)-cyclobutanebutanal (β-caryophyllone aldehyde, 236 g mol^{-1}) and 3,3-dimethyl-y-oxo-2- (3-oxobutyl)-cyclobutanebutanal (β-nocaryophyllone aldehyde, 238 g mol^{-1}; [29, 100]). These compounds exhibit low volatility (being thermally stable until $\sim$300 $^{\circ}$C; [29]) and can readily form aerosol. Formaldehyde and its subsequent products were also observed in abundance and are thought to make up $\sim$10% of the product composition in the gas phase [29, 81, 125]. [100] presented the most comprehensive β-caryophyllene ozonolysis speciation so far, identifying 17 compounds in both the gas and aerosol phases for a combined carbon yield of 65%; based on these studies, the mass-average molecular weight of the SOA is estimated to be 250 g mol^{-1} [97].

The aerosol formed during β-caryophyllene ozonolysis can act as CCN [50, 97, 208] yet SOA from sesquiterpenes are less hygroscopic and CCN-active than monoterpene SOA [97, 208]. [208] observed the hygroscopicity of β-caryophyllene SOA to decrease with ageing. Predicting the CCN activity of the SOA requires assumptions for its solubility and surfactant characteristics. [97] used an "effective solubility" (i.e., one common solubility for all compounds present in the SOA), which ranges around 0.10 g g^{-1} H_2O for monoterpene and sesquiterpene SOA; other studies assume complete

solubility of the SOA (e.g., [155]). Surface tension at the point of activation is often assumed to be equal to that of water, although recent studies relax this assumption [28, 55, 182, 14]. Even if the usage of simplifying assumptions for thermodynamic properties (e.g., complete solubility and constant surface tension) reproduce the measured CCN activity, this does not imply that they reflect the true nature of the aerosol [55].

There is currently little work on the link between SOA volatility and CCN activity and the potential effect of semi-volatile organic compounds on aerosol hygroscopicity and CCN properties [6, 19, 105, 109]. The volatility of VOC oxidation products largely control their gas-to-particle partitioning [151], and if water-soluble, their CCN activity. Chamber and ambient studies have measured the volatility for ageing SOA [6, 19, 78, 107], coupled with hygroscopicity measurements [66, 104, 105, 203]. Results suggest that SOA formed by OH oxidation is more volatile than the SOA formed during reactions with other oxidants (e.g., O_3) [105]; non-volatile hygroscopic organic material that forms may resemble the water uptake properties of $(NH_4)_2SO_4$ [66], although the hygroscopic water uptake measured for SOA below water saturation may not accurately reflect their CCN activity [155].

A major issue that is set to be elucidated is the effect of composition on droplet growth kinetics. Complex growth kinetics can arise from numerous mechanisms, such as incomplete solubility [184, 181], slow dissolution kinetics of solute [**?**], and organic films which can potentially decrease α, the "effective" water vapor accommodation coefficient. Values of $\alpha \sim 0.042$ is associated with H_2O uptake coefficients used in earlier cloud modeling studies for inorganic aerosol [123]. More recent aerosol-cloud droplet closure studies show a range of α from 0.04 to 1 [135]. [39], [137], and [70] conducted aerosol-cloud droplet closure using in-situ observations of cumuliform and stratiform clouds formed in polluted and clean air masses; both studies achieved closure for α between 0.03 and 1.0, with optimum estimates (i.e., both average error and

standard deviation within experimental uncertainty) between 0.03 and 0.06. [196], using a static diffusion chamber combined with a model of the instrument estimated α=0.07 for ambient biogenic CCN sampled during the CELTIC experiment. [170] also observed a wide range of growth kinetics for ambient aerosol sampled in sites across the Northern Unites States.

In this study we investigate the droplet formation characteristics of ageing β-caryophyllene SOA generated via seedless dark ozonolysis. Employing two different CCN counters, we comprehensively characterize the CCN activity and droplet kinetics of the SOA, and explore the role of its volatile fraction on droplet formation. From filter samples of SOA obtained during these experiments, surfactant characteristics, molar volumes and droplet growth kinetics of the water-soluble component are determined with Köhler Theory Analysis (KTA) [14, 16, 150]. SOA and WSOC measurements are then combined to infer the soluble fraction of SOA, as well as the impacts of chemical ageing thereon. Finally, we explore the impact of composition (i.e., insoluble fraction) on droplet growth kinetics, by combining the CCN activation measurements with comprehensive models of the CCN instrumentation; growth kinetics is parameterized in terms of an "effective" water vapor uptake coefficient, which is then expressed as a function of WSOC fraction.

4.2 Experimental methods

4.2.1 SOA formation and online measurements

Experiments in this study were conducted in the Carnegie Mellon University 12 m^3 Teflon SOA chamber (Welch Fluorocarbon), suspended inside a temperature-controlled room (Fig. 13). Details of the smog chamber and its operation are reported elsewhere [157, 156, 194]. As shown in Fig. 13, the aerosol from the chamber inlet is classified by a scanning mobility particle sizer (SMPS 3080) and differential mobility analyzer (DMA 3081). The total aerosol concentration (CN) of the monodisperse

particles is counted by a condensation particle counter (TSI CPC 3010) and the CCN concentration is measured by a DH Associates-M1 Static Diffusion (SD) CCN Counter and a DMT Continuous-Flow Streamwise Thermal Gradient (CFSTG) CCN Counter [122, 164]. The SOA was formed in unseeded dark ozonolysis of β-caryophyllene (Fluka $>$ +98.5%). For each dry chamber experiment, oxidation occurred at 22 $^\circ$C at low relative humidity (3-8%); aerosol measurements commenced after the injection of sesquiterpene and lasted up to 11 hours. Table 16 summarizes the initial ozone and sesquiterpene concentrations for particle nucleation in our experiments. 0.5 ml of 2-butanol was used as hydroxyl radical (OH) scavenger so oxidation could occur in the presence and absence of OH (Table 16).

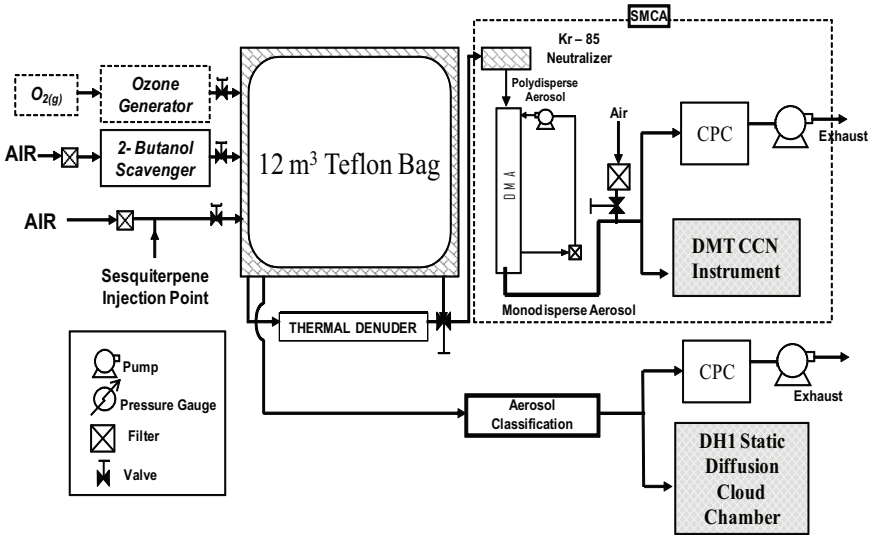

Figure 13: Experimental set-up for SOA generation and online analysis.

Experiment 2 and 6 (Table 16) focused largely on the relationship between volatility and CCN activity. The SOA (formed in the presence of OH) was at times passed through a thermodenuder (TD) at 35 $^\circ$C for $\sim$15 seconds before introduction to aerosol classification and CCN measurements. The temporal conditions in the thermodenuder simulate and closely resemble those in the CFSTGC.

The counting frequency and operating conditions of the two CCN instruments are

very different. The SD CCN counter requires 7.5 minutes per datum (∼0.002 Hz); to capture the impacts of ageing on CCN activity, the SD is operated at 0.60% ± 0.02% supersaturation in experiments 1,2 and 6, and is supplied with 100 nm diameter classified aerosol. Additional experiments (4 and 5) were performed with the SD counter to estimate the activation diameter, d, (i.e., the dry diameter of the aerosol particle with critical supersaturation, s_c). For these experiments, a similar analysis and set-up (not shown here) to that presented in [41] are used. Two classifying systems are employed; the first DMA selects a monodiserpse aerosol, and the second DMA scans several sizes and measures the distrbution of particles. The method uses the activated fraction (CCN/CN) to determine the fraction of particles in each distribution with a diameter greater than d.

The CFSTG is considerably faster (∼1 Hz) than the SD counter, allowing for a comprehensive characterization of size resolved CCN activity using Scanning Mobility CCN Analysis (SMCA) [142] which couples the CFSTG CCN counter with a SMPS. By keeping the CFSTG supersaturation, s, constant during the scanning cycle of the SMPS, we obtain the time series of CN and CCN counts; an inversion procedure then leads to the CCN/CN ratio as a function of dry mobility diameter [142]. This procedure is repeated over multiple supersaturations (e.g., 0.65 % and 1.09 %), giving a characterization of the size-resolved CCN properties for a range of supersaturations every 2.25 minutes. SMCA has been evaluated for calibration, laboratory and ambient aerosol, SOA filter samples, biomass burning aerosol [14, 16, 142, 150] and monoterpene SOA [55].

SMCA also provides size-resolved droplet growth measurements as the DMT CCN counter sizes particles of $D_p > 1$ μm with an optical particle counter (OPC). SOA, when exposed to the same s profile, will grow to the same wet diameter, D_p, provided that the mass transfer coefficient of the water vapor to the growing droplet and the critical supersaturation is the same [141]. The dependence of droplet size on the

supersaturation profile and particle size can then be used to study the impact of organics on the droplet growth kinetics [14, 55, 122, 139, 170]. Changes in growth kinetics are quantified by *i*) comparison against the droplet size attained by CCN composed of pure $(NH_4)_2SO_4$, and, *ii*) using comprehensive models of the instruments to infer growth kinetic parameters of the SOA.

4.2.2 Characterizing the water-soluble fraction of SOA

$\beta-$caryophyllene SOA oxidized in the presence of OH and O_3 (Table 16) was collected on a Teflon filter and subsequently used to characterize the properties of its water-soluble organic carbon (WSOC) fraction. The WSOC in the filter samples was extracted with 20 ml of ultra-pure water (18 Mohms) during a 1.5 hour sonication process with heat (bath water temperature $\sim 60\,^{\circ}$C;)[14, 16, 199]. The WSOC concentration was measured with a Total Organic Carbon (TOC) Turbo Siever analyzer [199] and found to be 10.8 μg C mL^{-1}. The extracted sample is subsequently atomized, dried, size selected, and characterized for its CCN activity (following the procedure of [14]) using SMCA between 0.2 and 1.4% supersaturation. This procedure is repeated for pure WSOC and mixture with $(NH_4)_2SO_4$ using the procedure of [14]. The composition of the salted mixtures are verified with ion chromatography (IC) analysis. Köhler Theory Analysis (KTA) combined with the CCN activity measurements, are used to infer the molecular weight, surface tension [14, 150, 139], and droplet growth kinetic characteristics [14].

The concentration of WSOC extracted from filter samples is often too low ($\sim$100 mg L^{-1}) to have a measurable impact on surface tension; σ measurements relevant for CCN activation need to be obtained at much higher WSOC concentrations (>500 mg C L^{-1}) [14]. Although concentrating these solutions is possible [16], obtaining the required volume of organic sample is often impractical [14]. It is possible, however, to infer the surfactant characteristics of the SOA from the CCN activity of pure WSOC

and mixtures with $(NH_4)_2SO_4$, following the procedure of [14] and [139]

4.3 Data Analysis

4.3.1 Köhler theory analysis of WSOC

Köhler Theory Analysis (KTA), (method b_1) [16, 150] is used to infer the average molar volume (molecular weight, M_o, over density, ρ_o) of the water-soluble organic fraction. KTA employs measurements of the activation diameter, d, to obtain a Fitted CCN Activity (FCA) factor, ω, as $s_c = \omega d^{-3/2}$. If the organic is assumed to be composed of a soluble and insoluble organic fraction, FCA can be used to infer the average organic molar volume, $\frac{M_o}{\rho_o}$, as

$$\frac{M_o}{\rho_o} = \frac{\varepsilon \nu_o}{\frac{256}{27}\left(\frac{M_w}{\rho_w}\right)^2\left(\frac{1}{RT}\right)^3 \sigma^3 \omega^{-2}} \tag{21}$$

where R is the universal gas constant, T is droplet temperature. M_w and ρ_w are the molecular weight and density of water, respectively, ε is the soluble fraction, and σ is the surface tension of the droplet at the point of activation (Section 4.3.2). For aerosol composed solely of WSOC, we assume that $\varepsilon = 1$, and the organic effective van't Hoff factor, $\nu_o = 1$.

$\frac{M_o}{\rho_o}$ is computed for each s_c, d point and an average value is obtained. The average molecular weight, M_o, is then computed by assuming an average organic density of 1500 kg m^{-3} [117]. The standard deviation in $\frac{M_o}{\rho_o}$ is then compared against the estimated molar volume uncertainty, $\Delta\left(\frac{M_o}{\rho_o}\right) = \sqrt{\sum_x \left(\Phi_x \Delta x\right)^2}$, where Δx is the uncertainty of each of the measured parameters x, (i.e., any of σ, ω, and ν) and Φ_x is the sensitivity of molar volume to x, $\Phi_x = \frac{\partial}{\partial x}\left(\frac{M_o}{\rho_o}\right)$ (Table 17)[150, 14, 16].

KTA, when applied to organic aerosol of known composition, has been shown to yield organic molar volumes to within 20% [150]. KTA has also been applied to biomass burning aerosol [16], WSOC from alkene ozonolysis [14] and marine organic matter [139], where inferred σ was in agreement with direct measurements using the

pendant drop technique. KTA has also been used to infer the soluble fraction and the molecular weights of water-soluble components of monoterpene SOA [55].

4.3.2 Inferring Surface Tension

If CCN activity data is available for mixtures of WSOC and a salt (e.g., $(NH_4)_2SO_4$), KTA can be used to concurrently infer $\frac{M_o}{\rho_o}$ and σ (as a function of WSOC concentration) using an iterative procedure [139]. However, if enough salt is present in the sample, the contribution of organic solute is negligible; the effect of the organic on CCN activity amounts to its impact on surface tension, and can be inferred as [14],

$$\sigma = \sigma_w \left(\frac{s_c}{s_c^*} \right)^{2/3} \tag{22}$$

where s_c is the measured critical supersaturation, and s_c^* is the predicted value (from Köhler theory), assuming $\sigma = \sigma_w$, the surface tension of pure water computed at the average CFSTGC column temperature [14],

$$s_c^* = \frac{2}{3} \left(\frac{4 M_w \sigma_w}{RT \rho_w} \right)^{1.5} \left(\frac{3 \varepsilon_i \nu_i \rho_i M_w d^3}{M_i \rho_w} \right)^{-0.5} \tag{23}$$

where the subscript i denotes the inorganic salt properties. In this study, both methods are applied to infer σ as a function of carbon concentration.

4.3.3 Inferring the WSOC fraction in the SOA

The SOA formed during the ozonolysis can to first order be described as a mixture of a water-soluble and insoluble fractions. Assuming the extracted WSOC (Sect. 4.3.1) is similar to the soluble fraction of SOA, we can use the M_o and σ of the WSOC estimated by KTA (Sect. 4.3.1) to infer the ε for the SOA. This is done by solving Eq. 21 for ε,

$$\varepsilon = \frac{256}{27} \left(\frac{M_w}{\rho_w RT} \right)^3 \left(\frac{M_o}{\rho_o} \right) \left(\frac{\rho_w}{M_w} \right) \frac{\sigma^3 \omega^{-2}}{\nu_o} \tag{24}$$

4.3.4 Quantifying the droplet growth kinetics

The extent to which droplets grow in each instrument depends on the supersaturation profile, residence time, droplet growth kinetic behavior, and to a lesser degree, dry particle size [141]. We quantitatively describe the growth of SOA by simulating the process of droplet formation within each CCN counter using comprehensive computational fluid dynamic models: the SD chamber model of [141], and, the DMT CFSTGC model of [122]. Each of these models numerically simulates the temporal and spatial distributions of velocity, pressure, temperature and water vapor concentration throughout the growth chamber of each instrument (the particle and gas phases are coupled through release of latent heat and condensational loss of water vapor); the fields are then used to drive the condensation growth of a population of aerosol as it flows through the instrument. The kinetic model includes aerosol with size-dependant composition; condensation growth of aerosol is computed based on a size-dependant mass transfer coefficient [141] multiplied by the difference between gas-phase and equilibrium water vapor pressure. The latter is calculated with a comprehensive implementation of Köhler theory that accounts for multicomponent aerosol consisting of soluble, partially soluble and insoluble material. Organic surfactants can be present in any of these fractions.

The CCN models were initialized using the appropriate geometric dimensions and operating conditions of each CCN instrument (Sect. 4.2.1). A computational grid of 200 cells in the radial and 200 cells in the axial direction was used in each simulation; condensational growth and gravitational settling in the SD simulations commences after steady state is established for all gas-phase profiles. In CFSTGC simulations, the droplet diameter at the exit of the flow chamber is then compared against the measured size distribution, following the binning scheme used in the optical detection of the instrument [122]. Particles with diameter larger than 2 μm are counted as droplets in the SD simulations. Organics are allowed to affect the growth kinetics of

CCN, by modifying surface tension, equilibrium vapor pressure and the water uptake coefficient used to compute the water-vapor mass transfer coefficient [141, 122].

4.4 Results and Discussion

4.4.1 CCN activity of SOA

Figure 14 presents the CCN activity of 100 nm SOA particles (formed with and without OH), concurrently measured by the SD and CFSTG at $\sim 0.6\%$ supersaturation in experiments 1 and 2 and by the SD in experiment 6 (Table 16). CCN activity is presented in terms of an activated fraction, the ratio of CCN/CN. The gradual increase in CCN activity suggests active chemical ageing of the aerosol; this is in agreement with [50], although it is unclear if it is from oxidation in the gas or aerosol phase. Although both CCN instruments show an increase of activity with ageing, the magnitudes and trends of the activated fractions are remarkably different. First SOA formed in experiment 1 without OH appears more CCN active in the SD counter than SOA formed with OH oxidation in experiment 2, whereas the CFSTG measurements show the opposite. Secondly, according to the SD counter SOA ages more rapidly (i.e., CCN/CN has a larger slope) than the CFSTG data; the SD aerosol ages at a rate of 0.10 and 0.07 CCN/CN hr^{-1} for SOA formed without and in the presence of OH, respectively. Applying the same linear trend, the CFSTG counter ages at a rate of 0.02 and 0.04 CCN/CN hr^{-1} for SOA formed without and in the presence of OH, respectively. Finally, CCN are immediately measured in the SD, while up to 6 hours are required to register the first CCN counts in the CFSTGC (Figures 14,15). The discrepancy in measured CCN activity is most likely not an experimental artifact, as both instruments agree very well for calibration $(NH_4)_2SO_4$ and monoterpene SOA [55]. We postulate that β-caryophyllene SOA (at least the hygroscopic component) partially evaporates in the CFSTGC, given that it is operated at $\sim$10 $^\circ$C above the chamber temperature. Conversely, vapors may be condensing onto the CCN in the

SD (given that particles are exposed to supersaturation at ∼1 ° C below the chamber temperature), thus affecting the measured CCN properties of the aerosol. If true, this suggests that the hygroscopic fraction from the b-caryophyllene SOA formed during the reaction with O_3 tends to be more volatile than the hygroscopic SOA formed during the reaction with OH. The SD counter results in experimetns 1 and 2 also suggest that the ozonolysis products are better CCN than the products of OH reaction.

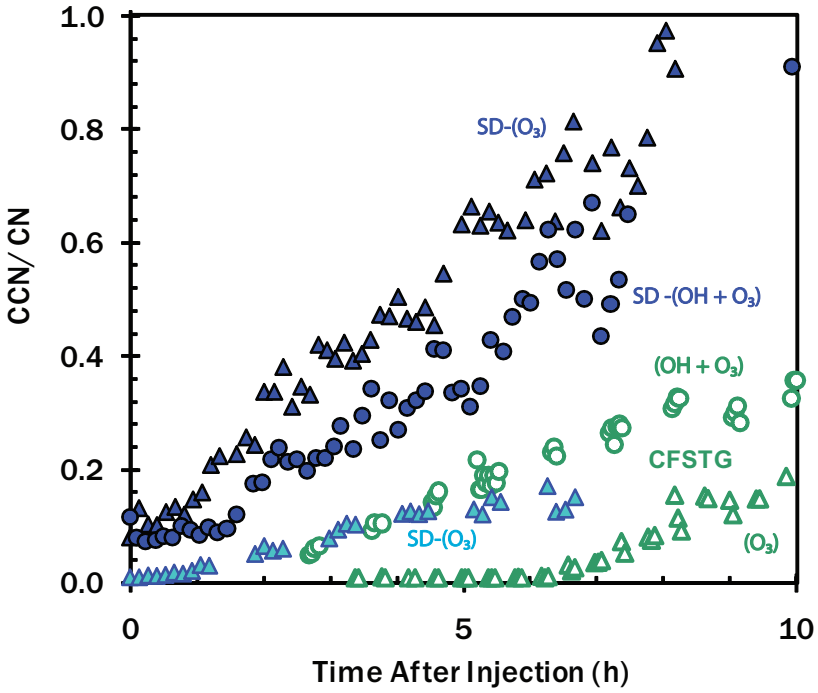

Figure 14: CCN activity (at ∼0.6% supersaturation) of 100 nm β-caryophyllene SOA formed in the presence of OH (circles) and without OH (triangles). Data obtained using the CFSTG and SD CCN counters are presented.

Similar behavior also seen at higher supersaturations; Figure 15 is similar to Figure 14, but the CFSTGC is operated at 1.09% supersaturation. Consistently with Figure 14, the SOA significantly age over time, and SOA formed in the absence of OH requires a very long time (≃4 hours) before any CCN counts are registered; SOA formed in the presence of OH form CCN almost immediately. The CCN/CN tends to exhibit a sigmoidal shape with time, unlike the data in Figure 14 where trends

exhibit a more linear dependence with time.

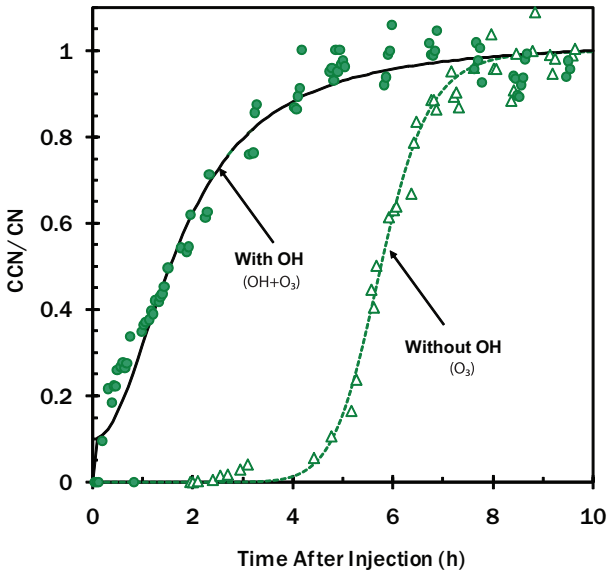

Figure 15: CCN activity of 100 nm β-caryophyllene SOA formed in the presence of OH (circles) and without OH (triangles). Measurements are obtained with the CFSTGC at 1.09% supersaturation.

4.4.1.1 Understanding the CCN activity

To characterize the time-dependant CCN behavior, SMCA is applied to SOA formed in the absence of OH at ∼1% supersaturation passed through the denuder and also for SOA of both types at ∼1% and ∼0.6% (Fig. 16). In these measurements, CCN activity is quantified by the activation diameter, d, defined as the size of particles with s_c equal to the instrument supersaturation; this is determined by the dry aerosol diameter for which CCN/CN=0.5. d is determined for measurements with the SD in experiments 4 and 5 using the methods of [41] (Sect. 4.2.1).

In the absence of OH, the SD counter initially measures $d \simeq 102$ nm at $s = 0.6\%$ and decreases gradually with time at a rate of -0.94 nm hr^{-1}. In the absence of OH, the CFSTGC cannot determine d within the first five hours due to insufficient CCN counts ($<$ 10 CCN cm^{-3}). Compared to the SD, the slope of d with time in

the CFSTGC is three times larger, suggesting that the volatility of the hygroscopic material in each SOA type may change with time. Beyond the sixth hour, the CCN activity of CFSTGC measurements (i.e., d) for both types of SOA (with and without OH oxidation in experiments 1 and 2) agree to within 5%, suggesting that the oxidized products of both SOA types become similar (Fig. 16). The consistency between aerosol types is supported by the measurements of [183], who suggested the addition of OH scavenger does not significantly affect the product distribution because only a small amount ($\sim$6% yield) of OH is formed during β-caryophyllene reaction with O_3. The CFSTGC measurements support this, as CCN activity for both SOA types agree to within 5% uncertainity at 0.6% supersaturation.

To verify that aerosol volatility accounts for the differences seen in the CCN activity between instruments, we pass the most volatile SOA (i.e., formed with OH absent) through a thermodenuder before introduction into the CFSTGC. SMCA is applied to measurements at 0.65% and 1.09% supersaturation; however, the lack of CCN counts at the lower supersaturation prohibits the determination of d. For similar reasons, the CCN activity of denuded SOA at 1.09% can not be determined during the first five hours of the experiment (Fig. 16); compared to the SOA, d is much larger ($\sim$25%) for the denuded aerosol . This suggests that the non-volatile aerosol exiting the thermodenuder is less CCN-active than the semi-volatile material, and that the latter is primarily responsible for the observed CCN activity of freshly formed SOA.

Since the CFSTGC is operated at conditions similar to the thermodenuder, some of the soluble material will evaporate in the CCN instrument and exhibit reduced CCN activity. In the SD instrument however, particles are exposed to supersaturation at one degree below chamber temperature (because the temperature difference between plates is 2$\sim$1 $^\circ$C, and s_{max} in the instrument is located halfway between plates. It is therefore expected that the SD measurements reflect the CCN activity of the particles in the SOA chamber, and any additional condensation of SOA in the SD chamber

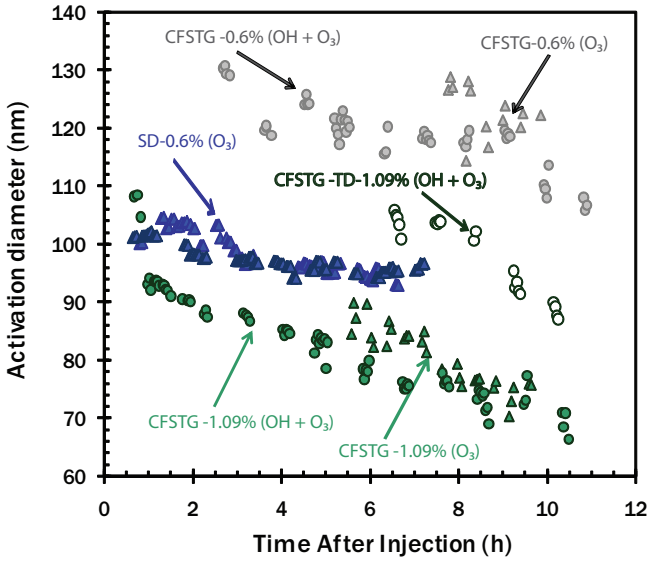

Figure 16: Activation diameter as a function of time, for β-caryophyllene SOA formed in the presence of OH (circles) and SOA formed without OH (triangles); CFSTG 1.09% supersaturation (green symbols), SD 0.6% supersaturation (blue symbols) and CFSTG 0.6% supersaturation (grey symbols) measurements are shown. Aerosol passed through the thermodenuder and exposed to 1.09% supersaturation in the CFSTGC are denoted by open green symbols. Assuming a linear dependence, the rate of decrease with d is -0.94, -2.8, -3.6, -4.6, -2.0, -2.6 nm hr^{-1}, for the SD-0.6% (O_3), CFSTG-1.09% (OH + O_3), CFSTG-1.09% (O_3), CFSTG-TD-1.09% (OH + O_3), CFSTG-0.6% (O_3)and CFSTG-0.6% (OH + O_3)respectively.

(because of the 1 degree difference) will have a minor impact on composition and CCN activity. The possibility that the SOA experiences significant kinetic limitations, enough to prohibit their activation in the CFSTGC within the measurement time frame (10-30s), is unlikely since the timescale of CCN activation in the SD is less than 5 s (Section 4.4.4).

The original SOA contains more hygroscopic material, as seen from the enhanced CCN activity (compared to CFSTGC measurments) at 0.6% (Fig. 16). Minor differences in CCN activity are seen between SOA from O3, and, O3+OH oxidation; this is seen in the SD measurements, as a smaller difference in CCN activity is observed

between the two SOA aerosol types (Fig. 14). After sufficient aging has occurred, the volatility of organic components may decrease enough for CCN activity measurements from the SD and CFSTGC to converge; this was not seen however over the duration of the experiments.

4.4.2 Characterization of the hygroscopic fraction

Figure 17 displays the s_c vs. d for β-caryophyllene SOA and WSOC. For comparison, we also present data for WSOC extracted from monoterpene SOA [55] and $(NH_4)_2SO_4$. The results show that aerosol generated from β-caryophyllene WSOC are more CCN-active than the original SOA, but less CCN active than $(NH_4)_2SO_4$. In fact, the CCN activity of WSOC from oxidation of monoterpenes and β-caryophyllene is remarkably similar. Gas Chromatography- Mass Spectrometry (GC-MS) analysis of the β-caryophyllene sample exclude the presence of monoterpenes; hence similarity of WSOC properties is not an experimental artifact but an inherent property of the WSOC. Despite this, the CCN activity of monoterpene and β-caryophyllene SOA is substantially different (the latter being less hygroscopic) [97, 55], suggesting that the WSOC fraction in sesquiterpene SOA is less than in monoterpene SOA.

The molecular weight of the WSOC fraction is estimated with KTA from the non-salted data set; a summary of the values employed in the analysis are summarized in Table 18. The average molecular weight of the WSOC was found to be 156 $\pm$ 44 g mol^{-1} (Tables 18, 20). This degree of WSOC CCN activity is similar to dicarboxylic organic species that are moderately surface active and of low ($<$ 200 g mol^{-1}) molecular weight (e.g. adipic acid, 146 g mol^{-1}; succinic acid 118 g mol^{-1}) [92, 150, 159] The molar volume uncertainty is estimated to be $\sim$ 25% (Table 20) and is consistent with the observed variability in the inferred $\frac{M_o}{\rho_o}$.

Low molecular weight species in the range of the KTA estimates have been identified in β-caryophllene SOA. [100] identify 3,3-dimethyl-2-(3-oxobutyl)-cyclobutane-methanal and 3,3-dimethyl-2-ethanal-cyclobutane, of molecular weight 192 and 154 g mol^{-1}, respectively in the aerosol phase. [125] using proton transfer reaction mass spectrometry (PTR-MS) measure several unknown compounds of mass charge ratio (m/z) < 250. In particular, [125] identify a compound with m/z $= 159$ in the ambient and laboratory experiments of β-caryophllene. Our WSOC analysis is derived from significantly aged ($\sim$ 12 hour) filter samples. As a result, more condensed species may form in the aerosol, including oligomers from formaldehyde (31 g mol^{-1}) that is in abundance in the gas phase [29, 100, 125] may be a source of low molecular weight oxidized products in the aerosol phase.

Addition of $(NH_4)_2SO_4$ to the WSOC mixture could produce better CCN than using pure $(NH_4)_2SO_4$ alone, if the organics depress surface tension. This is indeed the case, and shown in Figure 17b; the activation curve of the 92% aerosol should lie notably to the right of the pure $(NH_4)_2SO_4$. Instead, the organics (present in $\sim$10%) depress surface tension (by $\sim$5%, Table 19) so that the mixture behaves like pure $(NH_4)_2SO_4$. Similar CCN enhancement from surface tension depression is also seen in monoterpene and marine WSOC [55, 139], suggesting that this may be a robust characteristic of CCN containing water-soluble organics.

4.4.3 Estimating SOA Soluble Fraction

Once the surface tension and average molar volume of the WSOC is estimated from KTA, its volume fraction, ε, in the SOA can be inferred by applying Eq. 24 to the online CCN activation data. The results of this calculation is shown in Figure 18a, where ε is plotted against time for all the experimental data of Figure 16. CCN activity is only observed when sufficient amounts ($\varepsilon > 0.03$) of soluble non-volatile material exist in the aerosol phase (Figs. 16 and 18). Figure 18a suggests that

ε is minimum for aerosol processed in the thermodenuder, since that is when d is maximum (Figure 16), and is consistent with the hypothesis of volatile WSOC.

Analyzing the inferred ε trend over time (Fig. 18a) yields some very interesting aspects of the SOA ageing process. Early on in the experiment (0-5 h), the ε inferred from the CFSTGC 0.65% and 1.09% datasets is almost identical; this is consistent with the SOA being initially of uniform composition (and also confirms that the method to infer ε gives consistent results across a wide range of operation conditions and experiments). Later on in the experiment (5-11 h), ε between the two supersaturations diverge; the 1.09% dataset tends to infer a larger ε than for the 0.6%. This is consistent with size-dependant processing of the aerosol in the chamber; smaller particles (i.e., those with s_c=1.09%) would tend to age more quickly than larger particles (i.e., those with s_c=0.6%), because of differences in their surface-to-volume ratio. It is unclear however if this ageing is from the condensation of gas-phase species, or chemical ageing of material inside the aerosol.

Figure 18b presents the sensitivity of ε to the value of $\frac{M_o}{\rho_o}$ and σ used in Eq. 24; despite the large variation considered in aerosol properties, ε does not exceed 15%, supporting the postulation that the hygroscopic material mostly resides in the volatile fraction, and is present in small amounts in the aerosol. Because of the latter, any volatilization of the soluble fraction would have a strong impact on CCN activity.

4.4.4 Composition and Droplet Growth Kinetics

Figure 19 shows that more than six hours of ageing are required before the SOA with s_c=1.09% can grow to droplet sizes similar to those of $(NH_4)_2SO_4$; even more time is required for particles with s_c=0.65%. Since we evaluate the droplet growth kinetics by comparing the measured droplet sizes for particles with similar s_c, differences in the SOA and $(NH_4)_2SO_4$ Köhler curves do not account for the observed large droplet size difference. Combining the data in Figures 18 and 19 suggest that the SOA droplet

growth kinetics accelerate as ε increases, suggesting that *i*) the insoluble material may somehow form surface films that can delay growth, and, *ii*) the chemical ageing of the aerosol (expressed as an increase in ε) eventually diminishes the extent of this delay.

Figure 20 presents droplet sizes of WSOC (pure and mixed with $(NH_4)_2SO_4$) as a function of s_c. For comparison, droplet sizes for pure $(NH_4)_2SO_4$ and SOA CCN are presented. The WSOC (pure and salted) behave much like $(NH_4)_2SO_4$, as the wet diameters for all samples are within one size bin (0.5 μm) of the OPC sizing. This, combined with the marked delay in growth of SOA CCN (Figure 19) strongly suggests that the source of kinetic limitations in the latter arises from the "insoluble" component of the SOA.

To compare the observed droplet growth kinetics in both CCN counters, we derive the α from the simulations of the activation of CCN in each instrument. Figure 21 shows the simulated normalized droplet concentration in the viewvolume of the SD (used for determining the CCN concentration), as a function of time and α. The simulations suggest that α strongly influences the timing, but not the value, of peak droplet concentration; we therefore use the timing where the peak concentration is obtained to constrain α in the SD CCN measurements. The droplet formation timescale in the viewvolume was measured 4h (3.70 $\pm$ 0.60 s) and 8h (3.32 $\pm$ 0.50 s) into the experiments, and are shown as dotted lines in Figure 21; simulations suggest that the SOA water vapor uptake coefficient is low early on ($\alpha \sim 0.03$) and increases to values consistent with $(NH_4)_2SO_4$ (2.23 $\pm$ 0.19 s) and hydrophilic (monoterpene) SOA. These shifts are mostly outside the uncertainty of the droplet formation timescale measurements. Lower values of α are highly unlikely, since the timing difference in the peak concentration becomes very large (Fig. 21.

Figure 22a shows the simulated droplet size at the exit of the CFSTGC column as a function of α for CCN with s_c=1.09% (blue) and 0.65% (magenta). The size of

activated calibration $(NH_4)_2SO_4$ with corresponding critical supersaturations is also shown; simulations suggest that the α for $(NH_4)_2SO_4$ particles ranges between 0.04 and 0.06, which is consistent with the SD simulations for activation of $(NH_4)_2SO_4$ aerosol.

The simulations of Figure 22a are combined with the droplet size data of Figure 19 to infer the water vapor uptake coefficient for the activated SOA in the CFSTGC; this is shown in Figure 22b. Compared to the SD, growth kinetics in the CFSTGC (i.e., values of α) are substantially slower, with the following characteristics: *i*) aerosol thermally treated in the denuder exhibits the slowest growth, with 4 times lower α than $(NH_4)_2SO_4$, *ii*) aerosol that is not pretreated in the denuder exhibits slow growth kinetics early on in the experiment. Ageing gradually accelerates growth, until it reaches the levels of ammonium sulfate after 10 hours of ageing, and, *iii*) the growth at s_c=0.65% is slower than particles with s_c=1.09% and takes longer to reach the growth rate of $(NH_4)_2SO_4$.

The diverse range of uptake coefficients inferred for CCN in both instruments may at first seem counterintuitive, but is consistent with thermal structuring and processing of the SOA in the CFSTGC and denuder. Modification of CCN can happen in many ways; for example, evaporation of hygroscopic volatile compounds, preferentially from the surface layers of the aerosol (chemical reactions are presumed not to happen during the residence time in the instrument and denuder), and, sintering of insoluble material, especially if it exhibits "waxy" characteristics (i.e., changes viscosity in the 25-35 $^\circ$C range). In both cases, a "barrier" of insoluble and hydrophobic material could form between the hydroscopic fraction of the SOA, which would then decrease the growth rates of the activated CCN. The available data seems to support the above because:

1. aerosol processed in the denuder exhibits the slowest growth (evaporates the most hygroscopic material, and has the largest residence time at high T, hence

has best chance to reform the SOA surface).

2. CFSTGC data at 0.65% is growing slightly more than the denuded aerosol, because of the lower residence time at high temperature; less material evaporates and CCN surface layer is modified to a lesser degree.

3. CFSTGC data at 1.09% grows the fastest, because the WSOC fraction is higher, and, given that those particles are smaller (compared to those with s_c=0.65%), the amount of insoluble material (hence kinetic barrier) is much less and the aerosol establishes "rapid growth" kinetics towards the end of the experiment.

4. The SD is closest to activating CCN in their "native" state (i.e., as produced in the SOA chamber). This means that hygroscopic material (being secondary and semivolatile) would tend to be located at the surface layers of the aerosol, and growth kinetics would tend to be fast (i.e., α would approach that of $(NH_4)_2SO_4$). The growth kinetics measurements for the WSOC (Figure 20) and for very hygroscopic (e.g., monoterpene) SOA support this [55].

The activation of CCN in the CFSTGC can be kinetically limited for other reasons than proposed above. Limitations from dissolution kinetics of soluble material in the CCN [**?**] is unlikely, given that solute diffusivity (hence growth kinetics) should be faster at higher temperatures, contrary to what is seen in our experiments. Condensation/dissolution of material from the gas phase is also possible, but also unlikely, because the denuded aerosol would be expected to exhibit faster growth kinetics. Chemical reactions are also a possibility, but cannot be explore using the information available.

If volatilization of hygroscopic material (or sintering of insolubles) is responsible for the variability seen in droplet growth kinetics, a common scaling law could be derived between α and the amount of insoluble material in the particle (i.e., ε). Indeed, this is the case (Figure 23); the correlation between the quantities is quite

striking and clearly shows an explicit relationship between composition and growth kinetics.

4.5 Implications-Conclusions

A combination of theory with measurements of CCN activity, droplet growth kinetics and volatility provides a unique insight on the droplet formation characteristics of β-caryophyllene SOA. We find that the resulting CCN contain small amounts of hygroscopic material; hence, even if sesquiterpenes have higher aerosol yields than monoterpenes, they are less CCN-active. From our KTA estimates, the WSOC constitute roughly 10% of the SOA mass, moderately depresss surface tension and is composed (on average) of low molecular weight compounds (< 250 g mol^{-1}). Remarkably, these properties are similar to water-soluble organic carbon extracted from monoterpene oxidation (although the soluble volume fraction is much higher, between 70% and 100%, [55]). This suggests that WSOC in biogenic SOA may have similar CCN properties (solubility, molecular weight and surfactant characteristics), and that differences in the CCN activity of SOA from different parent hydrocarbons may be primarily arise from the WSOC mass fraction; if true, this can constitute the bases for a simple and mechanistically-based approach to represent the CCN activity of SOA as a function of atmospheric age.

A major finding of this study is that the hygroscopic material in β-caryophyllene SOA is volatile. The implications for CCN measurements are very important; the temperature at which CCN measurements are carried out, if the aerosol is volatile and composed of a low fraction of soluble material, may strongly affect the observed CCN activity. In our study, this bias shifted activation diameters between 25 and 30 %. Nevertheless, this problem can be identified and quantified if the aerosol is periodically passed through a thermodenuder, or, if CCN measurements are undertaken at different temperatures. The volatility of WSOC carries important implications for

atmospheric processes; since the temperature range in our measurements are typical of diurnal variations found during summertime conditions (where biogenic emissions and photochemical activity, hence SOA production, are maximum), volatilization of small amounts of aerosol may induce an unanticipated diurnal cycle of CCN activity.

Another major finding of this study is that the less volatile material in sesquiterpene SOA is not very hygroscopic, but can have a profound impact on CCN growth kinetics. The degree of kinetic limitations depend on the volume fraction of insoluble material in the SOA, and heating of the aerosol tends to decrease the droplet growth rates of the CCN. We postulate this to be result of soluble material evaporating from the surface of the SOA, potentially combined with redistribution (sintering) of "waxy" material to the CCN surface; both mechanisms would create a kinetic barrier that partially impedes water vapor condensation. An explicit relationship between the water vapor uptake coefficient (used here to represent variations in droplet growth kinetics) and WSOC fraction supports that one mechanism (that scales with particle volume) may primarily be responsible for delaying growth and that it is from the presence of insoluble material. The implications of these findings for cloud droplet formation are many: *i*) similar to CCN activity, a diurnal cycle of growth kinetics for biogenic aerosol may exist, with profound impacts on the droplet size distribution and aerosol-cloud interactions, *ii*) the concept of "external mixing" may not be only important for CCN activity (i.e., s_c), but also for droplet growth kinetics, *iii*) redistribution of SOA in the dry, free troposphere (which could partially evaporate SOA from dilution) would tend to form particles that are kinetically limited, and, *iv*) SOA systems with high soluble fractions (e.g., monoterpene SOA) may grow as quickly as inorganic salt CCN (e.g., $(NH_4)_2SO_4$), which is consistent with the limited data available to date [55]. Whether a simple relationship between α and ε exists in other SOA systems still remains to be found, but the approach outlined in this study could be the basis of parameterizing the elusive relationship between volatility, CCN

activity, growth kinetics and composition.

Table 16: Experimental conditions for the generation of β-caryophyllene SOA.

Experiment Number, Name	β-caryophyllene Concentration (ppb)	O_3 Concentration (ppb)	2–Butanol Present?	Oxidizing Agent	TD Used?	Peak SOA Mass (μg cm^{-3})	CCN Counter
1,without OH	22	300	Yes	O_3	No	27	SD, CFSTG
2,with OH	28	300	No	O_3 + OH	Yes	31.8	SD, CFSTG
3,with OH, filter collection	28	300	Yes	O_3	No	49.8	CFSTG
4,without OH	22	300	Yes	O_3	No	DNA	SD
5,without OH	32	300	Yes	O_3	No	DNA	SD
6,without OH	22	300	Yes	O_3	Yes	70	SD

DNA = Data Not Available

Table 17: Formulae for the sensitivity of $\frac{M_o}{\rho_o}$ to the dependant KTA parameters for β-caryophyllene experiments. These are applied for WSOC aerosol, where ε=1 and no inorganics are present.

Property	Sensitivity, $\Phi_x = \frac{\partial}{\partial x}\left(\frac{M_o}{\rho_o}\right)$
σ	$\Phi_\sigma = \left(\frac{3\times256}{27}\left(\frac{M_w}{\rho_w}\right)^2\left(\frac{1}{RT}\right)^3\frac{\sigma^2\omega^{-2}}{\upsilon_o}\right)\left(\frac{M_o}{\rho_o}\right)^2$
ω	$\Phi_\omega = \left(\frac{2\times256}{27}\left(\frac{M_w}{\rho_w}\right)^2\left(\frac{1}{RT}\right)^3\frac{\sigma^3\omega^{-3}}{\upsilon_o}\right)\left(\frac{M_o}{\rho_o}\right)^2$
ν_o	$\Phi_{\upsilon_o} = \frac{256}{27}\left(\frac{M_w}{\rho_w}\right)^2\left(\frac{1}{RT}\right)^3\left(\frac{M_o}{\rho_o}\right)^2\sigma^{-3}\omega^{-2}\nu_o^{-2}$

Table 18: Köhler Theory Analysis parameters and molar volume results for the water-soluble fraction of β-caryophyllene SOA.

Property (units)	Value
FCA, ω ($m^{1.5}$)	6.86×10^{-14}
σ (N m^{-1})	6.56×10^{-2}
$\left(\frac{M_o}{\rho_o}\right)$ (m^3 mol^{-1})	1.04×10^{-4}
M_o (g mol^{-1})[1]	156 ± 44

[1] ρ_s= 1500 kg m^{-3} [**?**]

Table 19: Average σ values inferred at the point of activation.

Sample Characteristics	σ (mN m^{-1})	$\pm\Delta\sigma$ (mN m^{-1})
WSOC with 96% $(NH_4)_2SO_4$	67.6	2.1
WSOC with 92% $(NH_4)_2SO_4$	65.6	2.1
WSOC with 64% $(NH_4)_2SO_4$	68.1	2.6
WSOC with 41% $(NH_4)_2SO_4$	67.8	1.6

Table 20: WSOC molar volume uncertainty analysis

Property x (units)	Δx	Φ_x (m^3 mol^{-1} x^{-1})	Molar Volume uncertainty %
σ	1.32×10^{-3}	4.62×10^{-3}	7.0
ω	1.01×10^{-15}	3.21×10^{9}	3.4
ν_o	0.20 [2]	1.02×10^{-4}	23.4
Total Uncertainty			24.8

[2]based on up to 20% disassociation observed for HULIS [46]

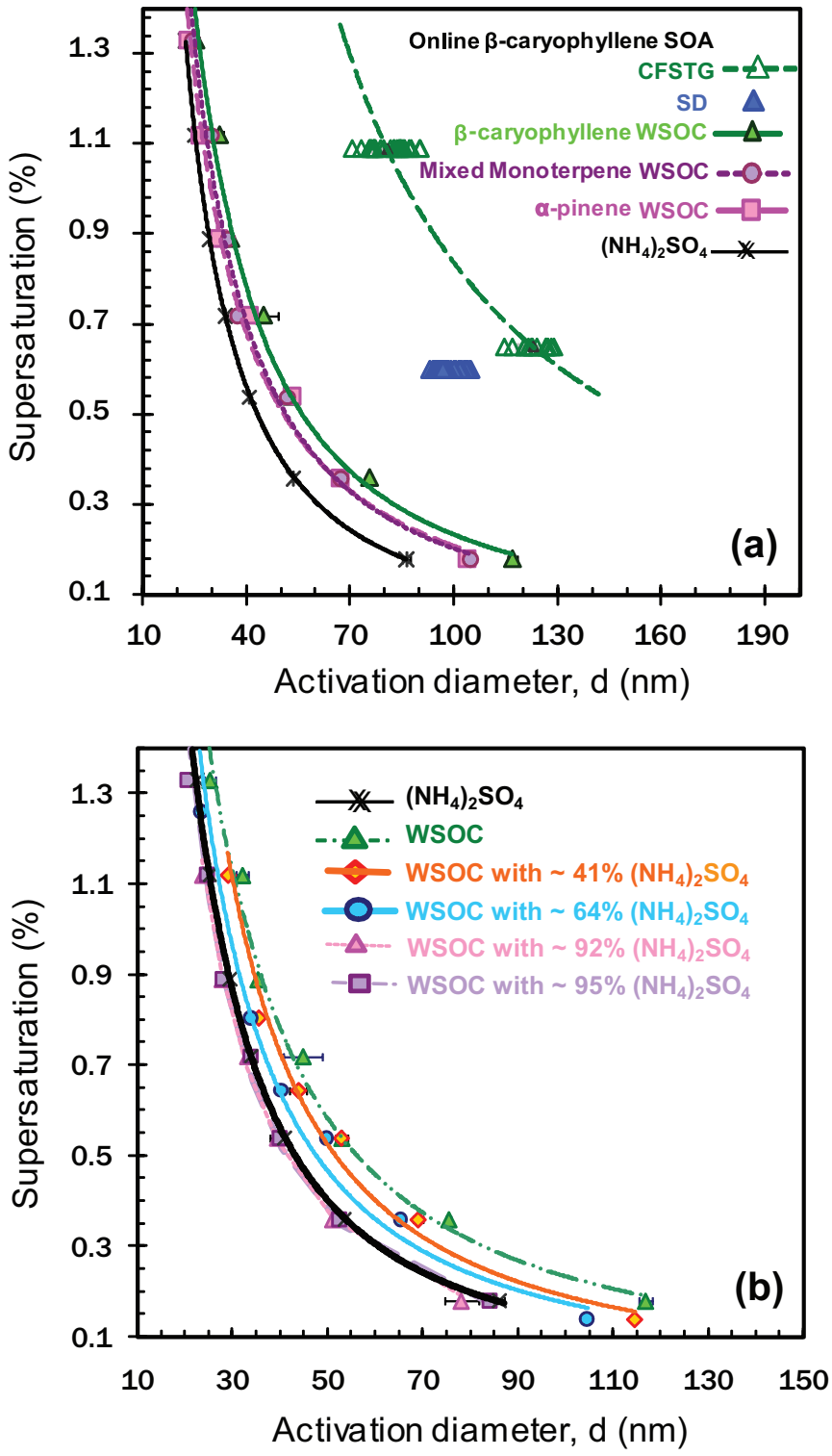

Figure 17: CCN Activity of WSOC from β-caryophyllene SOA. (a) SOA and $(NH_4)_2SO_4$ data are presented for comparison. WSOC from mixed monoterpene and α-pinene hydrocarbon pre-cursors [54] are also shown. (b) WSOC from β-caryophyllene SOA with mixed $(NH_4)_2SO_4$ fractions.

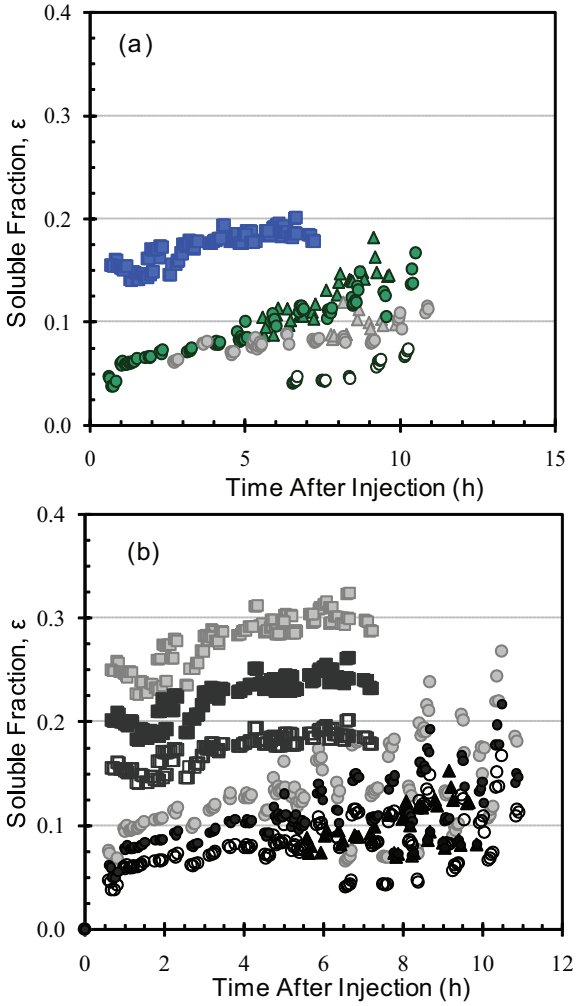

Figure 18: Estimated β-caryophyllene WSOC volume fraction as a function of ageing. (a) ε estimated using SD CCN activity at 0.6% (blue squares) and CFSTG CCN activity 1.09% supersaturation (green closed and open symbols), 0.6% supersaturation (grey symbols) and for aerosol passed through the thermodenuder and exposed to 1.09% supersaturation (open symbols) for σ=66 mN m^{-1} and M_o = 130 g mol^{-1}. (b) Soluble fractions are estimated assuming σ = 66 mN m^{-1} and M_o = 156 g mol^{-1}(open symbols), σ = 72 mN m^{-1} and M_o = 156 g mol^{-1}(closed symbols) and σ = 66 mN m^{-1} and M_o = 250 g mol^{-1}(grey symbols).

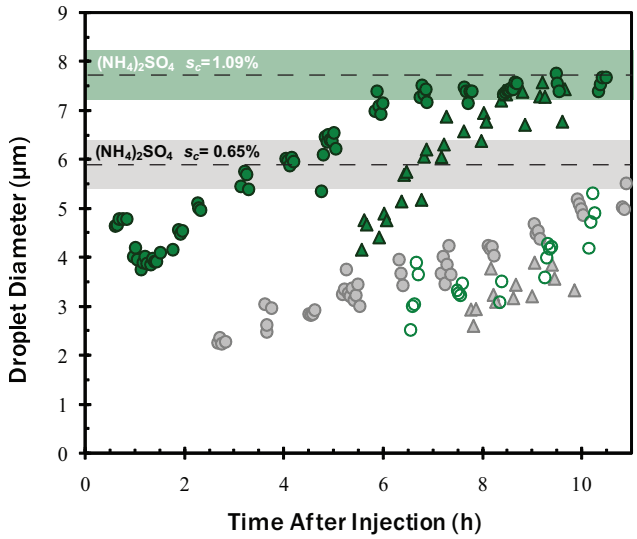

Figure 19: Droplet diameters of activated SOA particles with s_c equal to the instrument supersaturation. Results are shown for 1.09% (closed and open) and 0.6% (grey) supersaturation. Droplet diameters of aerosol passed through the thermodenuder are shown with open circles. The shaded black and grey bands represent the average droplet size of calibration $(NH_4)_2SO_4$ with critical supersaturation of 1.09% (7.7±0.25μm) and 0.65% (5.9±0.25μm), respectively.

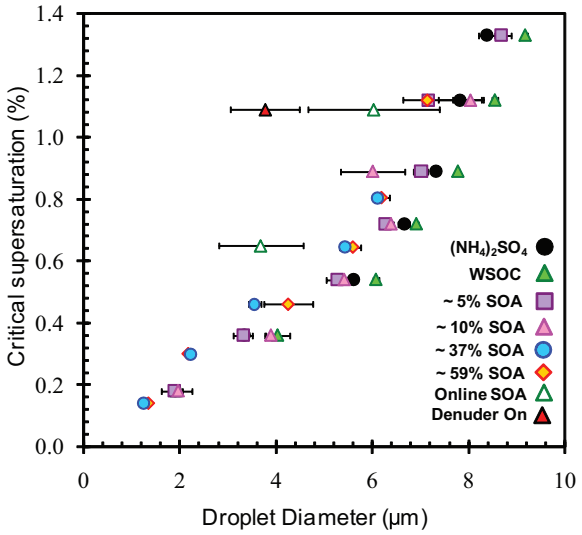

Figure 20: Droplet sizes of WSOC CCN with s_c equal to the instrument supersaturation. Corresponding droplet sizes for $(NH_4)_2SO_4$ and SOA CCN are also shown.

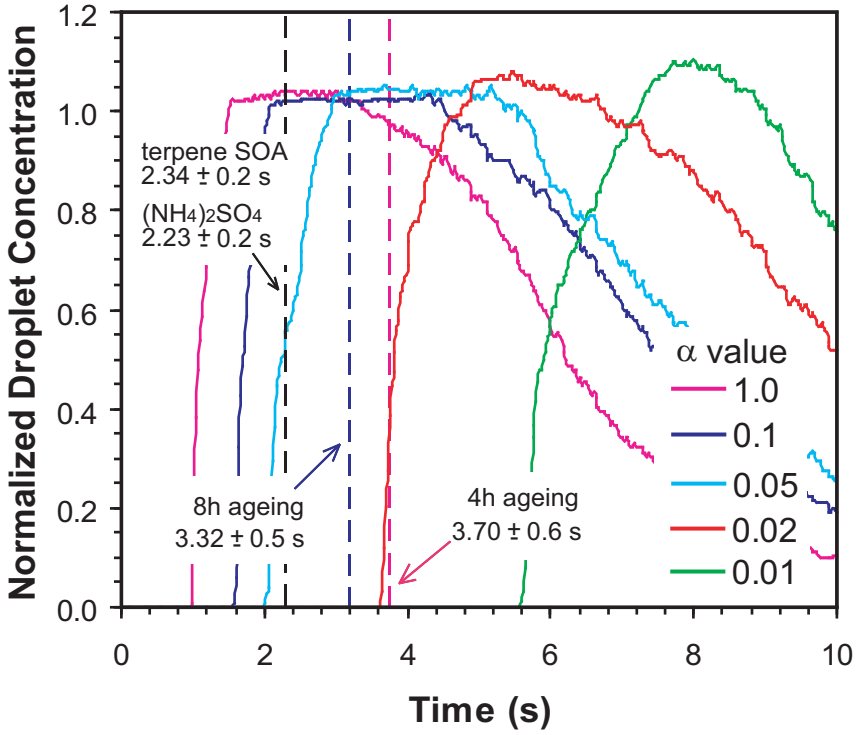

Figure 21: Simulated droplet concentration within the view volume of the SDCC as a function of time and water vapor uptake coefficient. Peak supersaturation in the counter is ∼0.6%, and initially filled with monodisperse (d=100 nm) β-caryophyllene SOA composed of 10% WSOC (with the composition shown in Table 18).

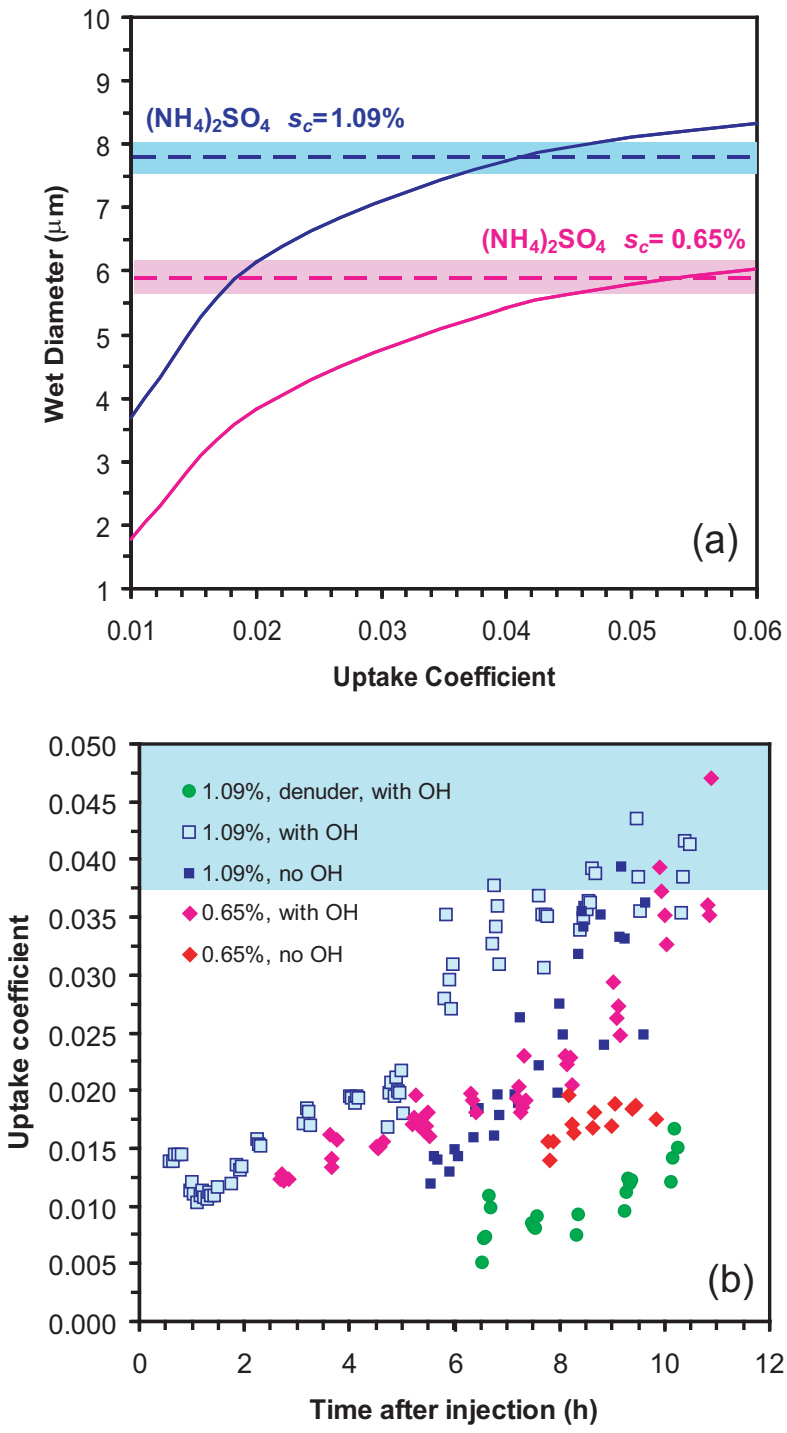

Figure 22: CFSTGC growth kinetics simulations. (a) Simulated droplet wet diameter at the exit of the CFSTGC as a function of α for CCN with s_c=1.09% (blue) and 0.65% (magenta). The size of activated calibration $(NH_4)_2SO_4$ is also shown for comparison. (b) Inferred water vapor uptake coefficient for the growth kinetic data of Figure 20. For comparison, the range of inferred α for $(NH_4)_2SO_4$ (panel a) is shown in the blue banded area.

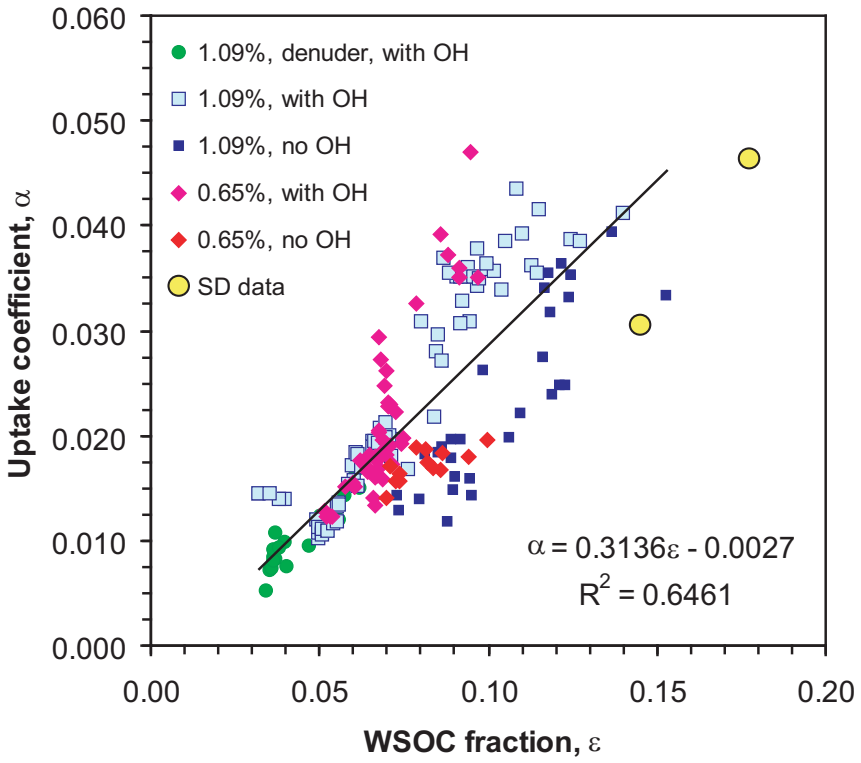

Figure 23: Inferred α as a function of ε for all the datasets obtained with the CFSTGC.

CHAPTER V

WSOC PROPERTIES FROM CLOUDWATER COLLECTED DURING MASE 2005

This study explores the CCN-relevant properties of water-soluble organic aerosol collected during the Marine Stratus/Stratocumulus Experiments (MASE) off the coast of Monterrey, California. In-situ chemical composition, CCN activity and surface tension measurements coupled with Köhler Theory Analysis are used to infer the molar volume and surfactant characteristics of organics contained in cloud droplets and aerosol below cloud base. Results indicate that the aerosol does not contain strong surfactants, and the carbonaceous material in cloud drops is far more hygroscopic than sub-cloud aerosol. The inferred molecular weights of the organic aerosol within cloud residuals are low (< 200 g mol^{-1}), consistent with carboxylic acids identified during cloud processing. Below cloud aerosol exhibits the properties of primary organic matter (molar mass $\sim$2400 kg mol^{-1}). The substantial changes in CCN-relevant properties of the organic fraction illustrate the strong impact of cloud chemistry thereon.

Note: This chapter appears as reference [15].

5.1 Motivation

It is known that water soluble organic compounds (WSOC) can enhance marine CCN number concentrations and cloud droplet number by 10 to 15% [2, 138, 147, 220]. The sources and chemical composition of marine organics vary; primary organic marine aerosol (POMA) generated during bubble bursting may be insoluble high molecular weight organic matter [147]. POMA concentrations vary with season [216]

and are attributed to emissions during phytoplankton blooms [109, 147, 216]. The production of secondary organic marine aerosol (SOMA) during cloud processing (mostly WSOC and carboxylic acids such as oxalate) is persistent in marine cloud regions [**?**]. SOMA can be produced through glyoxylic acid oxidation [192] via several aqueous phase intermediates [31, 57, 128]. Despite the ubiquitous existence and sources of these organics, organic marine matter and its interactions with water can be quite complex, as they can affect particle hygroscopicity, droplet surface tension, and droplet growth kinetics [45, 56, 60, 175, 176, 140]. In-situ chemical composition measurements and offline surface tension and CCN activity measurements are used to characterize thermodynamic properties and droplet growth of marine organic aerosol. CCN measurements have been used to constrain thermodynamic properties of aerosol relevant for cloud droplet formation [150, 154, 212]; this work uses Köhler Theory Analysis (KTA) [150] to infer molar volumes of the aggregate organic component of aerosol collected in-situ during airborne measurements. Surface tension at the droplet surface is directly measured and also inferred with Köhler Theory [14, 139]. Growth behavior of growing cloud droplets are observed and compared to $(NH_4)_2SO_4$. These analyses are presented for marine aerosol in sub-cloud regions that have the potential to form droplets and for aerosol from cloud water samples.

5.2 Aerosol sampling and chemical composition

5.2.1 Aerosol sampling and chemical composition

In-situ samples were obtained during the 2005 Marine Stratus/Stratocumulus Experiments (MASE) that took place off the coast of Monterrey, California. MASE was conducted from July through August of 2005 during the period of persistent formation of clouds in the boundary layer. During the experiments, the Center for Interdisciplinary Remotely-Piloted Aircraft Studies (CIRPAS) Twin Otter airplane sampled clear air and cloudy air masses. A full description of the aerosol and cloud

instrument payload aboard the plane can be found in [131].

For this study, we investigate aerosol samples obtained on July 13^{th} (with reported high organic acid concentrations) from within and below cloud (101 and 450 m cloud base and top, respectively [131]). NOAA Hysplit Back Trajectories indicate that the aerosol mass was mainly a mix of pacific marine air with a potential mix of fresh anthropogenic sources (Fig. 24).

Insert Back Trajectories

Two different inlets were employed for two different sampling stratergies. The activated aerosol (cloud water samples) are collected within cloud (WC) regions and aerosol sampled in clear skies are obtained within sub-cloud (SC) regions. The submicrometer aerosol chemical composition of both WC and SC aerosol were measured by a particle-into-liquid sampler (PILS, Brechtel Manufacturing Inc.)[192]. The counter-flow virtual impactor (CVI) [133, 144] inlet collected only cloud droplet residuals characterized by the WC aerosol.

In the PILS, submicrometer-sized ambient particles are exposed to supersaturated steam and grown into droplets sufficiently large to be collected by inertial impaction. Samples are deposited in vials held on a rotating carousel; each vial contains material representing a period of time between 3.5 and 5 min of flight. The contents of the vials are subsequently analyzed using a dual Ion Chromatography (IC) system (ICS-2000 with 25 μL sample loop, Dionex Inc.) for simultaneous anion and cation analysis. To preserve the samples, each are spiked with 5 μL of dichloromethane and frozen. The WSOC content of the WC and SC samples were measured offline by a Total Organic Carbon (TOC) Analyzer (Sievers Model 800 Turbo, Boulder, CO) (Table 21). The WSOC concentration is determined by the oxidation of organic compounds via ultraviolet irradiation. The amount of CO_2 in the stream is proportional to the measured conductivity, hence the concentration of WSOC found in the de-ionized sample.

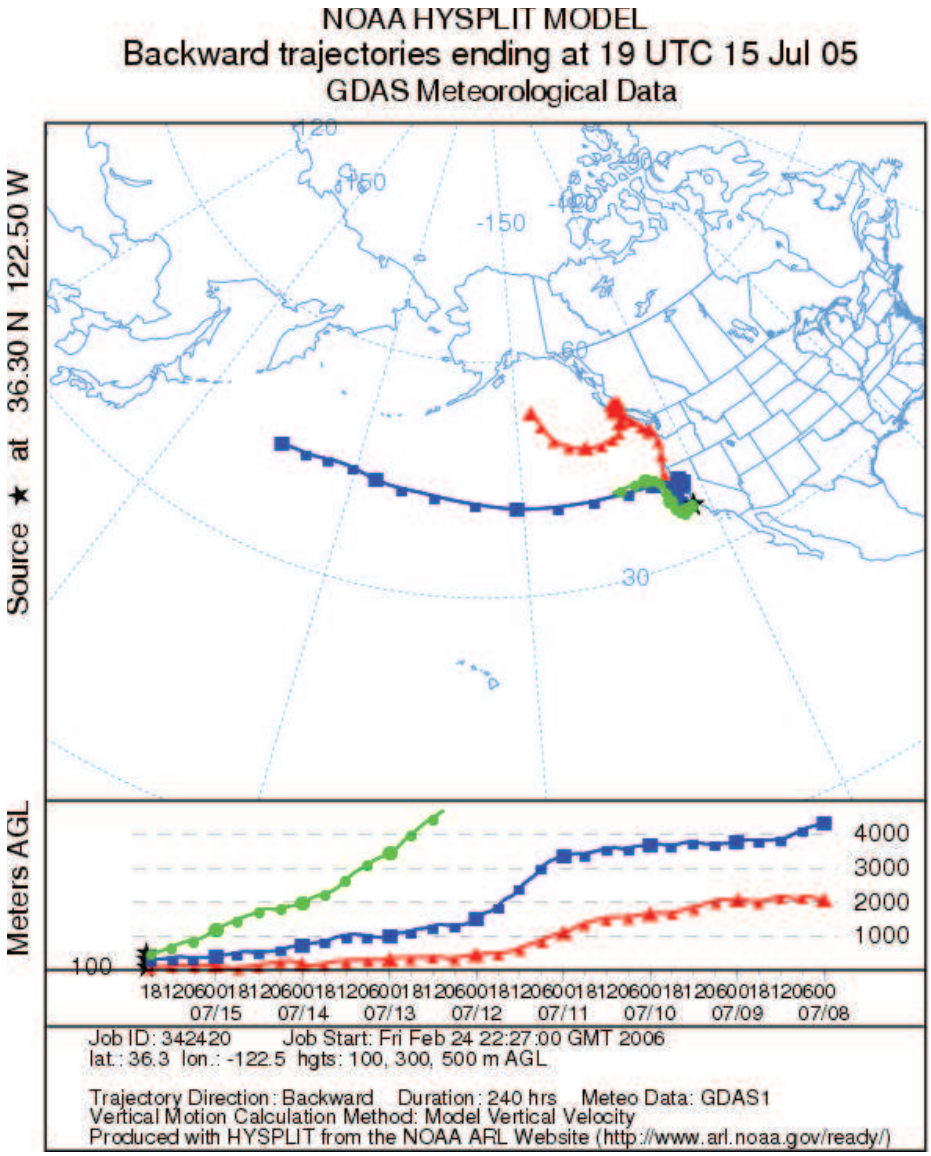

Figure 24: NOAA HYSPLIT Model Back Trajectories for July 13 2005

Table 21: Summary of WSOC (mg C L^{-1}) and ion concentrations(mg L^{-1}) and α and β parameters of the Szyszkowski-Langmuir model of each of the PILS samples

	Within Cloud Aerosol	Sub-Cloud Aerosol
WSOC	220 ± 14	202 ± 7
Ca^{2+}	3.10	2.75
Mg^{+}	0.07	0.58
Na^{+}	21.07	20.90
Cl^{-}	25.30	22.61
NH_4^{+}	21.00	36.38
NO_3^{-}	16.12	17.30
SO_4^{2-}	35.30	87.85
Oxalate	3.61	4.22
NH_4Cl	31.72	33.14
α (mN m^{-1} K^{-1})	8.99×10^{-4}	2.91×10^{-3}
β (L mg^{-1})	3.84×10^{-2}	1.63×10^{-2}

The concentration detection limit, calculated as the average concentration plus three standard deviations of the smallest detectable peak for each ion in the IC baseline noise (converted to air-equivalent units), is < 0.1 $\mu g/m^3$ for the inorganic ions (Na^{+}, NH_4^{+}, K^{+}, Mg^{2+}, Ca^{2+}, Cl^{-}, NO_2^{-}, NO_3^{-}, and SO_4^{2-}) and < 0.01 $\mu g/m^3$ for the organic acid ions (dicarboxylic acids C_2-C_9, acetic, formic, pyruvic, glyoxylic, maleic, malic, methacrylic, benzoic, and methanesulfonic acids). Oxalate was the only organic acid ion above detection limits. The flight also characterized two plumes from ship tracks of the coast and oxalate was reported in high concentrations above cloud top compared to below cloud base (Table 21).

5.2.2 CCN activity

Aerosol from the MASE samples are atomized and regenerated offline to measure CCN activity. Samples are atomized with a collision-type (University of Minnesota) atomizer (Fig. 25) operated at 5 psig pressure. The wet droplets are subsequently dried through two silica gel dryers, charged by a Kr-85 bipolar charger and classified with

Table 22: Aerosol chemical compositions inferred by ISOROPPIA II in terms of % concentration

	Within Cloud Aerosol	Sub-Cloud Aerosol
Organic	88.3	82
NH_4Cl	3.4	3.6
NaCl	0.6	0.0
$(NH_4)_2SO_4$	0.0	5.1
$NaNO_3$	2.3	0.0
NH_4NO_3	0.00	2.4
Na_2SO_4	4.1	7.0
Ca_2SO_4	1.1	0.0

a Differential Mobility Analyzer (DMA 3081) (Fig. 25). The classified monodisperse aerosol is then split and passed though a TSI 3025A Condensation Particle Counter (CPC) for measuring aerosol number concentration (CN); the other stream was sampled by a Droplet Measurement Technologies Continuous-Flow Streamwise Thermal Gradient CCN Counter (CFSTGC) [122, 164].s

Given the limited sample available size-resolved CCN activity and growth kinetics measurements are obtained using scanning mobility CCN Analysis (SMCA) [142]. SMCA couples CFSTGC measurements and a scanning mobility particle sizer (SMPS); as the SMPS scans from 10 and 250 nm dry mobility diameter for a fixed supersaturation, s, an inversion procedure obtains the ratio of CCN to CN as a function of aerosol size. The data is fit to a sigmoidal curve, neglecting the impact of doubly charged particle. The particle dry diameter size, d, for which 50% of the particle are CCN represents the dry diameter of the particle with critical supersaturation, s_c, equal to the instrument supersaturation. The activation experiments are repeated (a minimum of four times) at a given s, and for varying s from 0.2 to 1.2%. The dependence of d with respect to s is used to infer organic solute molar volume [16, 150] and the presence of surfactants [14] (Sect. 5.3).

The addition of inorganic salts to an aqueous solution containing surfactants can

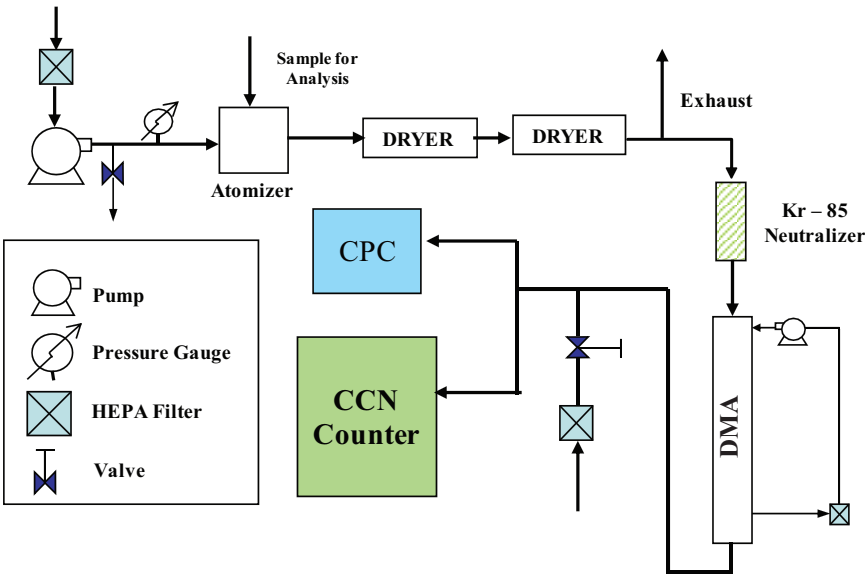

Figure 25: Experimental Set-up for CCN Activity

enhance surface tension depression [16, 111] and CCN activity [16]. Adding pre-calculated amounts of $(NH_4)_2SO_4$ to organic samples can determine the presence of surface active organics in secondary organic aerosol [14, 139]. We base the mass of organic, $m_{organic}$, in the MASE samples on the WSOC carbon concentration (Table 21) and assume that the total mass of organic is 3.75 times the mass of carbon; a value based on the carbon to organic carbon mass ratio of oxalic acid ($C_2H_6O_4$), 90 g mol^{-1})), the most abundant organic measured in-situ. The amount of salt to be added, m_{added}, is determined by the final inorganic mass fraction, α, desired and the amount of salt pre-existing in the sample, m_i. as follows;

$$m_{added} = \frac{\alpha}{(1-\alpha)} m_{organic} - m_i \tag{25}$$

where m_i is assumed to be known from measurements and inferred from ionic concentrations (Table 22) that are input into an aerosol thermodynamic equilibrium model, ISORPPPIA II [69].

5.2.3 Surface tension measurements

A CAM 200 pendant drop method goniometer was used for measurements of surface tension, using the procedure described in [150] and [16]. For each sample, the measurements of sample surface tension, σ, are subsequently fit to the Szyskowski-Langmuir equation [124]:

$$\sigma = \sigma_w - \alpha T \ln(1 + \beta c) \tag{26}$$

where T is the temperature, σ_w is the surface tension of pure water and c is the dissolved carbon concentration (mg C L^{-1}) of the sample. α, β are constants, used for fitting Equation 26 to the σ measurements. Equilibrium is assumed to be obtained during the typical timescale of a measurement (60 s, which allows for the organics in each pendant drop to partition between the bulk and surface layer [202]). Table 21 provides a summary of the α, β parameters for all samples considered.

5.2.4 Droplet growth measurements

The SMCA method, in addition to CCN activity, provides size-resolved droplet growth. This is because the optical particle counter in the DMT CFSTGC used for the activated droplet detection can provide the droplet size to within 0.5 μm. This information can be used to quantify the impact of organics on droplet growth kinetics [164, 14, 122, 139]. When exposed to the same s profile, the droplet size of activated CCN at the exit of the flow chamber, D_p, is constant if the mass transfer coefficient of water vapor to the growing droplet and the CCN critical supersaturation is the same [**?**]. To directly assess the impact of organics on CCN growth kinetics, we examine the D_p of CCN with s_c equal to the instrument saturation (i.e., CCN with a dry diameter equal to the cutoff diameter, d) of the activated SOA is observed and compared to $(NH_4)_2SO_4$ at identical s_c.

5.3 Analytical Theory

5.3.1 Inferring Molar Volumes

Köhler Theory Analysis (KTA) [150] can be used to infer the average molar volume (molecular weight, M_j, over density ρ_j) of the organic fraction, j, of CCN. The analysis employs a CCN activity spectrum (i.e., measurements of s versus d) to solve for the Fitted CCN Activity parameter (FCA), ω, (Table 23) a function of $\frac{M_j}{\rho_j}$ as follows [16, 150].

$$\frac{M_j}{\rho_j} = \frac{\varepsilon_j \upsilon_j}{\frac{256}{27}\left(\frac{M_w}{\rho_w}\right)^2\left(\frac{1}{RT}\right)^3\sigma^3\omega^{-2} - \sum\limits_{i\neq j}\frac{\rho_i}{M_i}\varepsilon_i\nu_i} \tag{27}$$

where M_w, ρ_w are the molecular weight and density of water, respectively, R is the universal gas constant, T is the ambient temperature, σ is the droplet surface tension at the point of activation, ε is the volume fraction and ν is the effective van't Hoff factor. Subscripts i, j refer to the inorganic and organic solutes contained within the aerosol, respectively. ε_k is related to the mass fraction of solute k (k being either of i or j), m_k, as:

$$\varepsilon_k = \frac{m_k/\rho_k}{\sum\limits_{i\neq j} m_i/\rho_i + m_j/\rho_j} \tag{28}$$

The independent variables (σ, ω, ε_i, ε_j, ν_i, and ν_j) employed in KTA analysis for each MASE sample is summarized in Table 23. For our calculations, we assume that the effective organic van't Hoff factor, $\varepsilon_{organic} = 1$. Molecular weights of the organic component are estimated assuming an average density of 1.4 g cm^{-3} [16, 204].

KTA can constrain molecular weight estimates to within 20% [150] for the organic component with mass fractions between 20-50% and has been applied to complex biomass burning aggregate organics mixtures to within 40% [16], secondary organic aerosol to within 30% uncertainty [14], and 25% with primary marine organic matter [139].

Table 23: Köhler Theory Analysis Properties and Molar Volume Results

Property (units)	Within Cloud Aerosol	Sub-Cloud Aerosol
σ (N m^{-1})	6.89×10^{-2}	6.58×10^{-2}
ω (m^1.5)	6.80×10^{-14}	8.75×10^{-14}
$\nu_{organic}$	1	1
ν_{NH_4Cl}	2	2
ν_{NaCl}	2	
$\nu_{(NH_4)_2SO_4}$		2.5
ν_{NaNO_3}	2	
$\nu_{(NH_4)NO_3}$		2
$\nu_{Na_2SO_4}$	3	3
$\nu_{aerosol}$	1.45	1.89
$\varepsilon_{organic}$	0.88	0.82
ε_{NH_4Cl}	0.10	0.09
ε_{NaCl}	0.01	
$\varepsilon_{(NH_4)_2SO_4}$		0.12
ε_{NaNO_3}	0.05	
$\varepsilon_{(NH_4)NO_3}$		0.06
$\varepsilon_{Na_2SO_4}$	0.07	0.10
$\rho_{organic}$	1.4	1.4
ρ_{NH_4Cl}	1.527	27
ρ_{NaCl}	2.16	
$\rho_{(NH_4)_2SO_4}$		1.77
ρ_{NaNO_3}	2.3	
$\rho_{(NH_4)NO_3}$		1.73
$\rho_{Na_2SO_4}$	2.68	2.68
$\rho_{aerosol}$	1.59	1.53
$\left(\frac{M_{aerosol}}{\rho_{aerosol}}\right)$	9.22×10^{-5}	3.10×10^{-4}
$\left(\frac{M_j}{\rho_j}\right)$	1.05×10^{-4}	1.72×10^{-3}
M$_{aerosol}$ (g mol^{-1})	143	458
M$_j$ (g mol^{-1})	157	2413

Derivations of the equations used in this study to calculate molar volume uncertainty, $\Delta\left(\frac{M_j}{\rho_j}\right)$, can be found in [150], [16] and [139]. Here we express the general form of the total uncertainty in inferred molar volumes as $\Delta\left(\frac{M_j}{\rho_j}\right) = \sqrt{\sum_{\text{for all x}} \left(\Phi_x \Delta x\right)^2}$, where Δx is the uncertainty in of each of the measured parameters x, (i.e., any of σ, ω, ε_i, ε_j, ν_i, and ν_j), and Φ_x is the sensitivity of molar volume to x,

$$\Phi_x = \frac{\partial}{\partial x}\left(\frac{M_o}{\rho_o}\right) \tag{29}$$

5.3.2 Inferring Surface Tension

For relatively low concentrations of carbon of our samples ($\sim$100 mg L^{-1}), the effective surface tension depression of the organic solution, $\frac{\Delta\sigma}{\sigma} = \frac{\sigma_w - \sigma}{\sigma_w}$, may be small, extrapolation to higher concentrations ($\sim$ 500 mg C L^{-1}) relevant for CCN activation may not be reliable [14].

If CCN activity data is available for mixtures of WSOC and a salt (e.g., $(NH_4)_2SO_4$), KTA can be used to concurrently infer $\frac{M_j}{\rho_j}$ and σ (as a function of WSOC concentration) using an iterative procedure [139]. However, if enough salt is present in the sample, the contribution of organic solute is negligible; the effect of the organic on CCN activity amounts to its impact on surface tension, and can be inferred as [14],

$$\sigma = \sigma_w \left(\frac{s_c}{s_c^*}\right)^{2/3} \tag{30}$$

where s_c is the measured critical supersaturation, and s_c^* is the predicted value (from Köhler theory), assuming $\sigma = \sigma_w$, the surface tension of pure water computed at the average CFSTGC column temperature [14],

$$s_c^* = \frac{2}{3}\left(\frac{4M_w\sigma_w}{RT\rho_w}\right)^{1.5}\left(\frac{\varepsilon_i\nu_i\rho_i M_w d^3}{M_i\rho_w} + \frac{\varepsilon_j\nu_j\rho_j M_w d^3}{M_j\rho_w}\right)^{-0.5} \tag{31}$$

Equations 30 and 31 are iterated for each data point until convergence is achieved. Each surface tension inference is then related to the WSOC concentration and fit to the Szyskowski-Langmuir adsorption isotherm (Eq. 26), as described by [139].

5.4 Results

5.4.1 Surface Tension

For the low carbon concentrations of our samples, organics have minimal effect on surface tension (Fig. 26). Hence, Eq. 30 is used to infer σ at carbon concentrations relevant for CCN activation. Inferred σ values shown in Fig. 26 indicate that neither sample contain organics that can significantly depress surface tension and is corroborated by nominal changes in effective surface tension depression from our direct surface measurements at limited concentrations. The inferred σ values for the SC aerosol shows potential for surface tension depression, ($-\frac{\Delta\sigma}{\sigma} \simeq 5\%$), at concentrations greater than 1000 mg C L^{-1} and are similar to results from [**?**]. Previous studies show that at concentrations relevant for activation, ($\sim$ 1000 mg L^{-1}) marine organics and HUmic-Like Substances (HULIS), can depress surface tension 25-42% [16, 111, 32], tenfold larger than in the samples of this study.

5.4.2 CCN Activity

Figure 27 shows the supersaturation, s as a function of WC and SC dry diameter, d. The data for $(NH_4)_2SO_4$ aerosol has been added for comparison and, consistent with the expectation that it is highly CCN active, lies to the left of both WC and SC samples.

The activation slope of completely soluble aerosol is consistent with traditional Köhler theory and exhibits a $d^{-1.5}$ dependence (Fig. 27) and [150].

At low supersaturations and dissolved aerosol concentrations($s = 0.5\%$ and [WSOC] > 1000 mg C L^{-1}), the WC and SC aerosol are assumed to be completely soluble yet neither activity is parallel to $(NH_4)_2SO_4$. At higher concentrations the WC and SC converge, as indicated by a -1.66 slope and -1.53 slope respectively. The WC aerosol contain material less hygroscopic than sulfate and more hygroscopic than the SC aerosol; SC has the lowest CCN activity (for a given s the d of the WC is

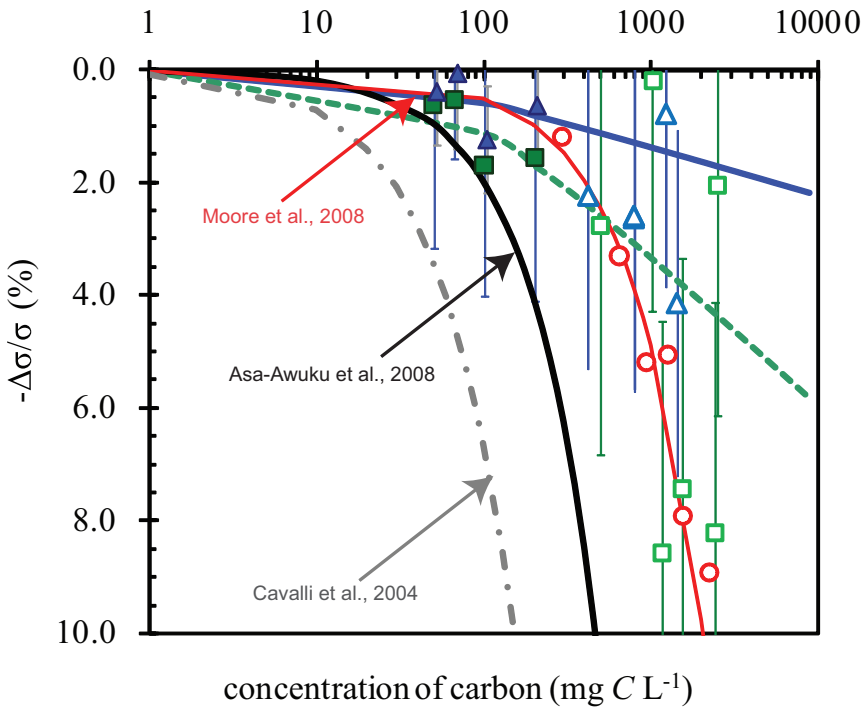

Figure 26: Surface Tension Depression as a function of dissolved carbon concentration. Measurements (closed symbols) and Inferred values (open symbols) of the WC (triangles) and SC aerosol (squares) are shown as data points. WC and SC curves (solid blue and green dashed lines, respectively) are based on Szyszkowski -Langmuir model parameters derived from measurements in Table 21. HULIS data (solid black line) is taken from [16], marine organic aerosol data (dash-dot grey line) taken from [32] and dissolved organic matter (solid red line and open circles) from [139] are added for comparison.

.

greater than SC), and the inferred $\frac{-\Delta\sigma}{\sigma}$ is small at low supersaturations (Fig. 27). This is consistent with [85] who found that for a given size particle the majority of aerosol forming cloud droplets were soluble and the insoluble particles preferentially remained in the interstitial air. At higher supersaturations ($> \sim 1\%$), the WC aerosol exhibits limited solubility (d^{-a} where $a > 1.5$) and the SC aerosol shows enhanced CCN activity as a result of a slight $\frac{-1\Delta\sigma}{\sigma} \sim 5\%$ (Fig. 26).

In addition, if one assumes that the MASE WC and SC aerosol are of a similar source, the intersection of CCN spectrum suggests that under atmospheric conditions

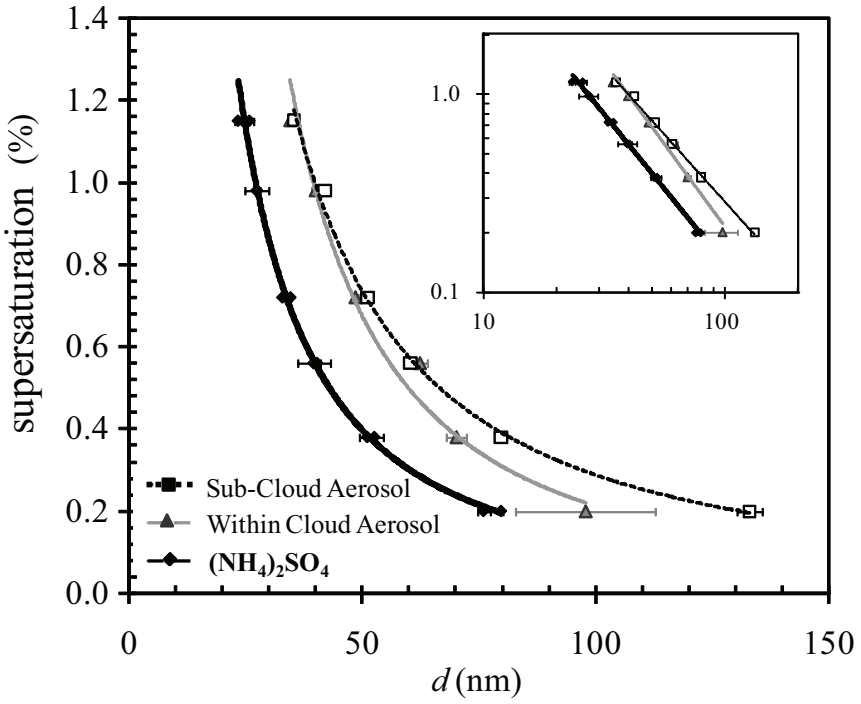

Figure 27: CCN Activity of SC and WC samples. $(NH_4)_2SO_4$ (solid black line) is added for comparison. Inset graph is the same data plotted on a logarithmic scale so that the slopes may be easily compared. The slopes for $(NH_4)_2SO_4$, WC, and SC are -1.51, -1.66, and -1.35, respectively and are within 10 % uncertainty of -1.5.

i) SC aerosol activated during strong updrafts where supersaturations exceeded 1% (conditions consistent with the definition of cumulus clouds formed in strong updrafts [179] and cloud type sampled during MASE); and *ii*) WC aerosol that forms as a result of SC aerosol cloud processing, produces organics of more hygroscopic behavior as supported by evidence of the production of organic acids in [190]. Both WC (Fig. 28a) and SC (Fig. 28 b) increase CCN activity with the addition of $(NH_4)_2SO_4$. However in both cases the CCN activity do not surpass that of $(NH_4)_2SO_4$), again suggesting neither WC nor SC aerosol contain significant amounts of strong surface active organic components such as HULIS [16].

5.4.3 Inferred molar volumes and uncertainties

The CCN spectrum of the both WC and SC aerosol that are shifted to the right of $(NH_4)_2SO_4$ both suggest that the aerosol that do not disassociate as readily have chemical components with molar volumes similar or greater than that of $(NH_4)_2SO_4$ (Table 22). Using a minimum aerosol density of 1.4 g mol^{-1}, the lower limit for the organic molecular weight in the WC aerosol is estimated to be 157$\pm$ 28 g mol^{-1} (Table 23). This value is within range of atmospheric small carboxylic acids (i.e mono and dicarboxylic acids C2-C9 $\sim$100 to 200 g mol^{-1}; oxalic, adipic, suberic, pimelic, azelaic, phthalic acids) and is consistent with the types of organics measured in marine regions [32, 192]. Though not as surface active, the SC sample most likely contain polycarboxylic acids such as HULIS, which have been shown to account for up to 5-25% in marine dissolved organic carbon [32, 87] and may originate from bubble bursting at the seawater surface [149]. As a result the estimated molar mass of aerosol is five times as much as the aerosol found within cloud samples. The aggregate organic molar mass is even larger for the ε is significant (0.8), and the contribution of soluble moles is less than one third of the effective inorganic moles. As a result, KTA estimates a large M_j = 2413$\pm$ 536, a value consistent with less

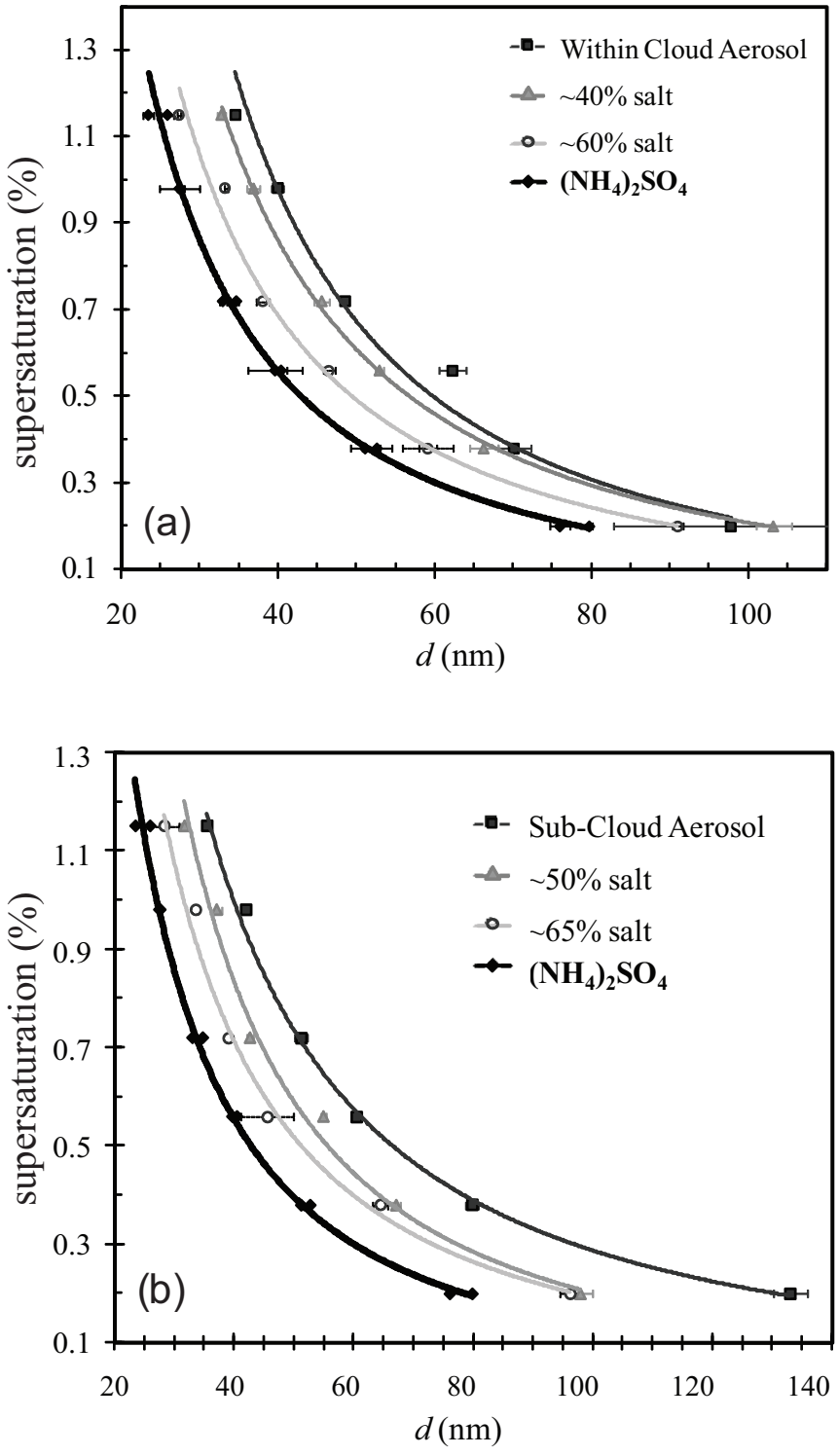

Figure 28: CCN Activity of MASE samples with the addition of $(NH_4)_2SO_4$. Approximate mass fractions of salts are given in percentages. (a) WC sample obtained within cloud regions. (b) SC sample obtained in sub-cloud regions

hygroscopic polycarboxilic materials and corroborated by the SC aerosol potential to depress surface tension. As with other KTA estimates, molar mass values are within 30% uncertainty; the greatest sources of error stem from the FCA parameter, then σ and chemical composition analysis Table 24 and 25.

Table 24: Molar Volume Sensitivity Analysis for WC Organic Marine Aerosol.

Property x (units)	Δx	Φ_x (m^3 mol^{-1} x^{-1})	Molar volume uncertainty (%)
σ (N m^{-1})	1.38×10^{-3}	3.83×10^{-3}	5.72
ω ($m^{1.5}$)	4.43×10^{-15}	2.59×10^{9}	12.42
ν_{NH_4Cl}	0.5	6.43×10^{-6}	3.49
ν_{NaCl}	0.5	1.54×10^{-6}	0.83
$\nu_{(Na)NO_3}$	0.5	4.18×10^{-6}	2.27
ε_{NH_4Cl}	1.95×10^{-3}	8.50×10^{-4}	0.79
$\varepsilon_{(NaCl}$	2.03×10^{-3}	8.25×10^{-4}	0.80
$\varepsilon_{organic}$	6.36×10^{-3}	4.10×10^{-3}	2.82
$\nu_{organic}$	0.20	4.39×10^{-5}	9.52
Total Uncertainty, %			**17.5**

Table 25: Molar Volume Sensitivity Analysis for SC Organic Marine Aerosol.

Property x (units)	Δx	Φ_x (m^3 mol^{-1} x^{-1})	Molar volume uncertainty (%)
σ (N m^{-1})	1.32×10^{-3}	1.97×10^{-2}	8.37
ω ($m^{1.5}$)	4.43×10^{-15}	9.89×10^{9}	14.13
ν_{NH_4Cl}	0.5	6.35×10^{-5}	10.24
$\nu_{(NH_4)_2SO_4}$	0.5	3.74×10^{-6}	0.60
$\nu_{(NH_4)NO_3}$	0.5	2.82×10^{-6}	0.45
ε_{NH_4Cl}	1.95×10^{-3}	4.21×10^{-3}	2.64
$\varepsilon_{(NH_4)_2SO_4}$	2.03×10^{-3}	4.10×10^{-3}	2.69
$\varepsilon_{organic}$	6.36×10^{-3}	4.63×10^{-3}	9.50
$\nu_{organic}$	0.20	7.21×10^{-5}	4.65
Total Uncertainty, %			**22.2**

5.4.4 Droplet growth kinetics

Figure 29 illustrates the droplet size measurements at the OPC for all supersaturations and samples considered. The flow rate within the instrument was maintained at 0.5 L min^{-1} and the sheath to aerosol ratio was 10:1 to generate similar supersaturation profiles for all data points. Similar to the WSOC droplet data presented in [14, 55, 139], almost all of the growth droplet data lie within the measurement uncertainty. Hence the growth kinetics (or water vapor mass transfer coefficient) of the SC and WC aerosol are assumed to be uniform and similar to that of $(NH_4)_2SO_4$. The WSOC SC that contain components of higher molecular weight with mild surface active characteristics they do not affect the droplet growth kinetics.

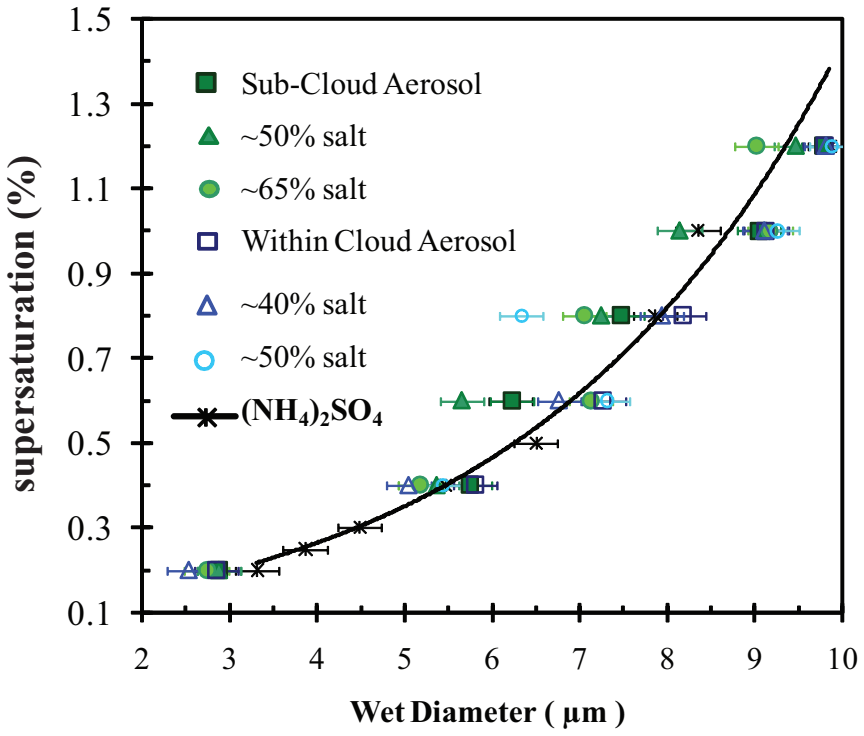

Figure 29: Off-line Droplet size measurements. Within-cloud samples (WC, solid symbols), Sub-cloud samples (SC,open symbols) and $(NH_4)_2SO_4$ (solid black line) wet droplet sizes are plotted for each supersaturation.

5.5 Summary and implications

CCN activity, chemical composition and droplet growth measurements of within-cloud and sub-cloud samples collected during MASE 2005 are explored. This work presents a novel sampling method in combination with offline measurements to elucidate similarities and differences of the aerosols collected in and out of stratocumulus cloud regions. Several analytical techniques exploiting CCN activity are employed to characterize the thermodynamic properties, chemical composition, and surfactant behavior of the organic containing aerosol. The WC aerosol was more hygroscopic than the SC aerosol and mostly likely contains SOMA formed during cloud processing. The direct and inferred surface tension measurements show neither sample contained strong surfactants and as both material is soluble their droplet growth is similar to $(NH_4)_2SO_4$. A similar analysis performed in regions where phytoplankton blooms are prominent may show indicate the presence of strong aerosol surfactants within sub cloud regions and potentially within cloud regions as well.

CHAPTER VI

WSOC PROPERTIES FROM CLOUDWATER COLLECTED DURING GOMACCS 2006

Little is understood about the water-soluble organic composition and properties required to model droplet growth and predict CCN number. The CCN activity analysis of cloud water samples provides insight into the thermodynamic properties of ambiently activated organic aerosol. The experimental technique is revisited and applied to aerosol obtained from a particle-in-liquid sampler (PILS) during the Gulf of Mexico Atmospheric Composition and Climate Study (GoMACCs) in 2006. The sampling and experimental strategy employed characterize the potential differences in aerosol that have been activated within cloud regions (top, middle, and bottom) and below cloud regions. Specifically, samples are obtained from two inlets; already activated aerosols incorporated in cloud droplets are first sampled by a counter-flow virtual impactor (CVI) then PILS within cloud regions and sub-cloud and interstitial aerosols are sampled by the PILS in regions below cloud levels. The molar mass and surfactant characteristics of the average aerosol constituents are estimated using Köhler theory analysis. Droplet size measurements are also presented and quantify the water-soluble growth kinetics of inorganic and organic mixtures in urban environments. The inferred values presented are of particular importance for they can be incorporated into CCN closure studies and aid in the agreement of predicted and measured values.

Note: This chapter appears as reference [10].

6.1 Motivation

Aerosol have the potential to indirectly change cloud properties such that increasing the number of atmospheric cloud-forming aerosols, cloud condensation nuclei (CCN), may yield a larger number of smaller droplets and brighter clouds for a given amount of condensable water vapor (otherwise referred to as the "Twomey effect") [99, 205, 130]. However quantifying the global annual influence of the anthropogenic indirect aerosol effect is subject to uncertainty [130, 34, 158, 90, 99] mainly due to a lack of understanding of the physical based parameters (i.e., chemical composition, hygroscopicity, growth kinetics etc.,) incorporated in global climate models to constrain cloud droplet formation [68, 193].

Köhler theory is an ideal and commonly used thermodynamical model used to predict CCN concentrations. Traditional theory is aptly applied to inorganic salts and low molecular weight (< 250 g mol^{-1}) hygroscopic species and constrain CCN concentrations well [41, 159]. Yet the ideal theory is less successful for partially soluble compounds and less hygroscopic compounds and inorganic/organic mixtures [41, 159]. This is especially true for ambient predictions in polluted areas [36, 207, 196, ?] that can be influenced by partially soluble organics that may contribute surface active materials, affect hygroscopicity, dissolution rates, and influence droplet growth kinetics [64, 35, 60, 45, 184, 74, 140, 12].

The aerosol sampled within cloud regions and below cloud regions can be of significantly different organic composition [15]. Cloud processing that produces monocarboxylic and dicarboxylic organic acids is known to occur ubiquitously at cloudtop [190]; whereas sub-cloud aerosol, such as marine organics generated from the bubble bursting of dissolved matter are more likely to contain weakly hygroscopic, polycarboxlic organics of considerably larger (> 250 g mol-1) molar mass [146, 147, 32, 139, 15, 171]. These differences in chemical composition and hygroscopicity will effect CCN behavior, cloud droplet number and the indirect effect and thus must be

explored.

During the 2006 Texas Air Quality Study (TexAQS) and Gulf of Mexico Atmospheric Composition and Climate Study (GoMACCS), research flight experiments aboard the Center for Interdisciplinary Remotely-Piloted Aircraft Studies (CIRPAS) Twin Otter probed aerosol cloud properties and radiative effects. Chemical, physical, and optical, properties of the aerosol in the Eastern Texas and Gulf of Mexico region were investigated; in particular the properties and behavior of urban and industrial aerosol that affect regional haze, the aerosol direct and indirect radiative forcing of climate were explored.

From measurements of in-situ samples, we investigate the behavior of urban aerosol that has already been activated within cloud and out of cloud using the experimental and analytical techniques first presented with marine cloud water samples in stratocumulus cloud regions [15]. In this previous work, it was shown that cloudwater aerosol are more hygroscopic than the type found below cloud [15]. The water-soluble component of already-activated aerosol are of particular interest because their thermodynamic organic properties will help constrain estimates of cloud droplet number. The water-soluble properties of the aerosol obtained below cloud will aid in the agreement of CCN measurement and predictions for ground-based and airborne CCN Closure studies [**?**].

6.2 Experimental Methods

6.2.1 In-Flight Measurements

6.2.1.1 Aerosol sampling

For this study, we investigate aerosol samples obtained on seven research flights (Table 26). These flights sampled aerosol in key pollutant regions of Eastern Texas: downwind of the Parish Power Plant plume, in the Houston Ship Channel (a conglomerate of oil refineries located close to the city, in the Gulf Air stream, and the

metropolitan area of Houston, Fig. 30).

As with the cloud water experiments during the Marine Statrocumulus Experiments (MASE I), two different inlets were employed; one for sampling cloud droplets; activated aerosols within cloud (AWC) regions and another for sampling in clear skies, (above and below cloud regions, AC and BC respectively) and interstitial aerosol within the cloud (IWC). The inlet of the counter-flow virtual impactor (CVI) [133, 144]) collected cloud droplet residuals (AWC). The sub-micrometer aerosol chemical composition was subsequently measured by a particle-into-liquid sampler (PILS, Brechtel Manufacturing Inc) [189, ?, 191] and collected for offline measurements. IWC, AC and BC samples collected within cloud and in clear skies were sampled from the PILS inlet, measured for chemical composition and then collected for analysis. Some samples are not obtained near cloud regions, as a result their names are characterized by the location with which the PILS sampled and collected (i.e., Transit refers to aerosol obtained over the Gulf as the aircraft flew to its intended destination, Ship Channel and Plume are collected within their respective regions and the Gulf air sample is characteristic of a cleaner air mass (Fig. 31).

6.2.1.2 Chemical composition Measurements

In the PILS, submicrometer-sized ambient particles are exposed to supersaturated steam and grown into droplets sufficiently large to be collected by inertial impaction. Samples are deposited in vials held on a rotating carousel; each vial contains material representing a period of time between 3.5 and 5 minutes of flight. The contents of the vials are subsequently analyzed using a dual IC system (ICS-2000 with 25 μL sample loop, Dionex Inc.) for simultaneous anion and cation analysis. To preserve the samples for offline measurements, each vial was spiked with 5μL of dichloromethane and frozen.

The detection limit, calculated as the average concentration plus three standard

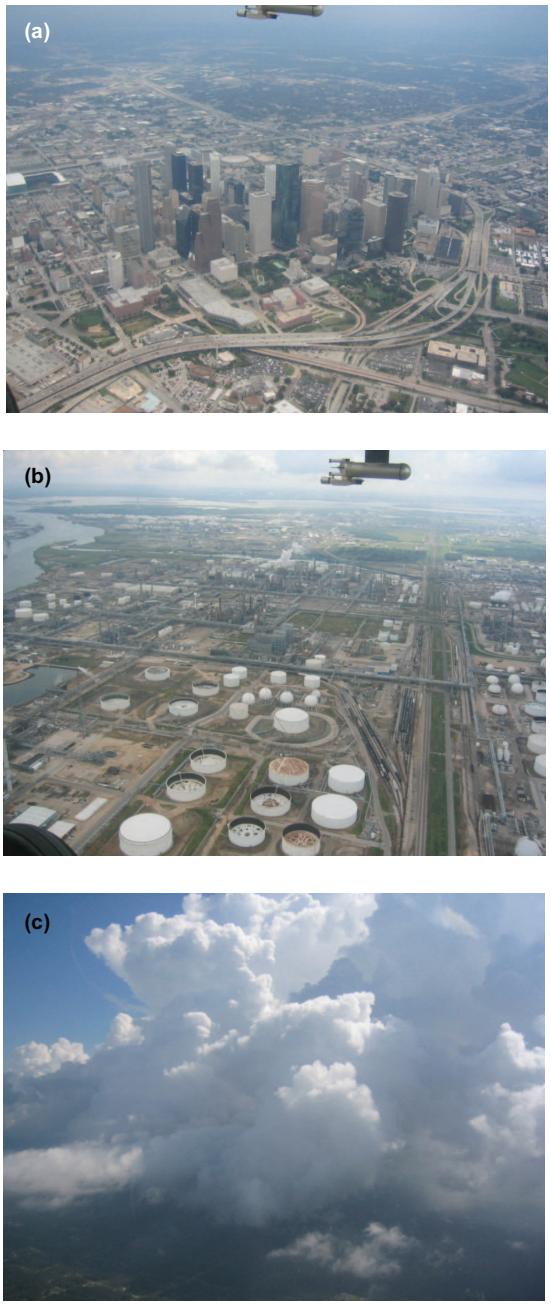

Figure 30: An aerial view of the sampling locations studied. (a) Downtown Houston (b) Houston Ship Channel (c) Clouds Sampled during TexAQS/ GoMACCS

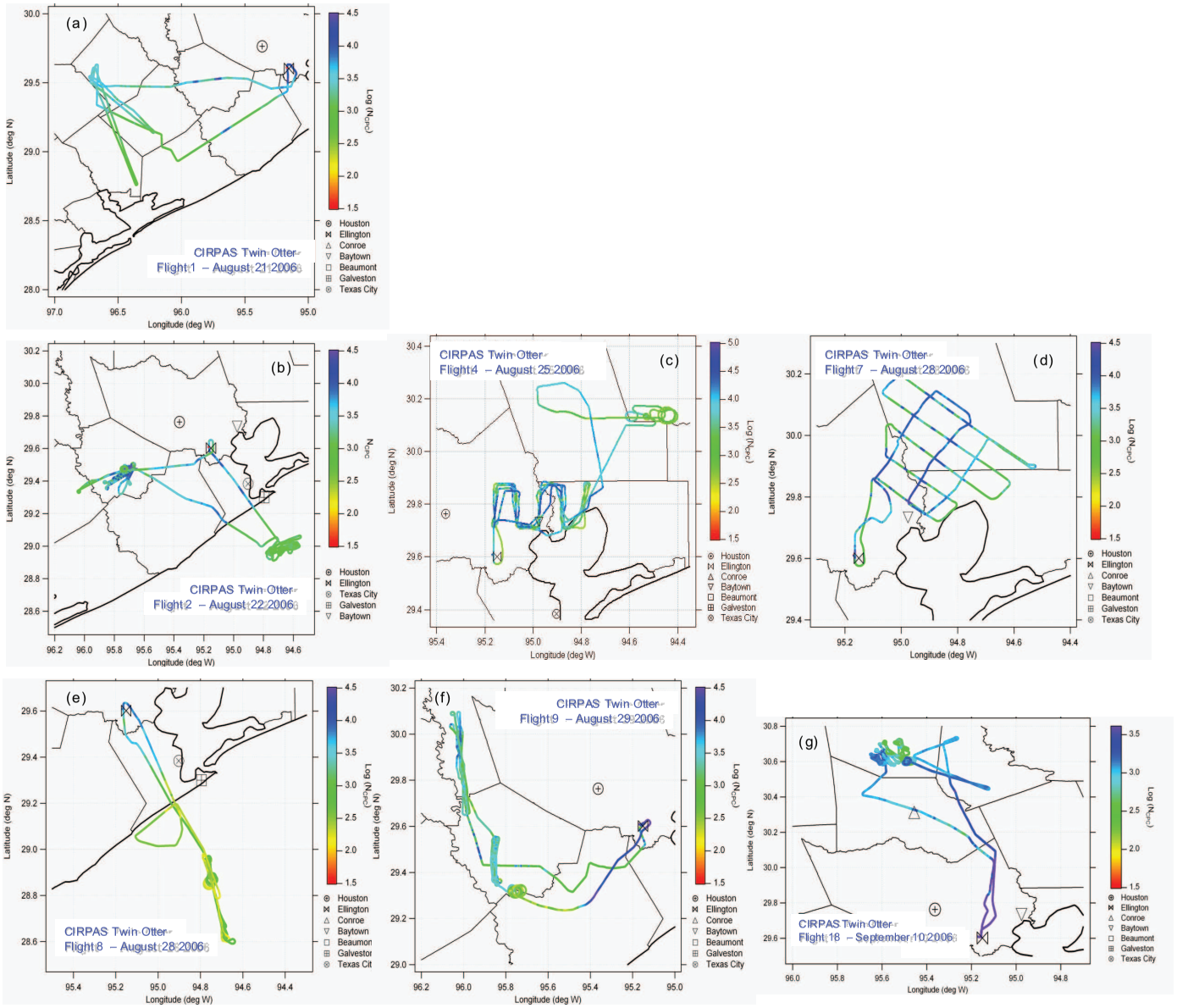

Figure 31: Research Flights during TexAQS/GoMACCS. Aerosol Concentrations are plotted as a function of intensity and changes in altitude correspond to the color scales shown.

Table 26: WSOC samples investigated. Samples obtained on the same research flight are separated by regions of collection and the concentration of the organic acid mass measured by PILS is shown.

Research Flight RF#	Flight Date	Sample Type	Total Mass (μg L^{-1})	Organic Acid Mass (μg L^{-1})	Cloud Rating	Flight Notes
1	Aug 21 2006	CVI	0.60	0.03		Parish Plume Study
1		Interstitial	0.87	0.06		
1		Above Cloud	0.65	0.06		
1		Below Cloud	0.53	0.01		
2	Aug. 22 2006	CVI	1.78	0.04	$\star\star$	Parish Plume Study; Clouds near point
2		Transit	1.05	0.04		source, good clean clouds over ocean
4	Aug. 25 2006	CVI	0.85	0.05	$\star\star$	Ship Channel Study; Clouds near
4		Below Cloud	2.15	0.04		point source
7	Aug. 28 2006	Ship Channel	2.85	0.05		Baytown Study; Clouds near
7		Plume	2.23	0.02		point source; Saharan Dust is Likely
8	Aug. 28 2006	Gulf Air	4.51	0.06		No plume; No Cloud
9	Aug. 29 2006	CVI	1.74	0.05	$\star\star$	Parish; good polluted
9		Below Cloud	1.84	0.03		clouds
9		Above Cloud	1.21	0.03		
18	Sep 10 2006	CVI	0.93	0.08	$\star\star\star$	Very good single cloud
18		Below Cloud	2.98	1.82		
18		Above Cloud	0.17	0.02		

deviations of the smallest detectable peak for each ion in the IC baseline noise (converted to air-equivalent units), is < 0.1 μg m^3 for the inorganic ions (Na^+, NH_4^+, K^+, Mg^{2+}, Ca^{2+}, Cl^-, NO_2^-, NO_3^-, and SO_4^{2-}) and < 0.01 μg m^3 for the organic acid ions (dicarboxylic acids C2-C9, acetic, formic, pyruvic, glyoxylic, maleic, malic, methacrylic, benzoic, and methanesulfonic acids). The average aerosol composition is presented in Table 27.

6.2.2 Off-line Measurements

Aerosols from the TexAQS/GoMACCS samples are atomized and regenerated offline. CCN activity and droplet sizes are measured with an identical experimental set-up and analysis as presented in [**?**]. Such that samples are atomized with a collision-type (University of Minnesota) atomizer operated, subsequently dried, charged classified with a Differential Mobility Analyzer (DMA 3081). The classified monodisperse aerosol is then split and passed though a TSI 3025A Condensation Particle Counter (CPC) for measuring aerosol number concentration (CN). CCN concentrations are measured in the other stream by a Droplet Measurement Technologies Continuous-Flow Streamwise Thermal Gradient CCN Counter (CFSTGC) [122, 164].

Scanning mobility CCN Analysis (SMCA) [142] is used to obtain size-resolved CCN activity and growth kinetic measurements for small sample amounts. At a fixed supersaturation, s, the ratio of CCN to CN is measured for a range of dry mobility diameter (between 10 and 250 nm). The SMCA data is fit to a sigmoidal curve, neglecting the impact of doubly charged particle. The particle dry diameter size, d, for which 50% of the particle are CCN represents the dry diameter of the particle with critical supersaturation, s_c, equal to the instrument supersaturation. The activation experiments are repeated (a minimum of four times) at a given s, and for varying s from 0.2 to 1.2%. The dependence of d with respect to s is used to infer organic solute molar volume [16, 150] and the presence of surfactants [14].

Table 27: Composition Data from PILS. Concentrations are measured in μg L^{-1}. The naming convention of each sample is denoted by RF-flight#-aerosol type

Sample	NH_4^+	NO_3^-	SO_4^{2-}	Cl^-	Ca^{2+}	Mg^{2+}	K^+	Na^+	formate	acetate	oxalate	$\frac{NH_4}{SO_4}$	Organic Acid	Total
RF1-AWC	0.06	0.04	0.41	0.04	0.00	0.00	0.00	0.01	0.00	0.00	0.02	0.35	0.03	0.60
RF1-IWC	0.09	0.06	0.61	0.01	0.01	0.01	0.00	0.01	0.00	0.00	0.05	0.30	0.07	0.87
RF1-AC	0.10	0.06	0.35	0.03	0.01	0.03	0.00	0.01	0.01	0.00	0.04	0.31	0.07	0.65
RF1-BC	0.08	0.02	0.39	0.01	0.01	0.00	0.00	0.01	0.00	0.00	0.01	0.18	0.01	0.53
RF2-AWC	0.29	0.08	1.18	0.12	0.02	0.00	0.00	0.03	0.00	0.01	0.03	0.81	0.04	1.78
RF2-Transit	0.16	0.08	0.71	0.04	0.01	0.00	0.00	0.01	0.00	0.00	0.03	0.69	0.04	1.05
RF4-AWC	0.14	0.08	0.52	0.02	0.00	0.00	0.01	0.03	0.01	0.00	0.03	1.01	0.05	0.85
RF4-BC	0.52	0.14	1.40	0.01	0.01	0.00	0.01	0.02	0.00	0.00	0.04	1.95	0.04	2.16
RF7-Ship Channel	0.58	0.14	2.00	0.05	0.00	0.00	0.00	0.02	0.01	0.00	0.01	1.17	0.05	2.85
RF7-Plume	0.48	0.12	1.53	0.03	0.00	0.00	0.01	0.03	0.00	0.00	0.01	0.86	0.02	2.23
RF8-Gulf Air	0.37	0.23	0.92	0.06	0.00	0.00	0.02	0.09	0.01	0.01	0.03	1.91	0.05	1.74
RF9-AWC	0.94	0.34	2.77	0.18	0.00	0.00	0.01	0.19	0.01	0.01	0.02	2.30	0.06	4.51
RF9-BC	0.47	0.22	1.08	0.02	0.00	0.00	0.00	0.02	0.01	0.00	0.02	0.73	0.03	1.84
RF9-AC	0.26	0.19	0.65	0.02	0.00	0.00	0.01	0.04	0.00	0.00	0.02	0.79	0.03	1.21
RF18-AWC	0.22	0.10	0.42	0.04	0.00	0.00	0.01	0.08	0.01	0.00	0.06	2.14	0.08	0.95
RF18-BC	5.10	0.58	1.49	1.15	0.01	0.02	0.04	0.02	0.02	0.01	0.05	1.26	1.82	2.98
RF18-AC	0.02	0.02	0.08	0.02	0.00	0.00	0.00	0.01	0.00	0.00	0.02	0.30	0.02	0.17

Size-resolved droplet growth of wet particle size $Dp > 1$ μm are measured with the DMT with an optical particle counter (OPC). Aerosol exposed to the similar s profiles within the instrument, will grow to the same wet diameter, D_p, provided that the mass transfer coefficient of the water vapor to the growing droplet and the critical supersaturation is the same [141, 164, 122]. The droplet sizes of WSOC are compared to droplet sizes measured from pure $(NH_4)_2SO_4$ so that the growth kinetics may be quantified.

6.3 Analytical Theory

6.3.1 Köhler Theory Analysis

Köhler Theory Analysis (KTA) [150] is used to infer molar volumes (molecular weight, M_o, over density ρ_o) of the aggregate organic component, o, of CCN. As previously shown, the analysis employs a CCN activity spectrum (i.e., measurements of s versus d) to solve for the Fitted CCN Activity parameter (FCA), ω. $\left(\frac{M_o}{\rho_o}\right)$ is also a function of the molecular weight and density of water, of M_w and ρ_w respectively, the universal gas constant, R, the ambient temperature, T ,the droplet surface tension at the point of activation, σ, the mass fraction, m volume fraction ε and the effective vant Hoff factor ν is for organic components, o, and inorganic components, i. m_i is assumed to be known from measurements and inferred from ionic concentrations. Using an iterative procedure, KTA can the surface tension at the droplet surface, σ for salted samples [139, 14]. If enough salt is present in the sample, the contribution of organic solute is small and the effect of the organic on CCN activity amounts to its impact on surface tension [14].

6.4 Results

The main component of aerosol mass collected during the study are inorganics. On average sulfates make up 84% $\pm$ 14% of the water-soluble fraction observed in the Texas region [**?**]. Sulfates from industrial and urban sources are the most abundant

Table 28: KTA properties of the Samples Studied

Sample	Name	ω ($m^{1.5}$)	$\overline{(\frac{M}{\rho})}_{aerosol}$ (m^3 mol^{-1})	M (g mol^{-1})
RF2	CVI	4.12×10^{-14}	6.05×10^{-5}	76.5
RF2	Transit	4.68×10^{-14}	1.26×10^{-4}	121.2
RF4	CVI	3.98×10^{-14}	6.97×10^{-5}	71.5
RF4	BelowCloud	4.60×10^{-14}	7.01×10^{-5}	95.6
RF7	ShipChannel	4.93×10^{-14}	8.29×10^{-5}	137.2
RF7	Plume	4.96×10^{-14}	9.22×10^{-5}	111.0
RF8	GulfAir	5.23×10^{-14}	9.82×10^{-5}	123.6
RF9	CVI	5.31×10^{-14}	9.62×10^{-5}	127.3
RF9	BelowCloud	4.92×10^{-14}	7.43×10^{-5}	109.3
RF9	AboveCloud	5.42×10^{-14}	9.05×10^{-5}	132.7

ions in the data presented (Table 27). As a result, the average properties from all flights show that the CCN are very hygroscopic, of low molecular weight and behave a lot like sulfate (Fig. 32 and Table 28).

The CCN activity of samples obtained during RF-2 concur with [15] and find that the AWC contain more hygroscopic materials than aerosol sampled over the Gulf. The estimated molar masses of the CCN are statistcally different (they are not the within the typical 30% uncertainty [139, 16, 14]) and suggest that the AWC contains low molecular weight species, most likely to be organic acids.

During RF-4 the cloud sampled is close to the sulfate plume source. The mass loading of water-soluble components measured BC is almost twice that measured WC (Table 27). Despite the addition of water-soluble mass in the BC aerosol, AWC shows enhanced CCN activity, surpasses that of $(NH_4)_2SO_4$ aerosol, and likely contains surface active materials (Fig. 32). The estimated molar mass of the AWC and BC aerosol are within uncertainty of each other and thus are presumably of similar source. However the differences in the small water-soluble organic fraction, brought about by

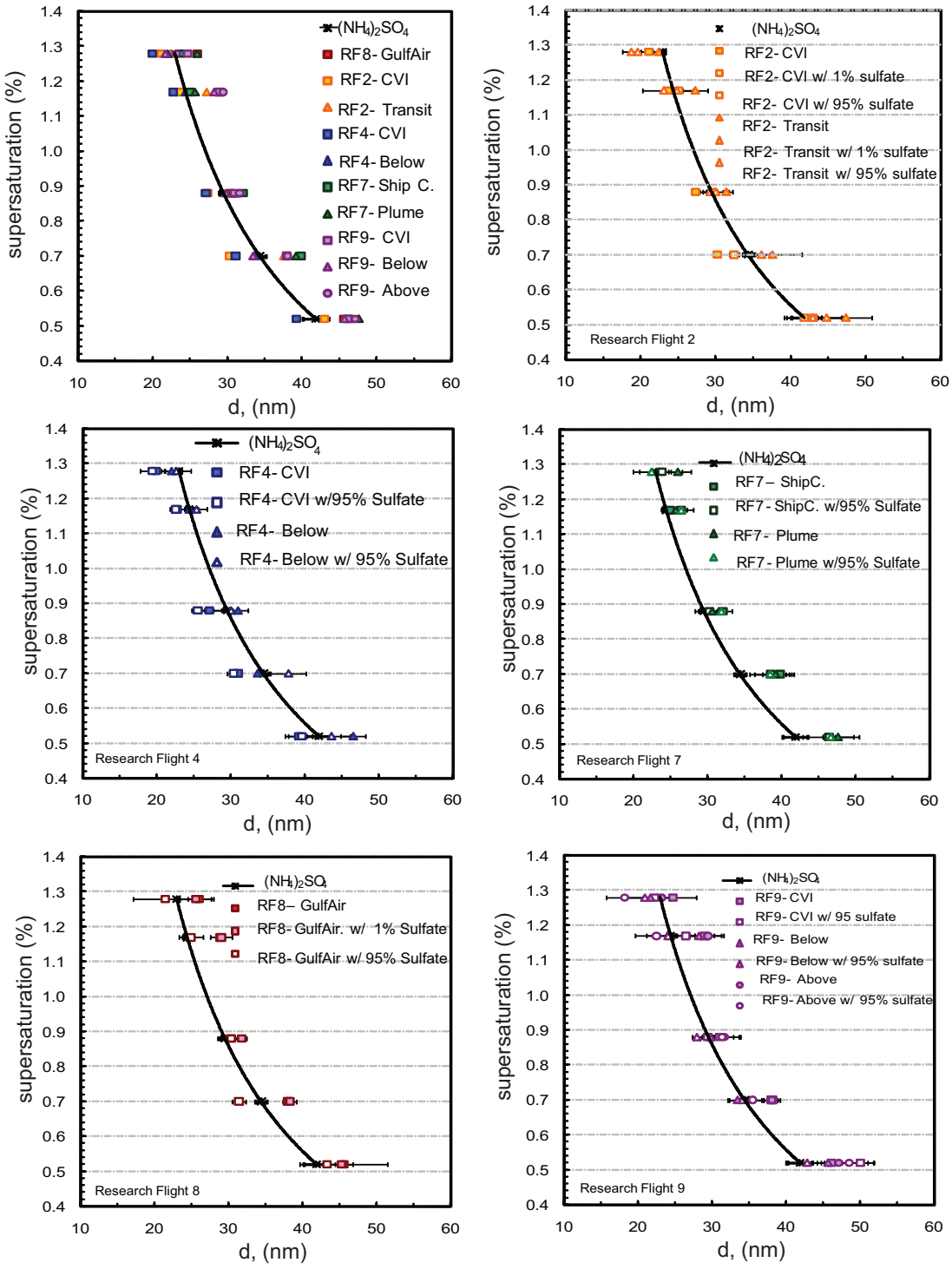

Figure 32: CCN Activity Spectrum. $(NH_4)_2SO_4$ is added for comparison (a) measurements of the research flights studied. Figures (b), (c), (d), (e) and (f) are measurements from the individual flight, including their respective salted fractions

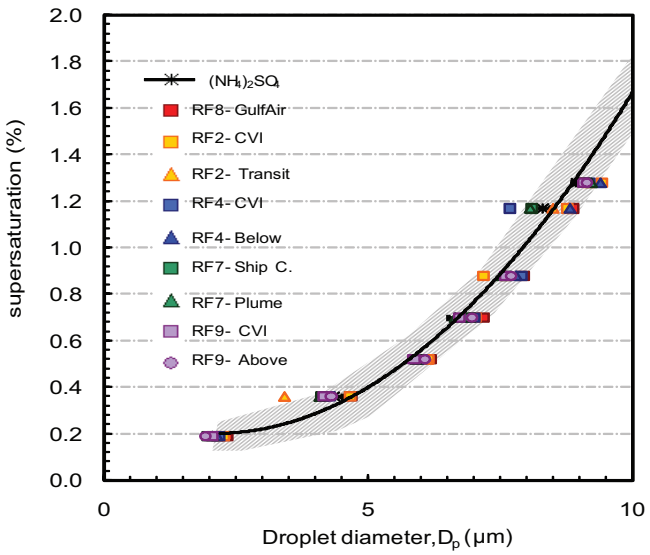

Figure 33: Droplet growth spectrum. $(NH_4)_2SO_4$ is added for comparison.

cloud processing, can account for the effects of reduced hygroscopicity in BC sample and enhanced surfaced activity in AWC samples.

RF-7 that characterized industrial plumes and ship channel sources contained the most soluble mass (Table 27). Consistently we observe that the samples obtained near the Parish Power Plant (RF-4,7,9) all behave like sulfate. Furthermore, the CCN activity of RF-7 suggests CCN from industrial and urban plumes are alike. RF-8 that studied cleaner air masses from the gulf region are more likely to contain sea-salt sulfates and dissolved organic marine materials. The average CCN material is less hygroscopic than sulfate and a slight enhancement of surface activity is observed in CCN measurements (Fig. 32).

The droplet growth of water-soluble material does not differ from $(NH_4)_2SO_4$ (Fig. 33). In addition the aerosol collected within and out of cloud regions grows to similar sizes. This suggests that droplet formation in urban areas where abundant water soluble mass is present is similar regardless of location or plume source.

6.5 Summary and Implications

Use of a CVI and PILS is a viable method we can use to assess ambient CCN properties and infer aerosol composition. The data set from the PILS and the estimated molar mass of the aerosol presented suggests that the majority of components from the sampled regions are low molecular weight species (< 250 mol^{-1}). The organic mass fraction can vary up to 50% in this region, and consequently the resulting molecular weight of the organic component as inferred from the overall molar mass of the aerosol can vary on the order of $\sim$100 to $\sim$1000 g mol^{-1}, depending on the dissociatative and hygroscopic properties. This quantity will be constrained in future work. Though CCN Activity varied between locations, the organic constituents in the water-soluble component do not alter droplet growth kinetics. Regardless of composition, the water-soluble fraction grows like $(NH_4)_2SO_4$, and suggests that any kinetic limitation on droplet growth beyond what is expected for sulfate aerosol is likely from the presence of insoluble species (i.e., not water soluble surfactants). Additional Aeroodyne Mass Spectrometer data, not yet available from this mission will aid in quantifying soluble and insoluble organic influences.

CHAPTER VII

CLOUD CONDENSATION NUCLEI IN URBAN PLUMES: AIRBORNE CCN MEASUREMENTS AND CLOSURE DURING THE TEXAS AIR QUALITY STUDY OF 2006

In August through October, airborne measurements of cloud condensation nuclei (CCN) were conducted with a Continuous-Flow Streamwise Thermal Gradient CCN counter aboard the National Oceanic and Atmospheric Administrations (NOAA) WP-3D platform during the 2006 Texas Air Quality Study/Gulf of Mexico Atmospheric Composition and Climate Study (TexAQS/GoMACCS) over eastern Texas and the northwestern Gulf of Mexico. Many of these experiments were conducted downwind of the Houston, Texas ship channel and were heavily influenced by industrial and urban pollution sources. The time series of aerosol measurements show the evolution of CCN downwind of plumes and suggest the ageing of aerosol via sulfate deposition, coating or coagulation, or organic oxidation may enhance CCN activity. CCN measurements are compared to predictions derived from traditional Köhler Theory. Mixing state (internal/external) assumptions along with bulk and chemical size-resolved data are used to constrain and improve estimates of CCN concentration in the closure study. Results concur with previously published literature that suggest that chemical composition size resolved data may improve predictions. Our predictions further indicate that in discrete cases organic properties such as molecular weight, surface tension, hygroscopicity, and effect solute disassociation may enhance the agreement between measurements and predictions.

Note: This chapter appears as reference [11].

7.1 Motivation

The global annual influence of the anthropogenic indirect aerosol effect is subject to large uncertainties [130, 34, 158, 90, 99]. Much of this uncertainty is due to a lack of understanding of the physical based parameters (e.g., chemical composition, hygroscopicity) incorporated in global climate models to constrain cloud droplet formation [68, 193]. As a result several studies have experimentally investigated CCN properties on regional and global scales to improve model parameters [185, 33, 136, 196, **?**, 25, 209, 163, 36, 207, 40, 52, 217].

Köhler theory, an ideal thermodynamical model and the most popular model used to predict CCN concentrations, describes the formation of cloud droplets from CCN [115]. Köhler theory can be aptly applied to inorganic salts and low molecular weight hygroscopic species to constrain CCN concentrations well [41, 159], yet is less successful for partially soluble compounds that are less hygroscopic and inorganic/organic mixtures [41, 159]. This is especially true for ambient predictions in polluted areas [36, 207, 196] that can be influenced by partially soluble organics that may contribute surface active materials, affect hygroscopicity, dissolution rates, and influence droplet growth kinetics [64, 35, 60, 45, 184, 74, 140, 13].

The degree of agreement between field measurements and predicted CCN concentrations values is often (and will be henceforth) referred to as its CCN closure; a closure study tests the theoretical understanding of CCN activation and highlights appropriate simplifying assumptions that will improve predictions.

Undoubtedly, knowing the amount of water vapor necessary for activation, the critical supersaturation, s_c , is crucial for understanding CCN theory [**?**] and for reliable ambient measurements; the key aerosol parameter for obtaining good closure is size [53, **?**]. Yet in the presence of organics, predictions can be significantly improved by incorporating size-resolved chemical composition, soluble fraction, and hygroscopicity data [**?**, 136]. Size-resolved chemical composition data is commonly

measured with an aerosol mass spectrometer (AMS) and additional chemical composition and soluble fraction data maybe incorporated from particle-in-liquid samplers (PILS). Cloudwater samples obtained from PILS will also be of use to infer water-soluble organic molar mass and surface tension from CCN activity measurement [15, 10]. Organic hygroscopic properties that constrain droplet growth, may be measured by *i*) a Hygroscopic Tandem Differential Mobility Analyzers (HTDMA) or with *ii*) a humidograph system that exploits light scattering data at sub-saturated relative humidities, e.g., [40, **?**]. The growth parameters are subsequently applied to supersaturated conditions for CCN estimates [40, **?**, 185]. Incorporating organic surface tension depression will also improve predictions [33]. As suggested by [196] and [13], in polluted cases a more robust closure may be achieved by including the effects of growth kinetics. Utilizing several or any combination of these methods can achieve closure to within reasonable uncertainty [217, 52, **?**, 136].

Many closure studies are ground based measurements, e.g., but not limited to [30, 165, 217, 26, 136, 52, 25, 33, 161], a few airborne CCN measurements have been presented [185, 186, 36], and even fewer with fast time resolved measurements employing a Continuous-Flow Stream-wise Thermal Gradient CCN Counter (CFSTGC) [207]. For this study, airborne CCN concentrations were measured with a CFSTGC in Houston, Texas, USA, an urban and industrial area dominated by sulfates and organics [218, 63]. The evolution and ageing of CCN in plumes are presented. The measurements are compared to predictions that incorporate mixing state assumptions and measurements of aerosol size, bulk and size-resolved chemical composition. Droplet size data is presented and growth kinetic behavior is qualitatively assessed. Lastly, we determine the simplest of experimental, sampling techniques and modeling schemes that would best characterize and predict urban CCN concentrations.

7.2 Observational Data Set and Instrumentation

7.2.1 Study location and Flight Trajectories

The Texas Air Quality Study (TexAQS) and Gulf of Mexico Climate Change Study (GoMACCS) of 2006 (the second in the TexAQS series) used several platforms (e.g., ground based, airborne, ship, and satellite measurements) to probe the atmospheric chemistry and understand the transport of pollutants in the eastern Texas and Northern Gulf of Mexico region (Fig. 34). Among these platforms, the National Oceanic and Atmospheric Administration (NOAA) WP-3D aircraft explored physical and chemical aerosol characteristics of pollutants during the months of September through October in 2006.

The studied region is characterized by a strong petrochemical, industrial and urban influence; the Houston ship channel hosts several petrochemical refineries and numerous powerplants (e.g., Parish, Big Brown, Limestone) can be found in the Houston and Dallas metropolitan region (Fig. 34). Like other urban environments, much of the aerosol is dominated by sulfates and organics [218]. Specifically, the work of [63], simulate aerosol formation using the U.S Environmental Protection Agency's models-3 Community Multiscale Air Quality model (CMAQ) and ground-based and aircraft aerosol measurements of TexAQS 2000, predict roughly 30% sulfate, 32% organics (including elemental carbon (EC)) in the particulate phase. Roughly 10% ammonium is also found in the total PM2.5 mass. As a result the organic component are a significant component in urban aerosol and can potentially alter ideal CCN behavior. We report CCN measurements for 10 flights that characterized aerosol over the eastern Texas during the months of the mission and highlight several findings from a few of these days.

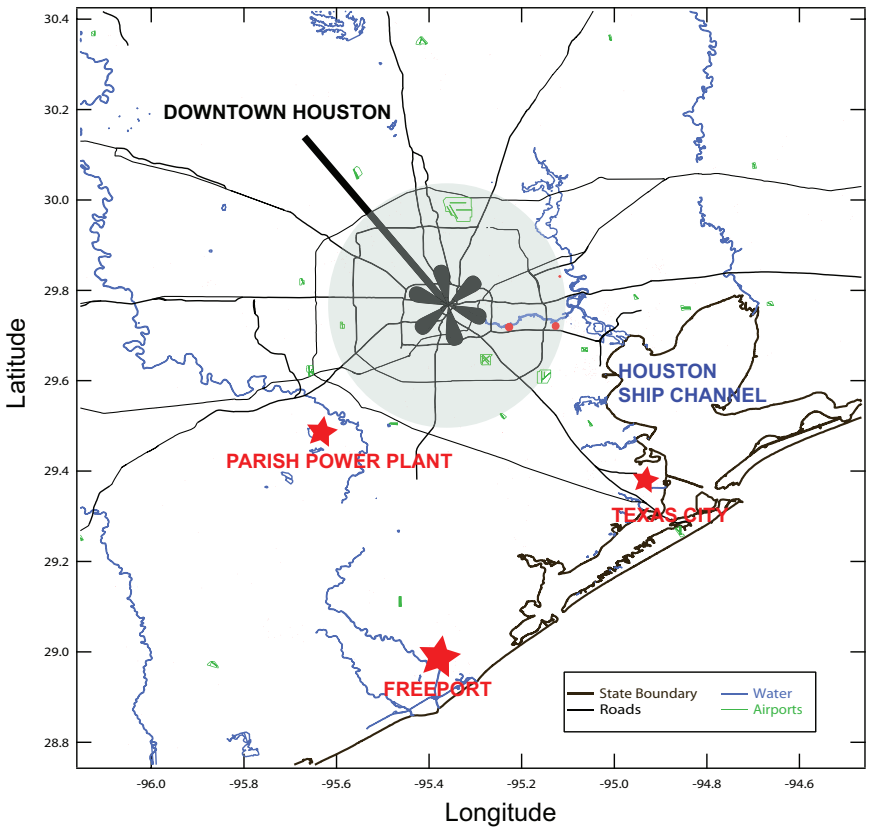

Figure 34: East Texas and Gulf of Mexico Region Explored by the NOAA WP3-D Aircraft during TEXAQS 2006. Key sources of industrial plumes are highlighted (e.g, power plants and the Houston Ship Channel. Research Flight 3 also explored aerosol Northward, in the Dallas Metropolitan area and influenced by large power plants not shown on the map

Table 29: Research Flights Studied in TEXAQS CCN Closure.

Research Flight(#)	Date	Aerosol Influences	Wind Direction	Instrument $\Delta T \pm 1^{\circ}$K	Average $s \pm 0.01\%$
1	September 20	Beaumont Port Arthur, Houston, Urban, Parish Power Plant, Isolated refineries	From the East	4.2°K	0.23%
2	September 21	Texas City, Houston Urban Plume	From the South	4.2°K	0.23%
3	September 25	Dallas, Houston Urban Plume, Big Brown and Limestone Power Plants emission characterization and chemical processing	From the North	5.2°K, 7.0°K	0.28%, 0.38%
4	September 26	Houston Urban Plume and Industrial Sources, Parish Power Plant, Beaumont-Port Arthur, Lake Charles emission characterization and chemical processing	From the North	5.2°K, 7.0°K	0.28%, 0.38%
5	September 27	Houston Urban Plume and Industrial Sources, Parish Power Plant	From the South West	5.2°K, 7.0°K	0.28%, 0.38%
6	September 29	Houston Urban and Industrial Parish Power Plant Emission characterization, chemical processing into the night	Light winds, from the East switching to the South	5.2°K, 7.0°K,	0.28%, 0.38%
7	October 05	Houston Urban and Industrial, Parish Power Plant Plume, Chemical Processing and Transport	Light winds, from the North East	5.2°K, 7.0°K	0.28%, 0.38%
8	October 06	Houston Urban and Industrial, Parish Power Plant Plume, Chemical Processing and Transport	From the North East	5.2°K, 7.0°K	0.28%, 0.38%
9	October 08	Houston Urban and Industrial Parish Power Plant Plume Emission Characterization, Chemical Processing and Transport into the night	Light winds, from the East	5.2°K, 7.0°K	0.28%, 0.38%
10	October 10	Oklaunion Power Plant, Near Vernon, Texas Emission characterization, chemical processing into the night	From the North to North West	5.2°K, 7.0°K	0.28%, 0.38%

7.2.2 Low Turbulence Aerosol Sampling Inlet

Aerosol instrumentation aboard the WP-3D sampled from a low turbulence inlet (LTI) [96, 213]. The LTI produces a laminar deceleration of the airstream with calculable effects on the particle concentrations. There is a potential for inertial enhancements of particle concentrations with the LTI and particle losses within the tubing however these issues are nominal for submicron aerosol measurements [213, 24].

7.2.3 Aerosol Size Measurements

Three instruments, coupled with a nonlinear inversion algorithm [132], measure the aerosol dry size distribution from from 0.003 to 8.3 μm diameter at a rate of 1 Hz aboard the aircraft. The measurement and analysis technique are identical to that employed aboard WP3-D during the New England Air Quality Study (NEAQS) of 2004 [24]. As in NEAQS 2004, the submicron urban aerosol dominates the particle number and surface area. The instrument specifically used to measure the ultra-fine particles (diameters < 0.1 μm), is composed of five condensation particle counters (CPC). The sample flowrate was maintained at 45 cm^3 s^{-1} and the sample air was warmed to 35 °C prior to detection, reducing the relative humidity (RH) for more than 90% of the samples to $<$ 50% RH. Size distributions were derived from the observed concentrations in the five size classes. Characterized with a 50% detection efficiency, the submicron aerosol is classified at 0.004, 0.008, 0.015, 0.030, and 0.055 μm sizes. Particles size distributions within the fine mode were classified with a second instrument, a modified Lasair 1001 laser optical particle counter (OPC, Particle Measuring Systems Inc., Boulder, CO, USA). Monodisperse aerosol were size selected in 64 size bins over a diameter range from 0.12 to 0.95 μm sampled at 5 cm^3 s^{-1}. A robust description of the instrument methodology and data analysis is provided in [24].

7.2.4 Black Carbon and Carbon Monoxide Measurements

Carbon monoxide (CO) and black refactory elemental carbon (BC) are anthropogenic tracers that can be used to quantify the origin of air mass in urban regions. BC aerosol, that is generated from fossil fuel and biomass burning emissions, is measured by a Single-Particle Soot Photometer (SP2). The SP2 uses an intense laser beam to vaporize the particles and detect the wavelength of resolved thermal radiation emissions to provide qualitative information on the BC mass of an individual particle in the size range of 0.2-1 μm. [178, 21, 195, 71]. CO is also measured aboard the aircraft every 1 second and reported in terms of ng m^{-3} [94].

7.2.5 Size Resolved Chemical Composition Measurements

The Aerodyne aerosol mass spectrometer (AMS), operated in mass spectrum mode measures size-resolved mass distributions and total mass loadings of non-refractory chemical species from submicron particles [102, 5, 103]. Within the instrument, the sampled particles are focused into a vaporizer located within the electron impaction ionization source region of a quadrupole mass spectrometer. When it is operated in the mass spectrum mode, mass spectra from m/z 1300 can be collected from several particles with good time resolution without particle size information. By extracting the mass spectral ion signals for various species, it has been shown to yield quantitative aerosol compositions for sulphate, nitrate, ammonium and total organic particulate matter [3, 4, 18, 177]. As expected the dominate composition in the fine particulate mode are sulfates and organics in the Eastern Texas Region. For our analysis, only soluble volume fraction, and not size information is extracted and applied to CCN closure.

7.2.6 CCN Measurements

A Continuous-Flow Streamwise Thermal Gradient CCN (CFSTG) counter developed by Droplet Measurement Technologies (DMT) measured CCN concentrations aboard

the NOAA WP-3D aircraft. Within the DMT CFSTG instrument, supersaturation, s is generated by applying a constant temperature gradient to the instrument walls; the difference in thermal and water vapor diffusivity generates a constant s at the centerline [164, 122, 168]. A heat transfer and fluid dynamics model of the CCN instrument developed in [141] and [122] is used to precise the actual s, caused by variations that arise from temporal and pressure fluctuations (mainly due to changes in altitude during flight) in the instrument profile . Calibration data with $(NH_4)_2SO_4$ is used to characterize the heat transfer across the wetted walls of the instrument and the fitted parameters are subsequently applied to calculate instrument s [122].

The DMT CFSTG CCN counter sampled from the LTI at a flow rate 1000 cm^3 min^{-1} and is capable of measuring CCN concentrations and droplet sizes between controlled supersaturations at 0.07% and 3% at a rate of $\sim$ 1 Hz [164]. To avoid instrument overheating during the hot Texas summer, the temperature gradient, ΔT was maintained below $<\sim$ 10 °K. During the earlier flights of the TexAQS 2006 mission, the temperature gradient, ΔT was kept constant at 4.2 °K (Table 29). For the later research flights, three different ΔT were cycled in 3 minute increments to explore measurements at different s. The time required to achieve temperature stability within the instrument for the smallest ΔT exceeded 2.5 minutes; thus the 30 second averaged data from the lowest s has been excluded from the following analysis.

7.3 Data Analysis and CCN Prediction

CCN closure was calculated using DMT CFSTG CCN measurements at 1 Hz, dry particle size distribution measurements at 1 Hz, and aerosol mass spectrometry (AMS) measurements at 0.1 Hz. Data from the CCN counter were filtered to remove temperature and pressure transients. Temporal variation between the measured CCN concentrations and particle size distributions arising from different instrumental residence times was accounted for by visually aligning the measured CCN counts to the

total CN counts as obtained from the integrated size distributions. It was observed that the size distribution measurements usually led the CCN measurements by approximately 10-15 seconds. For the closure analysis, all measurements were averaged over 30-second intervals to further reduce data noise.

7.3.1 The Application of Traditional Köhler Theory

Köhler theory is used to predict the fraction of the total particle distribution that is CCN active at a given supersaturation for particles of known composition. The critical activation diameter, d_c, is a function of the ability of aerosol composition to add solute (Raoult term) and reduce curvature (Kelvin Term) to depress the vapor pressure equilibrium at the droplet surface. d_c is calculated at each measurement timestep using Eq. 32 [136, 179].

$$d_c = s^2 \frac{27}{256} \left(\frac{\rho_w R T}{M_w \sigma} \right)^3 \left(\frac{\rho_s}{M_s} \frac{M_w}{\rho_w} \nu_s \varepsilon_s \right)^{-1/3} \tag{32}$$

where supersaturation, s, is that of the CCN counter at each timestep, as determined from instrument calibrations with $(NH_4)_2SO_4$. R is the universal gas constant, T is the average instrument temperature, σ is the droplet surface tension at the point of activation, M_s is the molar mass of solute, M_w is the molar mass of water, ρ_w is the density of water, ν_s is the effective vant Hoff factor, and ε_s is the volume fraction of soluble solute.

ε_s, is calculated as follows;

$$\varepsilon = \frac{\frac{m_s}{\rho_s}}{\frac{m_s}{\rho_s} + \frac{1-m_s}{\rho_s}} \tag{33}$$

where m_s is the soluble mass fraction and ρ_s is the density of the soluble components. The predicted CCN concentration is the sum of particles measured in the dry size

distributions whose diameters are greater than or equal to the critical activation diameter; the sum is subsequently compared to the measured CCN concentrations to determine the degree of closure. 5 different schemes are employed, (PRSULFATE, BULK-EX, BULK-INT, SR-EX, SR-INT), that assume different mixing states and soluble properties of the aerosol size distribution as outlined in Sections 7.3.1.1, 7.3.1.2, 7.3.1.3 and 7.3.1.4. The PRSULFATE scheme assumes that all aerosol are soluble and have properties of sulfate (M = 132 g mol $^{-1}$, ρ = 1500 kg m $^{-3}$). In the following closure methods, organics are assumed to be effectively insoluble and not surface-active (σ = 72 m Nm^{-1}, the value of water); although, this latter assumption can be relaxed by incorporating the empirically-determined surface tension depression of the organics obtained, for example, from measurements of PILS samples [10]. Furthermore, the soluble inorganic fraction is assumed to be entirely composed of ammonium sulfate with an average effective van't Hoff factor of 2.5 [23] (measured concentrations of other inorganic in the aerosol phase, such as nitrate, were observed to be negligible compared to ammonium and sulfate fractions). The aerosol composition are treated as either internal or external mixtures. Internally mixed aerosol are defined by homogeneous composition whereas externally mixed aerosol are considered to be of heterogenous nature and can be treated as completely separate insoluble and soluble fractions; the terminology can be applied to entire aerosol size distribution or individual bin sizes as follows:

7.3.1.1 BULK-EX

The BULK-EX scheme assumes an external aerosol mixing state and applies bulk composition measurements to the Köhler theory model. At each timestep, d_c, is calculated first by assuming $\varepsilon_s = 1$ in Eq. 33. The average mass fractions of soluble salts,m_s, and insoluble organics,$(1-m_s)$, from the entire size distribution are obtained from AMS data and ε_s is calculated using Eq. 33. The total number of particles where

$d > d_c$ are multiplied by ε_s to obtain the predicted CCN number at each measurement timestep.

7.3.1.2 BULK-INT

The BULK-INT scheme assumes an internal aerosol mixing state and applies bulk composition measurements to the Köhler theory model. At each timestep, the average mass fraction of soluble salts,m_s, and insoluble organics,$(1 - m_s)$, from the entire size distribution are obtained from AMS data and ε_s is calculated using Eq. 33. Subsequently, d_c, is calculated using Eq. 33. The predicted CCN number is then the sum of all particles in size bins where $d > d_c$.

7.3.1.3 SR-EX

The SR-EX scheme assumes an external aerosol mixing state and applies size-resolved composition measurements to the Köhler theory model. At each timestep, d_c, is calculated first by assuming $\varepsilon_s = 1$ in Eq. 33. The average mass fractions of soluble salts,m_s, and insoluble organics,$(1 - m_s)$, of size $d > d_c$ are determined and ε_s is calculated for each of these bins. The predicted CCN concentration is the sum of the number of particles in each bin size $d > d_c$ multiplied by the ε_s of that each sizebin.

7.3.1.4 SR-INT

The SR-INT scheme assumes an internal aerosol mixing state and applies size-resolved composition measurements to the Köhler theory model. The average mass fractions of soluble salts,m_s, and insoluble organics,$(1 - m_s)$, are determined for all size bins and ε_s is calculated for each of these bins. Subsequently, d_c, is calculated for every size bin with Eq. 33. The predicted CCN number is then the sum of all particles in size bins where $d > d_c$.

7.3.2 Closure Agreement: Predictions vs Observations

Predictions are presented using the 5 schemes described above and are compared to observations graphically. The extent of closure agreement (excellent agreement being predicted equal to measured values and within 5% uncertainties) is reported in terms of two error metrics, the Normalized Mean Error (NME) and the Normalized Mean Bias (NMB) (Table 30). NME and NMB are described as follows;

$$NME = \frac{\sum_{i}^{n} |P_i - O_i|}{\sum_{i}^{n} O_i} \quad \texttt{and} \quad NMB = \frac{\sum_{i}^{n} (P_i - O_i)}{\sum_{i}^{n} O_i} \tag{34}$$

where P_i is each predicted value and O_i is the measurement at each timestep, i. The NME indicates the degree of scatter between predictions and observations (small values suggest little if any scatter) and the NMB shows the degree of systematic errors (biases) between the predicted and measured values; a negative NMB value shows that the model underpredicts and positive values suggests overprediction. Predictions are calculated for dates where size distribution and chemical composition data are available.

7.4 Results and Discussion

Plumes within the Houston area can be broad and air masses may are comprised of a mixture of urban, ship channel, biogenic, and power point plume influences. The background air in the region is a "soup" of pollutants from these various sources that make it difficult to quantitatively assess the ageing of the aerosol. Unlike ground based measurements, the aircraft's sampling strategy at different points downwind of the plume does not correspond to a single time of emission; one transect might intersect a plume that was emitted during morning rush hour, and the next farthest transect might have been emitted in the early morning hours. As a result we focus on a few case studies and highlight significant shifts in the evolution of CCN downwind

Table 30: Closure Analysis for TEXAQS 2006 Data Set.

Research Flight	Date	s	Error	PRSULFATE	SR-INT	SR-EXT	BULK-INT	BULK-EXT
#1	September 20	0.23%	NME (%)	17.4	NAMS	NAMS	51.3	79.1
			NMB (%)	5.66	NAMS	NAMS	-51.3	-79.1
#2	September 21	0.23%	NME (%)	22.0	NAMS	NAMS	32.4	60.7
			NMB (%)	5.12	NAMS	NAMS	-27.2	-60.5
#3	September 25	0.28%	NME (%)	39.3	57.3	80.7	50.6	78.8
			NMB (%)	-22.1	-56.1	-80.7	-49.4	-78.8
		0.38%	NME (%)	38.0	54.3	82.6	47.6	79.5
			NMB (%)	-21.5	-53.3	-82.6	-47.5	-79.5
#4	September 26	0.28%	NME (%)	18.3	53.6	76.2	40.0	68.7
			NMB (%)	0.06	-53.2	-76.2	-39.4	-68.7
		0.38%	NME (%)	15.7	49.8	77.0	41.2	71.4
			NMB (%)	-11.5	-49.7	-77.0	-41.0	-71.4
#5	September 27	0.28%	NME (%)	11.0	35.0	67.3	30.1	67.2
			NMB (%)	-2.68	-34.7	-67.3	-29.7	-67.2
		0.38%	NME (%)	9.47	34.7	69.7	29.8	68.2
			NMB (%)	-6.58	-34.4	-69.7	-29.8	-68.2
#6	September 29	0.28%	NME (%)	10.8	36.5	69.8	21.7	59.1
			NMB (%)	7.79	-36.0	-69.8	-20.9	-59.1
		0.38%	NME (%)	7.96	37.4	72.0	29.0	63.6
			NMB (%)	-1.77	-37.3	-72.0	-28.8	-63.6
#7	October 05	0.28%	NME (%)	12.0	33.9	68.3	21.3	55.4
			NMB (%)	-7.56	-33.7	-68.3	-21.0	-55.4
		0.38%	NME (%)	11.8	33.5	71.9	23.0	58.4
			NMB (%)	-9.29	-33.3	-71.9	-22.5	-58.4
#8	October 06	0.28%	NME (%)	10.28	NAMS	NAMS	22.3	68.4
			NMB (%)	7.79	NAMS	NAMS	-21.5	-68.4
		0.38%	NME (%)	7.52	NAMS	NAMS	25.9	69.7
			NMB (%)	-1.59	NAMS	NAMS	-25.7	-69.7
#9	October 08	0.28%	NME (%)	7.48	NAMS	NAMS	21.0	63.6
			NMB (%)	-1.03	NAMS	NAMS	-21.0	-63.6
		0.38%	NME (%)	5.14	NAMS	NAMS	20.3	64.1
			NMB (%)	-2.60	NAMS	NAMS	-20.3	-64.1
#10	October 10	0.28%	NME (%)	19.5	NAMS	NAMS	7.61	54.5
			NMB (%)	19.3	NAMS	NAMS	-1.81	54.5
		0.38%	NME (%)	10.5	NAMS	NAMS	9.40	55.5
			NMB (%)	9.71	NAMS	NAMS	-8.56	-55.4

NAMS = No AMS Data Available

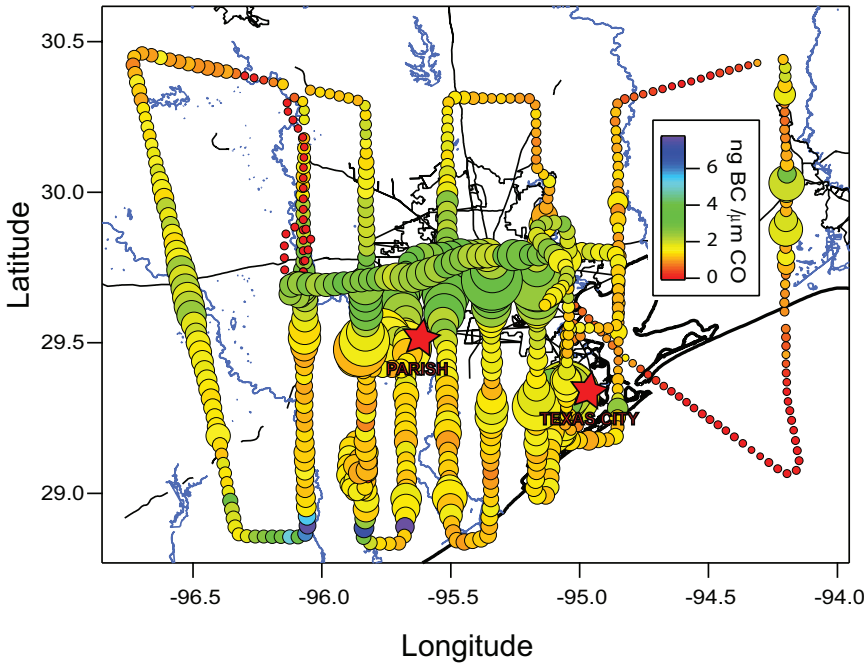

Figure 35: Flight Track of Research Flight #1 on September 20. Aircraft Position is plotted as a function of CN concentrations and the BC/CO ratio. The marker size reflects total CN concentrations and the WP3-D transects plumes blown by winds from the east.

of plumes. Closure from the different models schemes is used to quantify the extent to which horizontal mixing of existing pollutants effect freshly emitted plumes and CCN behavior.

7.4.1 Research Flight #1 September 20

Research flight #1, like flights 1-5, 7 and 8, was a 6.5 hour flight that focused on the daytime urban atmospheric chemistry and probed aerosol characteristics during the height of the boundary layer. The WP3-D, departed in the eastward direction from the field base at 3:54:00PM Coordinated Universal Time (UTC), traveling westward in a zig-zag flight pattern across industrial areas in the region. The aircraft transects two significant plumes (aerosol concentrations $> 50{\times}10^3$ cm^{-3}) transported from east to west across the region (Fig. 35). The highest CN concentrations are observed exiting the ship channel and downtown areas. The time series data indicates that

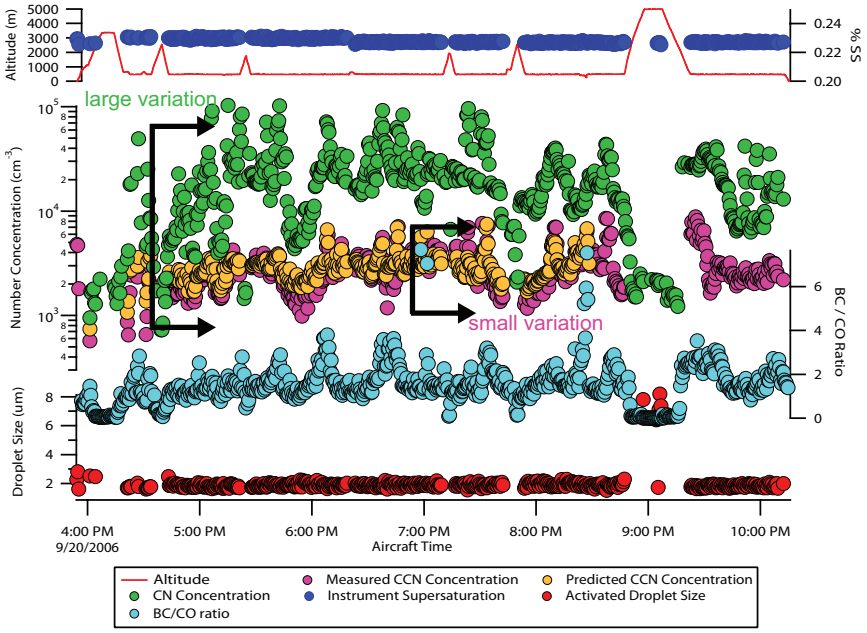

Figure 36: Research Flight #1. September 20 Time Series plot . Aircraft altitude, instrument supersaturation, BC/CO, measured CN and CCN concentrations and droplet size are plotted as a function of UTC Time. Predicted values are calculated with the PRSULFATE scheme.

the aerosol concentration varies greatly during the flight (on the order of 1 order of magnitude, $\sim 10^4$ to $\sim 10^5$, Fig. 36). Yet CCN concentrations remain fairly constant and account for roughly 10% (and even less in freshly emitted plumes) of the total CN population. It is presumed that much of the aerosol number on this day is dominated by sulfates in the superfine mode that are smaller than d_c, the organic components are more likely to have influence in size ranges $d > d_c$.

In the absence of size-resolved chemical composition measurement, the best closure is achieved using the PRSULFATE prediction scheme (Table 30). Small changes in instrument s during the flight (Δs <0.01%, Fig. 36) do not significantly affect measurments, however as the aerosol transects plumes and CN counts increase, closure agreement shifts (Fig. 37); aerosol in the background "Houston soup" treated as pure sulfate is overpredicted and contributes significantly to the positive PRSULFATE 5.66% NMB. Even though good closure is achieved (to within 20% error), better

closure may be achieved if background organic aerosol are not treated as completely soluble with properties of sulfate. At the other limit, treating the contributions of organics as insoluble (BK-INT and BK-EXT) severely underpredicts CCN counts and worsens predictions (NMB and NME < -50%) for all measured aerosol.

The aerosol measured in the downtown and ship channel must therefore be water-soluble. The external mixing state assumption worsens predictions and suggests that for the best closure partially soluble organics must be treated as homogenous mixtures with sulfate. In addition, within plume regions (CN > 50×10^3 cm^{-3}), the PRSULFATE closure agreement is best (Fig. 37). This may indicate that enhanced sulfate number in the superfine mode can act as a coating or facilitate the water-soluble properties (e.g, hygroscopicity, σ) of the organic aerosol. Research flight #1 suggests good closure can be achieved with the simplest of measurements and analysis; the instrument supersaturation is kept constant and size distribution and bulk chemical properties are the only other speciation data measured.

7.4.2 Research Flight #2 September 21

As with research flight #1, flight #2 also characterizes Houston urban and ship channel plumes (Fig. 38). The total CN concentrations are significantly higher in flight #1 than #2 (Figs. 36 and 39), for the aerosol plume intensities are greater. Research flight #2 is of particular interest because an obvious shift in CCN behavior is observed upwind of the plume after 7:00PM UTC (Figs. 36). Early on and close to the plume sources, CCN concentrations remain fairly stable and do not follow variances in CN concentration. As assumed in flight #1, close to the source the dominate mode of particles are ultrafine and not of relevant CCN size at the measured s. After significant dilution effects downwind (observed by the decreasing CN concentration trend in transects of the plume, Fig. 39), measured CCN concentration increase and have similar variance as CN concentrations. The closer agreement between measured CN

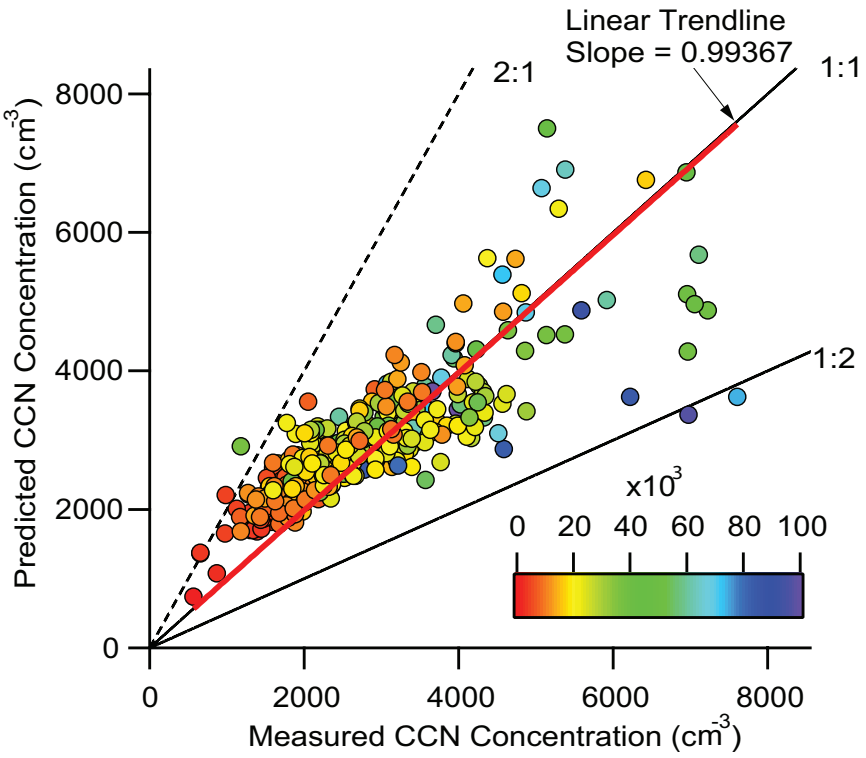

Figure 37: Research Flight #1. September 20 PRSULFATE Closure Plot. Predicted versus Measured values are plotted as a function of CN concentrations and dashed lines represent 50% uncertainty

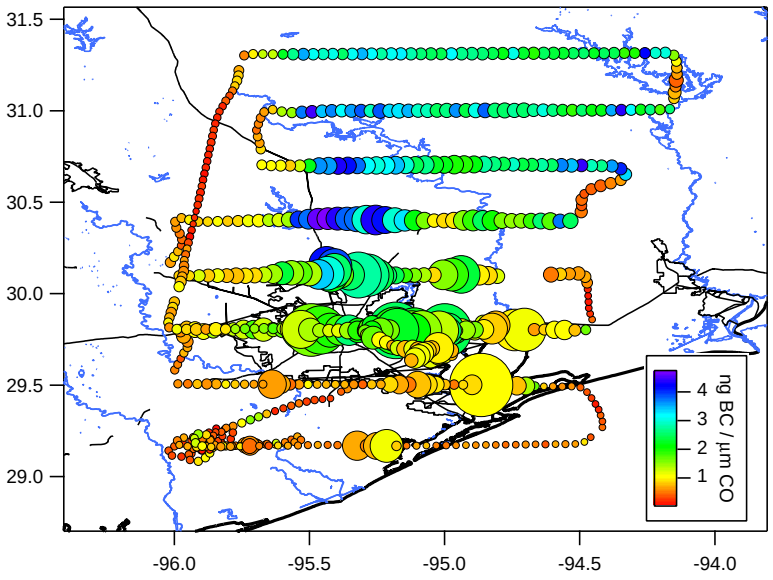

Figure 38: Flight Track of Research Flight #2 on September 21. Aircraft Position is plotted as a function of CN concentrations. The WP3-D transects plumes blown by winds from the south.

and CCN number concentrations indicates that aerosol have grown, the size distribution has shifted to the CCN relevant sizes, and ageing in the form of coagulation or either horizontal mixing with background airmass of larger aerosol sizes has occurred downwind of the plume.

The overall closure for flight#2 is good assuming PRSULFATE (NMB= 5.12%, NME= 22.0% and Fig. 40a) and worsens with other schemes that assume an insoluble organic component. Again the CCN measured in background air tend to overpredict suggesting that the organics in the background are partially soluble or are most likely of larger molecular weight than $(NH_4)_2SO_4$. Low CCN concentrations (< 1500 # cm^{-3}) regardless of CN concentrations, measured close to the source agree well with PRSULFATE, BK-INT, and BK-EXT predictions; though size-resolved composition is unavailable, it can be presumed that the organic component is not as influential earlier on in the plume transects and becomes more so as horizontal mixing and dilution processes from the background "soup" influence the plume.

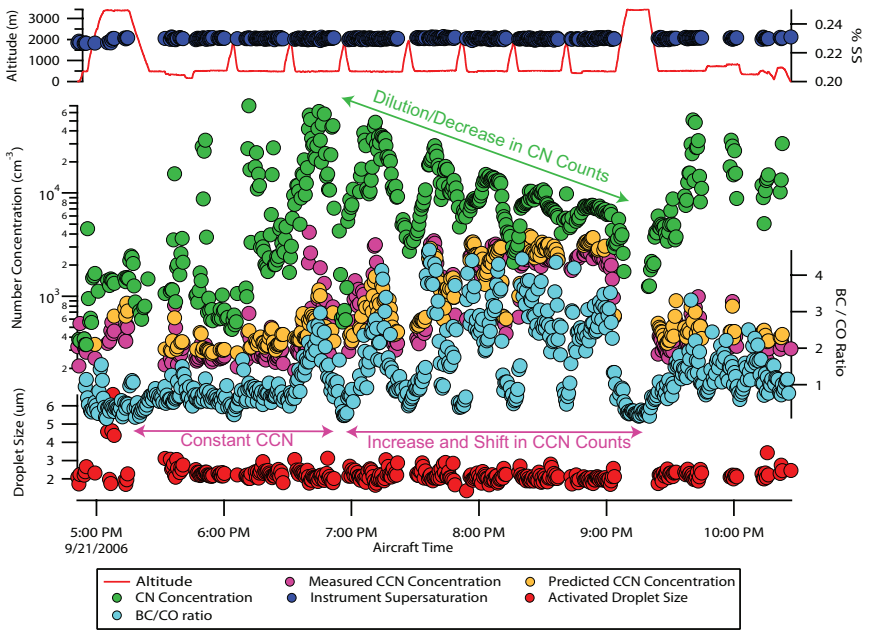

Figure 39: Research Flight #2, September 21 Time Series. Aircraft altitude, instrument supersaturation, measured CN and CCN concentrations and droplet size are plotted as a function of UTC Time. Predicted values are calculated with the PRSULFATE scheme.

7.4.3 Research Flight #3 September 25

During research flight #3, the WP3-D aircraft first headed north to Dallas and then made its way south towards the Houston metropolitan area. The daytime flight probed the mid-morning aerosol in the Dallas metropolitan area, emissions from the larger power plants in the area (Big Brown and Limestone) and the afternoon aerosol composition in the Houston Metropolitan. The aircraft transected plumes several times, as seen by the sharp increases in the total CN concentrations in Fig. 41 and Fig 42. During this (and subsequent flights) the CFSTGC was operated at multiple supersaturations. The measured CCN concentrations vary significantly and track the changes in total aerosol concentration (Fig 42) for much of the aerosol in the plume are of CCN relevant sizes.

CCN predictions are available for the leg of the flight towards and leaving Dallas area (between 4:30 and 7:30 UTC). CCN predicted by the PRSULFATE scheme

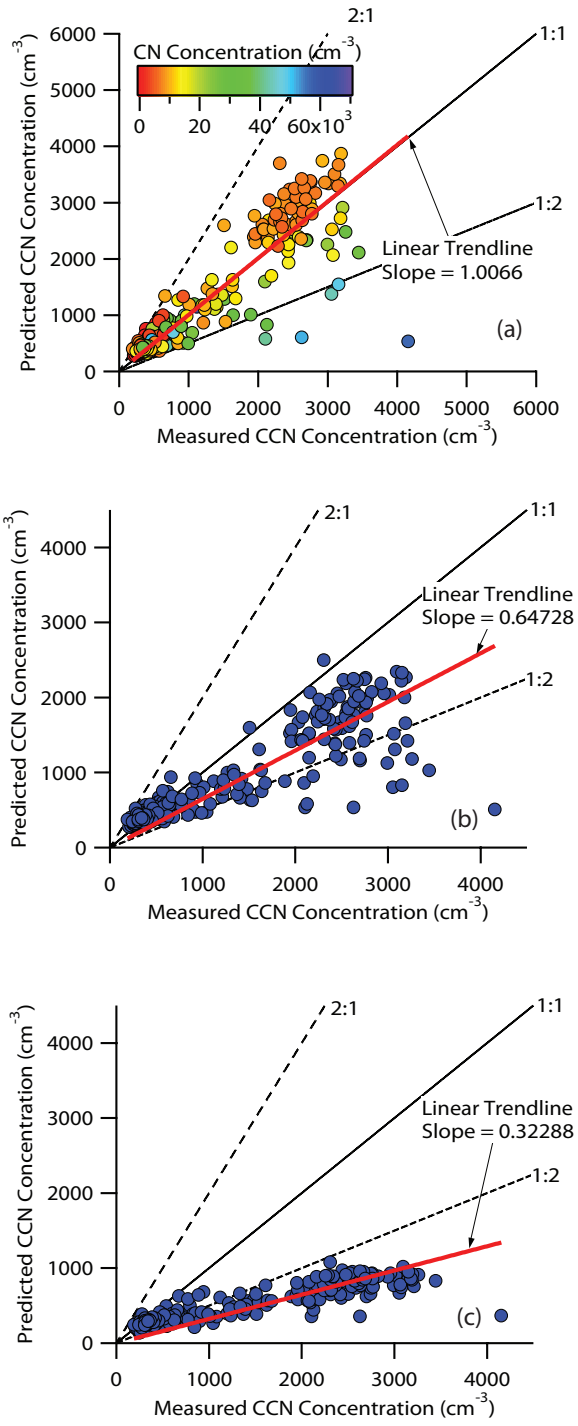

Figure 40: Research Flight #2. September 21 Closure Plot. Predicted versus Measured values are plotted as a function of CN concentrations and dashed lines represent 50% uncertainty (a)PRSULFATE (b)BK-INT (c)BK-EXT schemes are shown.

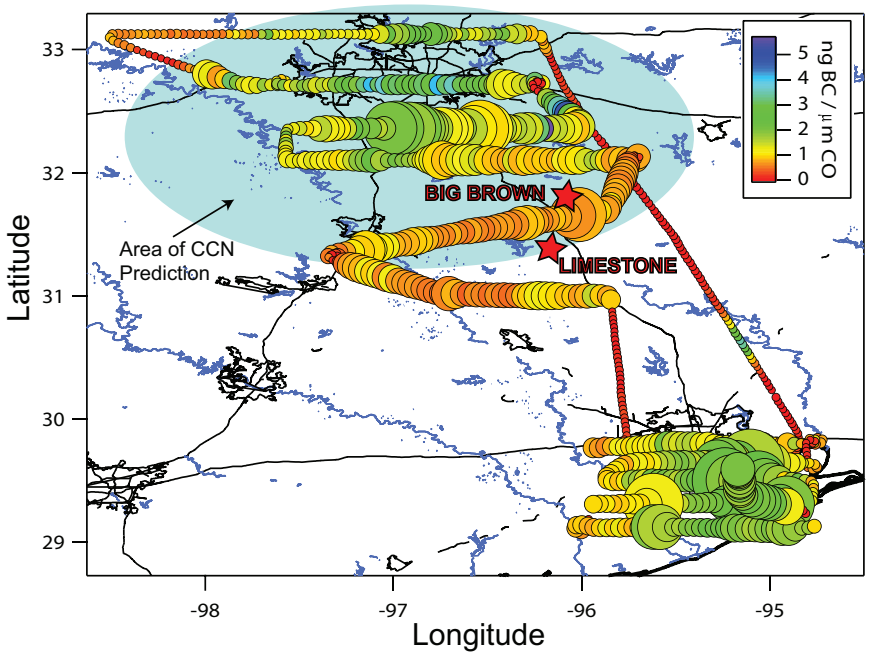

Figure 41: Flight Track of Research Flight #3 on September 25. Aircraft Position is plotted as a function of CN concentrations. Both Houston and Dallas areas are explored and emissions from large power plants (e.g., Big Brown, Limestone) are characterized. The WP3-D transects plumes blown by winds from the North.

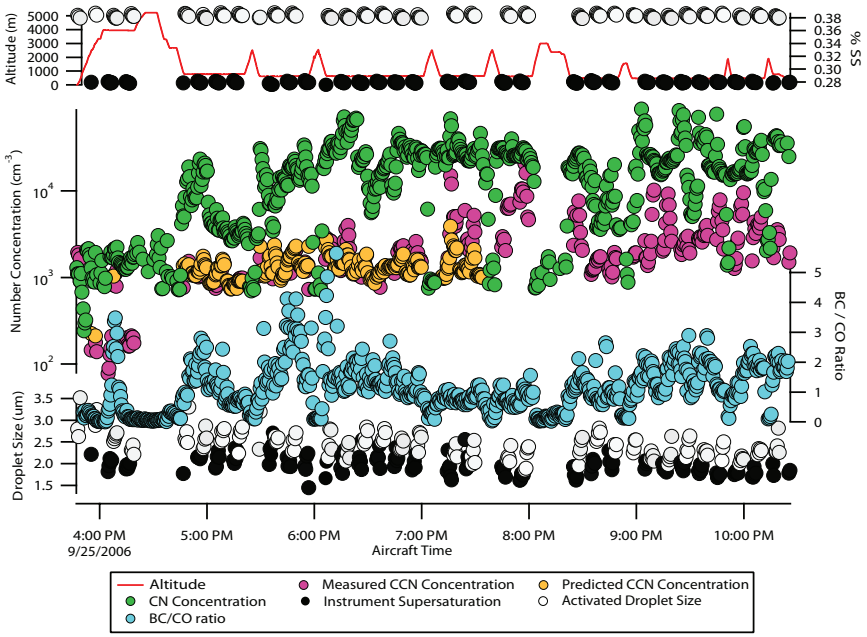

Figure 42: Research Flight #3. September 25 Time Series plot. Aircraft altitude, instrument supersaturation, measured CN and CCN concentrations and Droplet Size are plotted as a function of UTC Time. Predicted values are calculated with the PRSULFATE scheme.

agree well with measurements at low CN concentrations but deviate significantly (sometimes $> 50\%$) for high (CN $> 30\times10^3$ cm^{-3})concentrations (Fig 42).

The PRSULFATE CCN closure underpredicts above 2000 CCN cm^{-3} (Fig 43) but this is independent of instrument s and mostly a result of change in aerosol composition; greater CCN concentrations are expected at higher s, however NME ($\sim$-40% for PRSULFATE) and NMB ($\sim$-20%for PRSULFATE) are the same at both measured s (Table 30). This plume is transported south and is influenced by the outflow of aerosol produced in Dallas morning traffic, as reflected by BC/CO ratios above 1. The urban Dallas plume CCN that are significantly underpredicted in PRSULFATE are assumed to be completely soluble aerosol and the closure worsens for these aerosol when organic fraction is considered insoluble in the other schemes. In addition, the disassociation of organics is unlikely to surpass sulfate (one of the largest plausible reported values of organic atmospheric HULIS being $\nu = 1.25$ [48, 47]) and the molar

mass of organic component is most likely to be of comparable or larger size. Thus it can be inferred these aerosol contain surfactants and a significant depression in surface tension is required to obtain good closure for these particular aerosol in the Dallas plume.

Applying size-resolved (versus bulk composition) data improves overall predictions by roughly $< 10\%$ (Table 30). The external mixing assumption applied to the Dallas urban outflow significantly worsens predictions, and reinforces the importance of organic CCN as soluble and or surface active components.

7.4.4 Research Flight #4- September 26

Very good closure is obtained for the PRSULFATE case at low s during research flight #4 (NMB = 0.06%, Table 30). Predictions at higher s are accurate ($< 20\%$) but show a significant bias for underprediction. Assuming an insoluble organic fraction or an external mixing state worsens closure and as with flight #3, flight #4 suggests that homogeneous organic/inorganic mixtures play significant roles for enhancing CCN activity. (Fig. 45).

This is best observed in the PRSULFATE case at higher CCN concentrations that are significantly ($> 25\%$) underpredicted. Many of these underpredicted values are within plumes from the Parish Power plant (Figs. 44 and 47). In region 1 of the plume, soluble organic mass dominates (Fig. 46) and PRSULFATE CCN predictions match measurements well. As the aircraft transects plumes in region 2 and 3, two interesting phenomena occur *i.*) sulfate mass in the region of CCN relevant sizes becomes comparable to organic mass (especially for sizes below PRSULFATE d_c, Fig. 46) and *ii.*) measured CCN number increases and rival that of total CN counts ($\simeq 10^4$ cm^{-3}) suggesting an enhanced activity at smaller measured sizes due to a depression in the Kelvin term of the Köhler equation.

The organic in region 2, less than 50 km and measured only 10 minutes downwind,

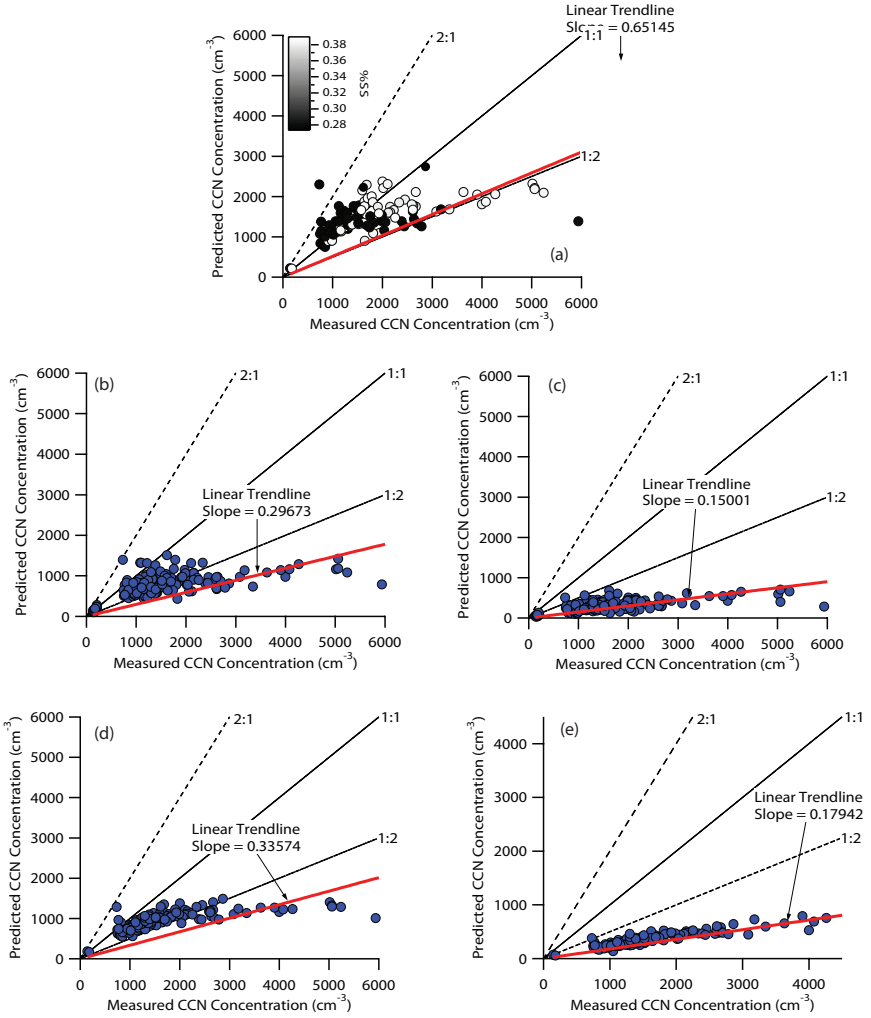

Figure 43: Research Flight #3. September 25 Closure Plot. Predicted versus Measured values are plotted as a function of CN concentrations and dashed lines represent 50% uncertainty (a) PRSULFATE, $s = 0.28\%$ (closed), $s = 0.38\%$(open symbols, (b) SR-INT, (c)SR-EXT (d)BK-INT and (e)BK-EXT are schemes are presented

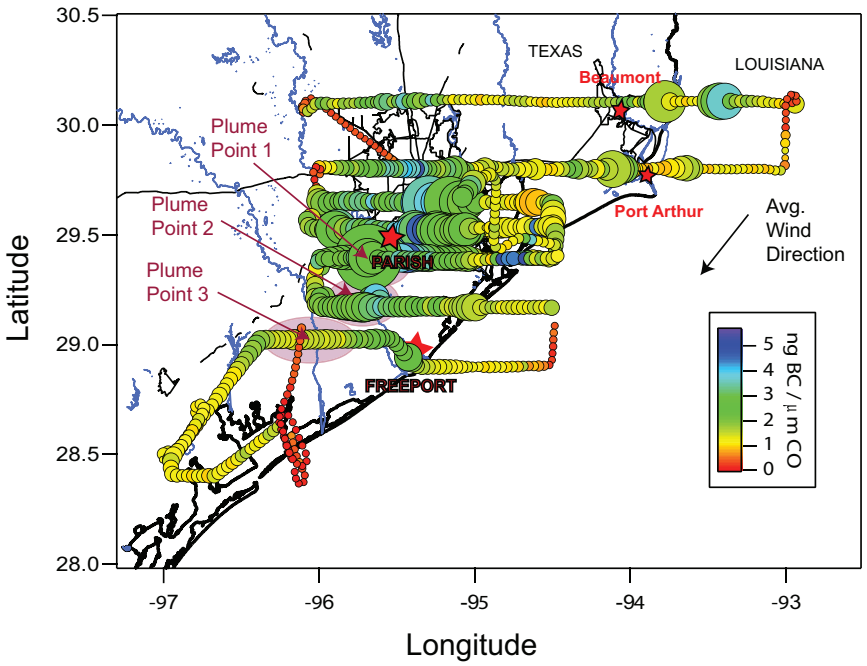

Figure 44: Flight Track of Research Flight #4 on September 26. The marker size reflects CN concentrations as a function of aircraft Position and the color gradient indicates the ratio of BC/CO. The urban Houston region and emissions from the Parish powerplant are characterized. The WP3-D transects plumes blown by winds from the North. Highlighted Areas 1,2 and 3 are characterized between , 19:27-1930, 19:41-19:58, and 20:36-20:47 UTC respectively.

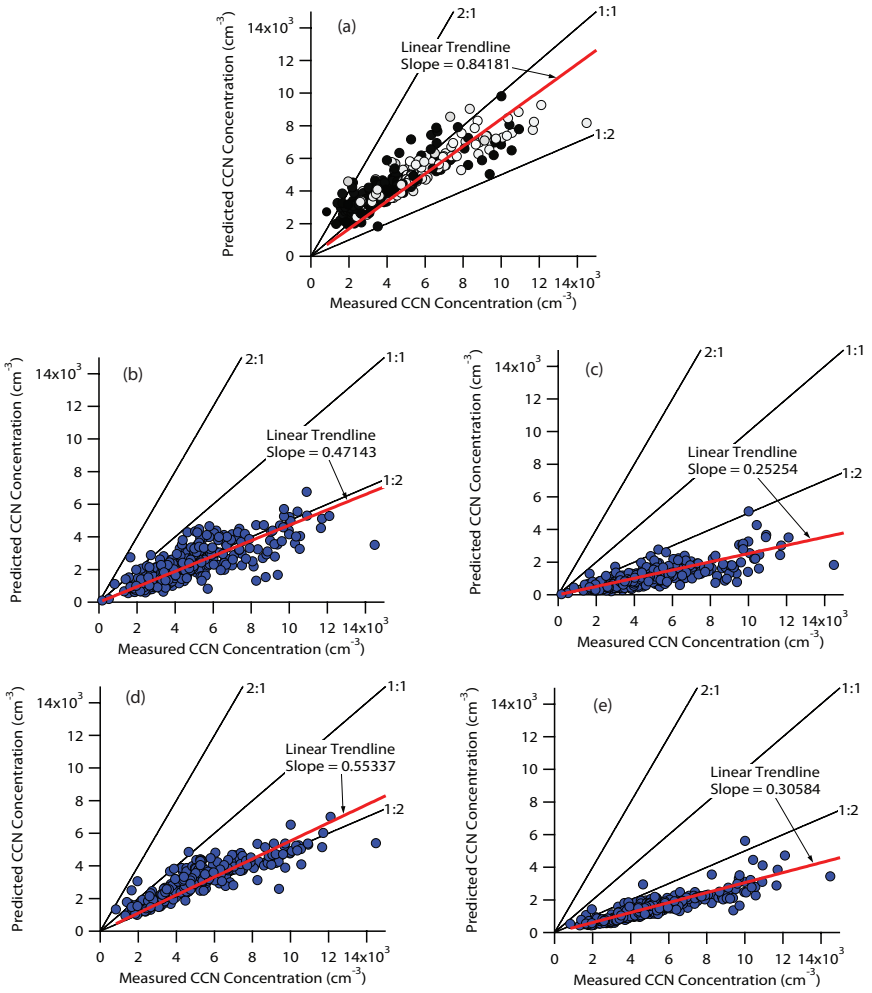

Figure 45: Research Flight #4. September 26 Closure Plot. Predicted versus Measured values are plotted as a function of CN concentrations and dashed lines represent 50% uncertainty (a) PRSULFATE, $s = 0.28\%$ (closed), $s = 0.38\%$(open symbols, (b) SR-INT, (c)SR-EXT (d)BK-INT and (e)BK-EXT are schemes are presented

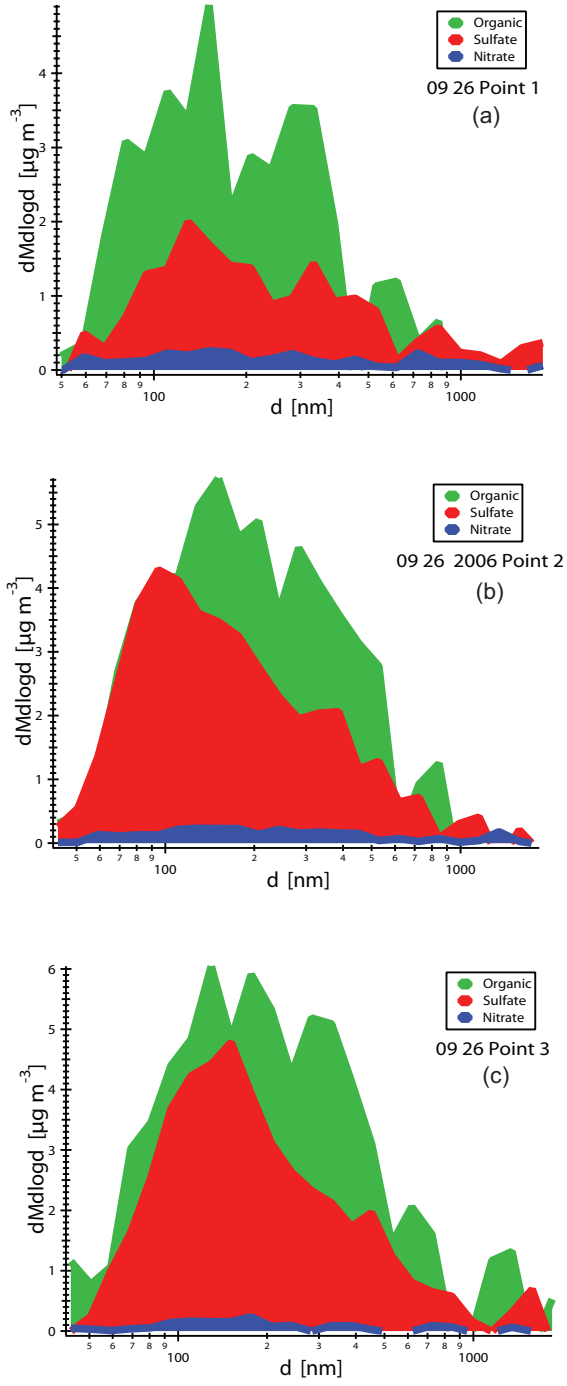

Figure 46: Mass distributions from AMS data in regions 1,2,and 3 of the Parish Power Plant during Research Flight #4. Much of the mass distribution is of CCN relevant sizes; d_c is ∼75 and ∼60 nm for s equal to 0.28% and 0.38%, respectively.

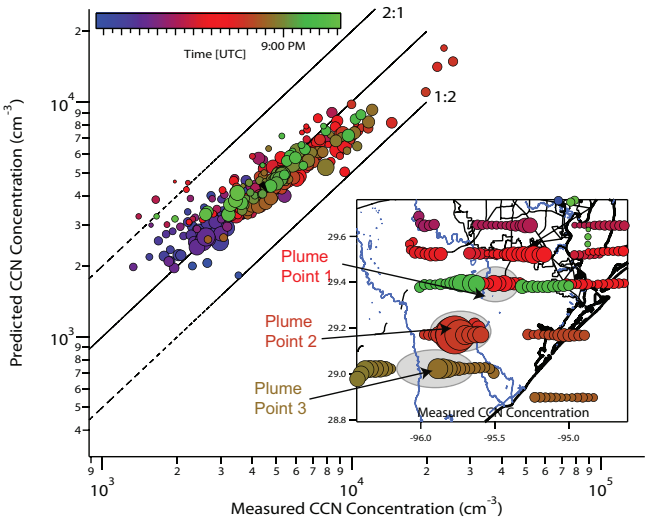

Figure 47: CCN Closure using the PRSULFATE scheme is re-plotted. Marker size is a reflection of measured droplet size. Transition in color reflects Aircraft time of Measurement. The inset graph shows the aircraft position. The Marker size is a reflection of CCN concentrations and the color scheme also reflects Aircraft Time in UTC.

are presumably of similar composition and solubility to region 1. Yet in regions 2 and 3, the sulfate fraction can partition more of these organics to the droplet surface and induce a "salting out effect" that has been previously shown in laboratory experiments to depress surface tension at the droplet surface and enhance CCN activity [111, 16]. The partitioning effect at low s becomes less significant for CCN predictions; solute is dilute at activation and as a result the NMB for low s is close to zero. In addition, measured droplet sizes in regions 2 and 3, especially for higher s where the dissolved solute activates at higher concentrations, are relatively smaller than those measured elsewhere during the flight($D_p \simeq 2$ μm, Figs. 48 and 47). This maybe indicative of film forming compounds that have the potential for slow growth [64].

7.5 Summary and Implications

The Eastern Texas and Gulf of Mexico region is dominated by aerosol composed of sulfate and organic materials. In general, the simplest and best closure scheme

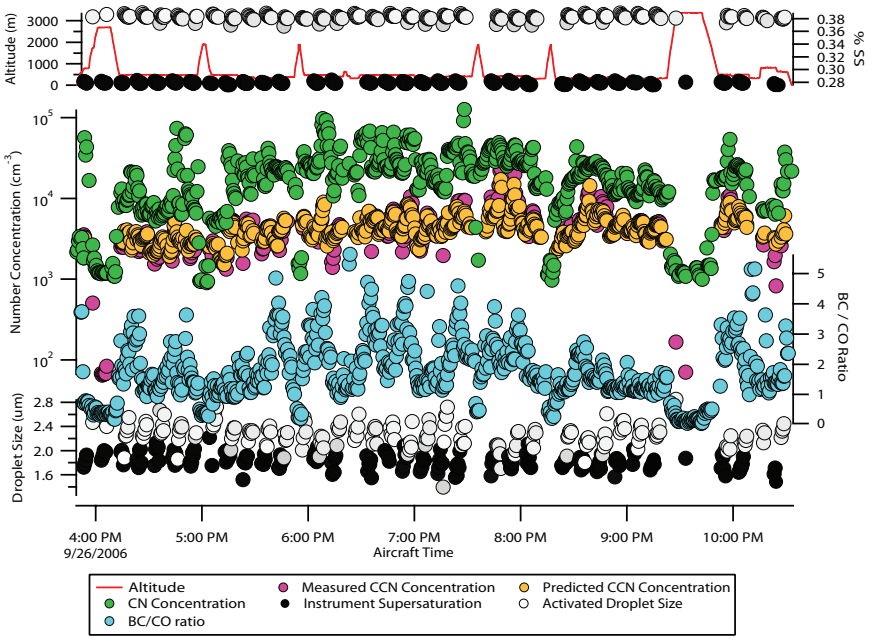

Figure 48: Research Flight #4. September 26 Time Series plot. Aircraft altitude, instrument supersaturation, BC/CO, measured CN and CCN concentrations and droplet size are plotted as a function of UTC Time. Predicted values are calculated with the PRSULFATE scheme.

assumes the aerosol is completely soluble and worsens considerably when organics are presumed to be insoluble. As a result, knowing the hygroscopic and thermodynamic properties of the water soluble organic component (WSOC) in regional urban aerosol will significantly improve CCN predictions. In specific cases we observe deviations from good closure and thus assuming ideal sulfate behavior should not always be applied; for these studies CCN closure will improve with mixing state, size-resolved chemical composition and organic surface tension inputs. In this study, the aerosol composition and CCN behavior close to plume sources differs significantly from the background aerosol masses. Though the age of this industrial "soup" has not been determined, it can significantly affect CCN measurements and predictions downwind of plumes.

Regardless of location, much of the aerosol contain sulfate and organics in the

accumulation mode, and as corroborated by our closure study are most likely internally mixed. More work is required to understand the morphology of the internally mixed aerosol especially as it ages; sulfates have the potential to act as organic aerosol coatings or may be evenly mixed with organics.

For most flights closure at high s is more likely to underpredict than at low s. this trend is consistent with and indicative of partially soluble surface active organic components; ideal models based on Köhler theory whose Kelvin and Raoult terms are more suspectable to changes with higher solute concentrations will show discrepancies in closure. At low s, partially soluble materials will not be overpredicted and at high s more dissolved organic solute can further depress σ and reduce underprediction. Our analysis and study, suggests more airborne measurements of fast-resolved CCN concentrations and WSOC properties are warranted to achieve good closure as a function of plume age.

CHAPTER VIII

FUTURE DIRECTIONS AND IMPLICATIONS

In this thesis we observed the interactions of organic and water vapor via the study of CCN. The wide array of aerosol types studied suggest that organic behavior cannot be easily generalized; age, aerosol mixing state, volatility and even soluble organic fraction can easily alter CCN activity. For example, HULIS observed in biomass burning aerosol could depress surface tension significantly, whereas smaller amounts potentially found in sub-cloud marine aerosol could have little if no effect on droplet surface tension at activation. Thus the question arises – "how much is the right amount?" Measurements of sesquiterpene SOA with several instruments revealed substantial volatility effects and potential instrumentation artifacts whereas no volatility effects were observed in similar experiments of SOA generated from monoterpenes. For water-soluble aerosol studied, droplet growth that differs from $(NH_4)_2SO_4$ is minimal, only significant differences are observed when insoluble non-hygroscopic fractions are present.

As initially stated organic aerosol is complex. Detailed speciation of all interactions is impractical and unwarranted for climate model improvements. Instead, future work should focus on categorizing the different states of aerosol ageing that could be any combination of the identified CCN activity and droplet growth kinetic factors (mixing state, volatility, soluble fraction). A more thorough understanding of these organic parameters will improve CCN and cloud droplet number predictions and will eventually lead to a better characterization of the aerosol-indirect affect.

REFERENCES

[1] Alfarra, M. R., Paulsen, D., Gysel, M., Garforth, A. A., Dommen, J., Prevot, A. S. H., Worsnop, D. R., Baltensperger, U., and Coe, H., "A mass spectrometric study of secondary organic aerosols formed from the photooxidation of anthropogenic and biogenic precursors in a reaction chamber," *Atmos. Chem. Phys.*, vol. 6, pp. 5279–5293, 2006.

[2] Alfonso, L. and Raga, G. B., "The influence of organic compounds on the development of precipitation acidity in maritime clouds," *Atmos. Chem. Phys.*, vol. 4, pp. 1097–1111, 2004.

[3] Allan, J. D., Alfarra, M. R., Bower, K. N., Williams, P. I., Gallagher, M. W., Jimenez, J. L., McDonald, A. G., Nemitz, E., Canagaratna, M. R., Jayne, J. T., Coe, H., and Worsnop, D. R., "Quantitative sampling using an aerodyne aerosol mass spectrometer 2. measurements of fine particulate chemical composition in two u.k. cities," *J. Geophys. Res.*, vol. 108, no. D3, 2003. 4091.

[4] Allan, J. D., Delia, A. E., Coe, H., Bower, K. N., Alfarra, M. R., Jimenez, J. L., Middlebrook, A. M., Drewnick, F., Onasch, T. B., Canagaratna, M. R., Jayne, J. T., and Worsnopf, D. R., "A generalised method for the extraction of chemically resolved mass spectra from aerodyne aerosol mass spectrometer data," *J. Aerosol Sci.*, vol. 35, no. 7, pp. 909–922, 2004.

[5] Allan, J. D., Jimenez, J. L., Williams, P. I., Alfarra, M. R., Bower, K. N., Jayne, J. T., Coe, H., and Worsnop, D. R., "Quantitative sampling using an aerodyne aerosol mass spectrometer 1. techniques of data interpretation and error analysis," *J. Geophys. Res.*, vol. 108, no. D3, 2003.

[6] An, W. J., Pathak, R. K., Lee, B. H., and Pandis, S. N., "Aerosol volatility measurement using an improved thermodenuder: Application to secondary organic aerosol," *J. Aerosol Sci.*, vol. 38, no. 3, pp. 305–314, 2007.

[7] Andreae, M. O. and Crutzen, P. J., "Atmospheric aerosols: Biogeochemical sources and role in atmospheric chemistry," *Science*, vol. 276, no. 5315, pp. 1052–1058, 1997.

[8] Arey, J., Crowley, D. E., Crowley, M., Resketo, M., and Lester, J., "Hydrocarbon emissions from natural vegetation in california south-coast-air-basin," *Atmos. Environ.*, vol. 29, no. 21, pp. 2977–2988, 1995.

[9] Asa-Awuku, A., Engelhart, G. J., Lee, B., Pandis, S. N., and Nenes, A., "Relating ccn activity, volatility, and droplet growth kinetics of β-caryophyllene secondary organic aerosol," *Atmos. Chem. Phys. Discuss.*, in preparation.

[10] Asa-Awuku, A., Lathem, T. L., Sorooshian, A., Flagan, R., Seinfeld, J., and Nenes, A., "The ccn activity of cloud water collected from gomaccs 2006," in preparation.

[11] Asa-Awuku, A., Moore, R., Brock, C. A., Bahreini, R., Middlebrook, A., Schwarz, J., Spackman, J. R., Holloway, J. S., Tanner, D. J., Huey, L., and Nenes, A., "Cloud condensation nuclei in urban plumes: Airborne measurements and ccn closure during the texas air quality study of 2006," in preparation.

[12] Asa-Awuku, A. and Nenes, A., "Effect of solute dissolution kinetics on cloud droplet formation: Extended köhler theory," *J. Geophys. Res.*, vol. 112, no. D22, 2007.

[13] Asa-Awuku, A. and Nenes, A., "Effect of solute dissolution kinetics on cloud droplet formation: Extended köhler theory," *J. Geophys. Res.*, vol. 112, no. D22, 2007. Asa-Awuku, A. Nenes, A.

[14] Asa-Awuku, A., Nenes, A., Gao, S., Flagan, R. C., and Seinfeld, J. H., "Alkene ozonolysis soa: inferences on composition, ccn and growth kinetics from khler theory analysis," *Atmos. Chem. Phys. Discuss.*, vol. 7, 2007.

[15] Asa-Awuku, A., Sorooshian, A., Flagan, R., Seinfeld, J., and Nenes, A., "Organic ccn properties of interstitial and cloud water aerosol collected during mase 2005," in preparation.

[16] Asa-Awuku, A., Sullivan, A. P., Hennigan, C. J., Weber, R. J., and Nenes, A., "Investigation of molar volume and surfactant characteristics of water-soluble organic compounds in biomass burning aerosol," *Atmos. Chem. Phys.*, vol. 8, pp. 799–812, 2008.

[17] Aschmann, S. M., Atkinson, R., and Arey, J., "Products of reaction of oh radicals with alpha-pinene," *J. Geophys. Res.*, vol. 107, no. D14, p. 4191, 2002. 4191.

[18] Bahreini, R., Jimenez, J. L., Wang, J., Flagan, R. C., Seinfeld, J. H., Jayne, J. T., and Worsnop, D. R., "Aircraft-based aerosol size and composition measurements during ace-asia using an aerodyne aerosol mass spectrometer," *J. Geophys. Res.*, vol. 108, no. D23, 2003. 8645.

[19] Baltensperger, U., Kalberer, M., Dommen, J., Paulsen, D., Alfarra, M. R., Coe, H., Fisseha, R., Gascho, A., Gysel, M., Nyeki, S.,

Sax, M., Steinbacher, M., Prevot, A. S. H., Sjoren, S., Weingartner, E., and Zenobi, R., "Secondary organic aerosols from anthropogenic and biogenic precursors," *Faraday Discuss.*, vol. 130, pp. 265–278, 2005.

[20] Baumann, K., Ift, F., Zhao, J. Z., and Chameides, W. L., "Discrete measurements of reactive gases and fine particle mass and composition during the 1999 atlanta supersite experiment," *J. Geophys. Res.*, vol. 108, no. D7, p. 8416, 2003. 8416.

[21] Baumgardner, D., Kok, G., and Raga, G., "Warming of the arctic lower stratosphere by light absorbing particles," *Geophys. Res. Lett.*, vol. 31, no. 6, 2004. L06117.

[22] Blanchard, D. C., "Sea-to-air transport of surface active material," *Science*, vol. 146, no. 364, p. 396, 1964.

[23] Brechtel, F. J. and Kreidenweis, S. M., "Predicting particle critical supersaturation from hygroscopic growth measurements in the humidified TDMA. Part I: Theory and sensitivity studies," *J. Aerosol Sci.*, vol. 57, pp. 1854–1871, 2000.

[24] Brock, C. A., Sullivan, A. P., Peltier, R. E.and Weber, R. J., Wollny, A., de Gouw, J. A., Middlebrook, A., Atlas, E., Stohl, A., Trainer, M. K., Cooper, O. R., Fehsenfeld, F. C., Frost, G., Holloway, J. S., Hubler, G., Neuman, J., Ryerson, T. B. andWarneke, C., and Wilson, J. C., "Sources of particulate matter in the northeastern united states in summer: 2. evolution of chemical and microphysical properties," *J. Geophys. Res.*, 2008.

[25] Broekhuizen, K., Chang, R. Y. W., Leaitch, W. R., Li, S. M., and Abbatt, J. P. D., "Closure between measured and modeled cloud condensation nuclei (ccn) using size-resolved aerosol compositions in downtown toronto," *Atmos. Chem. Phys.*, vol. 6, pp. 2513–2524, 2006.

[26] Broekhuizen, K., Chang, R. Y. W., Leaitch, W. R., Li, S. M., and Abbatt, J. P. D., "Coupling aerosol size distributions and size-resolved hygroscopicity to predict humidity-dependent optical properties and cloud condensation nuclei spectra," *J. Geophys. Res.*, vol. 111, no. D5, 2006. D05S13.

[27] Cachier, H., Liousse, C., Buatmenard, P., and Gaudichet, A., "Particulate content of savanna fire emissions," *J. Atmos. Chem.*, vol. 22, no. 1-2, pp. 123–148, 1995.

[28] Cai, X. Y. and Griffin, R. J., "Theoretical modeling of the size-dependent influence of surface tension on the absorptive partitioning of semi-volatile organic compounds," *J. Atmos. Chem.*, vol. 50, no. 2, pp. 139–158, 2005.

[29] Calogirou, A., Kotzias, D., and Kettrup, A., "Product analysis of the gas-phase reaction of beta-caryophyllene with ozone," *Atmos. Environ.*, vol. 31, no. 2, pp. 283–285, 1997.

[30] Cantrell, W., Shaw, G., Cass, G. R., Chowdhury, Z., Hughes, L. S., Prather, K. A., Guazzotti, S. A., and Coffee, K. R., "Closure between aerosol particles and cloud condensation nuclei at kaashidhoo climate observatory," *J. Geophys. Res.*, vol. 206, no. D22, pp. 28,711–28,718, 2001.

[31] Carlton, A. G., Turpin, B. J., Lim, H. J., Altieri, K. E., and Seitzinger, S., "Link between isoprene and secondary organic aerosol (soa): Pyruvic acid oxidation yields low volatility organic acids in clouds," *Geophys. Res. Lett.*, vol. 33, no. 6, 2006. L06822.

[32] Cavalli, F., Facchini, M. C., Decesari, S., Mircea, M., Emblico, L., Fuzzi, S., Ceburnis, D., Yoon, Y. J., O\Dowd, C. D., Putaud, J.-P., and Dell\Acqua, A., "Advances in characterization of size-resolved organic matter in marine aerosol over the north atlantic," *J. Geophys. Res.*, vol. 109, p. D24215, 2004.

[33] Chang, R. Y. W., Liu, P. S. K., Leaitch, W. R., and Abbatt, J. P. D., "Comparison between measured and predicted ccn concentrations at egbert, ontario: Focus on the organic aerosol fraction at a semi-rural site," *Atmos. Environ.*, vol. 41, no. 37, pp. 8172–8182, 2007.

[34] Charlson, R. J., Schwartz, S. E., Hales, J. M., Cess, R. D., Coakley, J. A., Hansen, J. E., and Hofmann, D. J., "Climate forcing by anthropogenic aerosols," *Science*, vol. 255, no. 5043, pp. 423–430, 1992.

[35] Chuang, P. Y., "Measurement of the timescale of hygroscopic growth for atmospheric aerosols," *J. Geophys. Res.*, vol. 108, no. D9, p. 4282, 2003.

[36] Chuang, P., Collins, D., Pawlowska, H., Snider, J., Jonsson, H. H., Breguier, J. L., Flagan, R. C., and Seinfeld, J. H., "Ccn measurements during ace-2 and their relationship to cloud microphysical properties," *Tellus B*, vol. 52, pp. 843–867, 2000.

[37] Ciccioli, P., Brancaleoni, E., Frattoni, M., Di Palo, V., Valentini, R., Tirone, G., Seufert, G., Bertin, N., Hansen, U., Csiky, O., Lenz, R., and Sharma, M., "Emission of reactive terpene compounds from orange orchards and their removal by within-canopy processes," *J. Geophys. Res.*, vol. 104, no. D7, pp. 8077–8094, 1999.

[38] Claeys, M., Wang, W., Ion, A. C., Kourtchev, I., Gelencser, A., and Maenhaut, W., "Formation of secondary organic aerosols from isoprene and its gas-phase oxidation products through reaction with hydrogen peroxide," *Atmos. Environ.*, vol. 38, no. 25, pp. 4093–4098, 2004.

[39] Conant, W. C., VanReken, T. M., Rissman, T. A., Varutbangkul, V., Jonsson, H. H., Nenes, A., Jimenez, J. L., Delia, A. E., Bahreini, R., Roberts, G. C., Flagan, R. C., and Seinfeld, J. H., "Aerosol-cloud drop concentration closure in warm cumulus," *J. Geophys. Res.*, vol. 109, no. D13, 2004.

[40] Covert, D. S., Gras, J. L., Wiedensohler, A., and Stratmann, F., "Comparison of directly measured ccn with ccn modeled from the number-size distribution in the marine boundary layer during ace 1 at cape grim, tasmania," *J. Geophys. Res.*, vol. 103, no. D13, pp. 16597–16608, 1998.

[41] Cruz, C. N. and Pandis, S. N., "A study of the ability of pure secondary organic aerosol to act as cloud condensation nuclei," *Atmos. Environ.*, vol. 31, no. 15, pp. 2205–2214, 1997.

[42] Cruz, C. N. and Pandis, S. N., "Deliquescence and hygroscopic growth of mixed inorganic-organic atmospheric aerosol," *Environ. Sci. Technol.*, vol. 34, no. 20, pp. 4313–4319, 2000.

[43] Decesari, S., "Source attribution of water-soluble organic aerosol by nuclear magnetic resonance spectroscopy," *Environ. Sci. Technol.*, vol. 41, no. 7, pp. 2479–2484, 2007.

[44] Decesari, S., Facchini, M. C., Fuzzi, S., and Tagliavini, E., "Characterization of water-soluble organic compounds in atmospheric aerosol: A new approach," *J. Geophys. Res.*, vol. 105, no. D1, pp. 1481–1489, 2000.

[45] Decesari, S., Facchini, M. C., Mircea, M., Cavalli, F., and Fuzzi, S., "Solubility properties of surfactants in atmospheric aerosol and cloud/fog water samples," *J. Geophys. Res.*, vol. 108, no. D21, p. 4685, 2003.

[46] Dinar, E., Mentel, T. F., and Rudich, Y., "The density of humic acids and humic like substances (hulis) from fresh and aged wood burning and pollution aerosol particles," *Atmos. Chem. Phys.*, vol. 6, pp. 5213–5224, 2006.

[47] Dinar, E., Taraniuk, I., Graber, E. R., Anttila, T., Mentel, T. F., and Rudich, Y., "Hygroscopic growth of atmospheric and model humic-like substances," *J. Geophys. Res.*, vol. 112, no. D5, p. D05211, 2007. D05211.

[48] Dinar, E., Taraniuk, I., Graber, E. R., Katsman, S., Moise, T., Anttila, T., Mentel, T. F., and Rudich, Y., "Cloud condensation nuclei properties of model and atmospheric hulis," *Atmos. Chem. Phys.*, vol. 6, pp. 2465–2481, 2006.

[49] Dommen, J., Metzger, A., Duplissy, J., Kalberer, M., Alfarra, M. R., Gascho, A., Weingartner, E., Prevot, A. S. H., Verheggen, B., and Baltensperger, U., "Laboratory observation of oligomers in the aerosol from isoprene/nox photooxidation," *Geophys. Res. Lett.*, vol. 33, no. 13, p. L13805, 2006. L13805.

[50] Donahue, N. M., Hartz, K. E. H., Chuong, B., Presto, A. A., Stanier, C. O., Rosenhorn, T., Robinson, A. L., and Pandis, S. N., "Critical factors determining the variation in soa yields from terpene ozonolysis: A combined experimental and computational study," *Faraday Discuss.*, vol. 130, pp. 295–309, 2005.

[51] Duarte, R. and Duarte, A. C., "Application of non-ionic solid sorbents (xad resins) for the isolation and fractionation of water-soluble organic compounds from atmospheric aerosols," *J. Atmos. Chem.*, vol. 51, no. 1, pp. 79–93, 2005.

[52] Dusek, U., Covert, D. S., Wiedensohler, A., Neususs, C., Weise, D., and Cantrell, W., "Cloud condensation nuclei spectra derived from size distributions and hygroscopic properties of the aerosol in coastal south-west portugal during ace-2," *Tellus B*, vol. 55, no. 1, pp. 35–53, 2003.

[53] Dusek, U., Frank, G. P., Hildebrandt, L., Curtius, J., Schneider, J., Walter, S., Chand, D., Drewnick, F., Hings, S., Jung, D., Borrmann, S., and Andreae, M. O., "Size matters more than chemistry for cloud-nucleating ability of aerosol particles," *Science*, vol. 312, no. 5778, pp. 1375–1378, 2006.

[54] Engelhart, G., Asa-Awuku, A., Nenes, A., and Pandis, S. N., "Ccn activity and droplet growth kinetics of fresh and aged monoterpene secondary organic aerosol," *Atmos. Chem. Phys. Discuss.*, vol. 8, pp. 95–135, 2008.

[55] Engelhart, G., Asa-Awuku, A., Nenes, A., and Pandis, S. N., "Ccn activity and droplet growth kinetics of fresh and aged monoterpene secondary organic aerosol," *Atmos. Chem. Phys. Discuss.*, vol. 8, pp. 95–135, 2008.

[56] Ervens, B., Feingold, G., Clegg, S. L., and Kreidenweis, S. M., "A modeling study of aqueous production of dicarboxylic acids: 2. implications for cloud microphysics," *J. Geophys. Res.*, vol. 109, no. D15, 2004. D15206.

[57] Ervens, B., Feingold, G., Frost, G. J., and Kreidenweis, S. M., "A modeling study of aqueous production of dicarboxylic acids: 1. chemical pathways and speciated organic mass production," *J. Geophys. Res.*, vol. 109, no. D15, 2004. D15205.

[58] Ervens, B., Feingold, G., and Kreidenweis, S. M., "Influence of water-soluble organic carbon on cloud drop number concentration," *J. Geophys. Res.*, vol. 110, no. D18, 2005. D18211.

[59] Facchini, M. C., Decesari, S., Mircea, M., Fuzzi, S., and Loglio, G., "Surface tension of atmospheric wet aerosol and cloud/fog droplets in relation to their organic carbon content and chemical composition," *Atmos. Environ.*, vol. 34, no. 28, pp. 4853–4857, 2000.

[60] Facchini, M. C., Fuzzi, S., Zappoli, S., Andracchio, A., Gelencser, A., Kiss, G., Krivacsy, Z., Meszaros, E., Hansson, H. C., Alsberg, T., and Zebuhr, Y., "Partitioning of the organic aerosol component between fog droplets and interstitial air," *J. Geophys. Res.*, vol. 104, no. D21, pp. 26821–26832, 1999.

[61] Facchini, M. C., Mircea, M., Fuzzi, S., and Charlson, R. J., "Cloud albedo enhancement by surface-active organic solutes in growing droplets," *Nature*, vol. 401, no. 6750, pp. 257–259, 1999.

[62] Falkovich, A. H., Graber, E. R., Schkolnik, G., Rudich, Y., Maenhaut, W., and Artaxo, P., "Low molecular weight organic acids in aerosol particles from rondonia, brazil, during the biomass-burning, transition and wet periods," *Atmos. Chem. Phys.*, vol. 5, pp. 781–797, 2005.

[63] Fan, J. W., Zhang, R. Y., Collins, D., and Li, G. H., "Contribution of secondary condensable organics to new particle formation: A case study in houston, texas," *Geophys. Res. Lett.*, vol. 33, no. 15, 2006.

[64] Feingold, G. and Chuang, P., "Analysis of the influence of film-forming compounds on droplet growth: Implications for cloud microphysical processes and climate," *J. Aerosol Sci.*, vol. 59, pp. 2006–2018, 2002.

[65] Fitzgerald, J. W., Hoppel, W. A., and Gelbard, F., "A one-dimensional sectional model to simulate multicomponent aerosol dynamics in the marine boundary layer - 1. model description," *J. Geophys. Res.*, vol. 103, no. D13, pp. 16085–16102, 1998.

[66] Fletcher, C. A., Johnson, G. R., Ristovski, Z. D., and Harvey, M., "Hygroscopic and volatile properties of marine aerosol observed at cape grim during the p2p campaign," *Environ. Chem.*, vol. 4, no. 3, pp. 162–171, 2007.

[67] Forstner, H. J. L., Flagan, R. C., and Seinfeld, J. H., "Secondary organic aerosol from the photooxidation of aromatic hydrocarbons: Molecular composition," *Environ. Sci. Technol.*, vol. 31, no. 5, pp. 1345–1358, 1997.

[68] Fountoukis, C. and Nenes, A., "Continued development of a cloud droplet formation parameterization for global climate models," *J. Geophys. Res.*, vol. 110, no. D11, 2005. D11212.

[69] Fountoukis, C. and Nenes, A., "Isorropia ii: A computationally efficient thermodynamic equilibrium model for k^+-ca^{2+}-mg^{2+}-nh^{4+}-na^+-$so_4{}^{2-}$-no3$^-$-cl$^-$-h2o aerosols," *Atmos. Chem. Phys.*, pp. 1893–1939, 2007.

[70] Fountoukis, C., Nenes, A., Meskhidze, N., Bahreini, R., Brechtel, F., Conant, W., Jonsson, H., Murphy, S., Sorooshian, A., Varutbangkul, V., Flagan, R., and Seinfeld, J., "Aerosol - cloud drop concentration closure for clouds sampled during (icartt)," *J. Geophys. Res.*, vol. 112, 2007.

[71] Gao, R. S., Schwarz, J. P., Kelly, K. K., Fahey, D. W., Watts, L. A., Thompson, T. L., Spackman, J. R., Slowik, J. G., Cross, E. S., Han, J. H., Davidovits, P., Onasch, T. B., and Worsnop, D. R., "A novel method for estimating light-scattering properties of soot aerosols using a modified single-particle soot photometer," *Aerosol Sci. Technol.*, vol. 41, no. 2, pp. 125–135, 2007.

[72] Gao, S., Keywood, M., Ng, N. L., Surratt, J., Varutbangkul, V., Bahreini, R., Flagan, R. C., and Seinfeld, J. H., "Low-molecular-weight and oligomeric components in secondary organic aerosol from the ozonolysis of cycloalkenes and alpha-pinene," *J. Phys. Chem.*, vol. 108, pp. 10147–10164, 2004.

[73] Gao, S., Ng, N. L., Keywood, M., Varutbangkul, V., Bahreini, R., Nenes, A., He, J. W., Yoo, K. Y., Beauchamp, J. L., Hodyss, R. P., Flagan, R. C., and Seinfeld, J. H., "Particle phase acidity and oligomer formation in secondary organic aerosol," *Environ. Sci. Technol.*, vol. 38, no. 24, pp. 6582–6589, 2004.

[74] Gill, P. S., Graedel, T. E., and Weschler, C. J., "Organic films on atmospheric aerosol-particles, fog droplets, cloud droplets, raindrops, and snowflakes," *Rev. Geophys.*, vol. 21, no. 4, pp. 903–920, 1983.

[75] Goldstein, A. H. and Galbally, I. E., "Known and unexplored organic constituents in the earth's atmosphere," *Environ. Sci. Technol.*, vol. 41, no. 5, pp. 1514–1521, 2007.

[76] Graber, E. R. and Rudich, Y., "Atmospheric hulis: How humic-like are they? a comprehensive and critical review," *Atmos. Chem. Phys.*, vol. 6, pp. 729–753, 2006.

[77] Graham, B., Mayol-Bracero, O. L., Guyon, P., Roberts, G. C., Decesari, S., Facchini, M. C., Artaxo, P., Maenhaut, W., Koll, P., and Andreae, M. O., "Water-soluble organic compounds in biomass burning aerosols over amazonia - 1. characterization by nmr and gc-ms," *J. Geophys. Res.*, vol. 107, no. D20, p. 8047, 2002.

[78] Grieshop, A. P., Donahue, N. M., and Robinson, A. L., "Is the gas-particle partitioning in alpha-pinene secondary organic aerosol reversible?," *Geophys. Res. Lett.*, vol. 34, no. 14, 2007. L14810.

[79] Griffin, R. J., Cocker, D. R., Flagan, R. C., and Seinfeld, J. H., "Organic aerosol formation from the oxidation of biogenic hydrocarbons," *J. Geophys. Res.*, vol. 104, no. D3, pp. 3555–3567, 1999.

[80] Griffin, R. J., Cocker, D. R., Seinfeld, J. H., and Dabdub, D., "Estimate of global atmospheric organic aerosol from oxidation of biogenic hydrocarbons," *Geophys. Res. Lett.*, vol. 26, no. 17, pp. 2721–2724, 1999.

[81] Grosjean, D., Williams, E. L., Grosjean, E., Andino, J. M., and Seinfeld, J. H., "Atmospheric oxidation of biogenic hydrocarbons - reaction of ozone with beta-pinene, d-limonene and trans-caryophyllene," *Environ. Sci. Technol.*, vol. 27, no. 13, pp. 2754–2758, 1993.

[82] Guenther, A., Archer, S., Greenberg, J., Harley, P., Helmig, D., Klinger, L., Vierling, L., Wildermuth, M., Zimmerman, P., and Zitzer, S., "Biogenic hydrocarbon emissions and landcover/climate change in a subtropical savanna," *Phys. Chem. Earth. B), Volume = 24, Number = 6, Pages = 659-667, Year = 1999.*

[83] Guenther, A., Geron, C., Pierce, T., Lamb, B., Harley, P., and Fall, R., "Natural emissions of non-methane volatile organic compounds; carbon monoxide, and oxides of nitrogen from north america," *Atmos. Environ.*, vol. 34, no. 12-14, pp. 2205–2230, 2000.

[84] Guenther, A., Hewitt, C. N., Erickson, D., Fall, R., Geron, C., Graedel, T., Harley, P., Klinger, L., Lerdau, M., McKay, W. A., Pierce, T., Scholes, B., Steinbrecher, R., Tallamraju, R., Taylor, J., and Zimmerman, P., "A global-model of natural volatile organic-compound emissions," *J. Geophys. Res.*, vol. 100, no. D5, pp. 8873–8892, 1995.

[85] Hallberg, A., Ogren, J. A., Noone, K. J., Okada, K., Heintzenberg, J., and Svenningsson, I. B., "The influence of aerosol-particle composition on cloud droplet formation," *J. Atmos. Chem.*, vol. 19, no. 1-2, pp. 153–171, 1994.

[86] Hamilton, J. F., Lewis, A. C., Reynolds, J. C., Carpenter, L. J., and Lubben, A., "Investigating the composition of organic aerosol resulting from cyclohexene ozonolysis: low molecular weight and heterogeneous reaction products," *Atmos. Chem. Phys.*, vol. 6, pp. 4973–4984, 2006.

[87] Hansell, D. A. and Carlson, C. A., *Biogeochemistry of Marine Dissolved Organic Matter*. Academic Press.

[88] Hansen, U. and Seufert, G., "Temperature and light dependence of beta-caryophyllene emission rates," *J. Geophys. Res.*, vol. 108, no. D24, 2003. 4801.

[89] Havers, N., Burba, P., Lambert, J., and Klockow, D., "Spectroscopic characterization of humic-like substances in airborne particulate matter," *J. Atmos. Chem.*, vol. 29, no. 1, pp. 45–54, 1998.

[90] Haywood, J. and Boucher, O., "Estimates of the direct and indirect radiative forcing due to tropospheric aerosols: A review," *Rev. Geophys.*, vol. 38, no. 4, pp. 513–543, 2000.

[91] Helmig, D., Ortega, J., Duhl, T., Tanner, D., Guenther, A., Harley, P., Wiedinmyer, C., Milford, J., and Sakulyanontvittaya,

T., "Sesquiterpene emissions from pine trees - identifications, emission rates and flux estimates for the contiguous united states," *Environ. Sci. Technol.*, vol. 41, no. 5, pp. 1545–1553, 2007.

[92] Henning, S., Rosenorn, T., D'Anna, B., Gola, A. A., Svenningsson, B., and Bilde, M., "Cloud droplet activation and surface tension of mixtures of slightly soluble organics and inorganic salt," *Atmos. Chem. Phys.*, vol. 5, pp. 575–582, 2005.

[93] Hoffmann, T., "Adsorptive preconcentration technique including oxidant scavenging for the measurement of reactive natural hydrocarbons in ambient air," *J. Anal. Chem.*, vol. 351, no. 1, pp. 41–47, 1995.

[94] Holloway, J. S., Jakoubek, R. O., Parrish, D. D., Gerbig, C., Volz-Thomas, A., Schmitgen, S., Fried, A., Wert, B., Henry, B., and Drummond, J. R., "Airborne intercomparison of vacuum ultraviolet fluorescence and tunable diode laser absorption measurements of tropospheric carbon monoxide," *J. Geophys. Res.*, vol. 105, no. D19, pp. 24251–24261, 2000.

[95] Holmberg, K., *Surfactants and polymers in aqueous solution.* Hoboken, NJ: John Wiley & Sons, 2nd ed., 2003.

[96] Huebert, B., Bertram, T., Kline, J., Howell, S., Eatough, D., and Blomquist, B., "Measurements of organic and elemental carbon in asian outflow during ace-asia from the nsf/ncar c-130," *J. Geophys. Res.*, vol. 109, no. D19, 2004.

[97] Huff-Hartz, K. E., Rosenorn, T., Ferchak, S. R., Raymond, T. M., Bilde, M., Donahue, N. M., and Pandis, S. N., "Cloud condensation nuclei activation of monoterpene and sesquiterpene secondary organic aerosol," *J. Geophys. Res.*, vol. 110, no. D14, p. D14208, 2005. D14208.

[98] Hunter, R. J., *Foundations of colloid science.* Oxford ; New York: Oxford University Press, 2nd ed., 2001. Includes bibliographical references and index.

[99] Intergovernmental Panel on Climate Change (IPCC), *Summary for Policymakers. In: Climate Change (2007): The physical science basis. Contribution of working group I to the fourth assessment report of the Intergovernmental Panel on Climate Change.* Cambridge, United Kingdom and New York, NY, USA: Cambridge University Press, 2007.

[100] Jaoui, M., Leungsakul, S., and Kamens, R. M., "Gas and particle products distribution from the reaction of beta-caryophyllene with ozone," *J. Atmos. Chem.*, vol. 45, no. 3, pp. 261–287, 2003.

[101] Jaoui, M., Lewandowski, M., Kleindienst, T. E., Offenberg, J. H., and Edney, E. O., "beta-caryophyllinic acid: An atmospheric tracer for beta-caryophyllene secondary organic aerosol," *Geophys. Res. Lett.*, vol. 34, no. 5, 2007. L05816.

[102] Jayne, J. T., Leard, D. C., Zhang, X. F., Davidovits, P., Smith, K. A., Kolb, C. E., and Worsnop, D. R., "Development of an aerosol mass spectrometer for size and composition analysis of submicron particles," *Aerosol Sci. Technol.*, vol. 33, no. 1-2, pp. 49–70, 2000.

[103] Jimenez, J. L., Jayne, J. T., Shi, Q., Kolb, C. E., Worsnop, D. R., Yourshaw, I., Seinfeld, J. H., Flagan, R. C., Zhang, X. F., Smith, K. A., Morris, J. W., and Davidovits, P., "Ambient aerosol sampling using the aerodyne aerosol mass spectrometer," *J. Geophys. Res.*, vol. 108, no. D7, 2003.

[104] Johnson, G. R., Ristovski, Z. D., D'Anna, B., and Morawska, L., "Hygroscopic behavior of partially volatilized coastal marine aerosols using the volatilization and humidification tandem differential mobility analyzer technique," *J. Geophys. Res.*, vol. 110, no. D20, 2005. D20203.

[105] Jonsson, A. M., Hallquist, M., and Saathoff, H., "Volatility of secondary organic aerosols from the ozone initiated oxidation of alpha-pinene and limonene," *J. Aerosol Sci.*, vol. 38, no. 8, pp. 843–852, 2007.

[106] Kalberer, M., "Analysis of oligomers in atmospheric aerosol particles - analytical challenges," *Anal. Bioanal. Chem.*, vol. 385, no. 1, pp. 22–25, 2006.

[107] Kalberer, M., Paulsen, D., Sax, M., Steinbacher, M., Dommen, J., Prevot, A. S. H., Fisseha, R., Weingartner, E., Frankevich, V., Zenobi, R., and Baltensperger, U., "Identification of polymers as major components of atmospheric organic aerosols," *Science*, vol. 303, no. 5664, pp. 1659–1662, 2004.

[108] Kalberer, M., Sax, M., and Samburova, V., "Molecular size evolution of oligomers in organic aerosols collected in urban atmospheres and generated in a smog chamber," *Environ. Sci. Technol.*, vol. 40, no. 19, pp. 5917–5922, 2006.

[109] Kanakidou, M., Seinfeld, J. H., Pandis, S. N., Barnes, I., Dentener, F. J., Facchini, M. C., Van Dingenen, R., Ervens, B., Nenes, A., Nielsen, C. J., Swietlicki, E., Putaud, J. P., Balkanski, Y., Fuzzi, S., Horth, J., Moortgat, G. K., Winterhalter, R., Myhre, C. E. L., Tsigaridis, K., Vignati, E., Stephanou, E. G., and Wilson, J., "Organic aerosol and global climate modelling: a review," *Atmos. Chem. Phys.*, vol. 5, pp. 1053–1123, 2005.

[110] Keywood, M. D., Varutbangkul, V., Bahreini, R., Flagan, R. C., and Seinfeld, J. H., "Secondary organic aerosol formation from the ozonolysis of cycloalkenes and related compounds," *Environ. Sci. Technol.*, vol. 38, no. 15, pp. 4157–4164, 2004.

[111] Kiss, G., Tombacz, E., and Hansson, H. C., "Surface tension effects of humic-like substances in the aqueous extract of tropospheric fine aerosol," *J. Atmos. Chem.*, vol. 50, no. 3, pp. 279–294, 2005.

[112] Kiss, G., Tombacz, E., Varga, B., Alsberg, T., and Persson, L., "Estimation of the average molecular weight of humic-like substances isolated from fine atmospheric aerosol," *Atmos. Environ.*, vol. 37, no. 27, pp. 3783–3794, 2003.

[113] Kiss, G., Varga, B., Galambos, I., and Ganszky, I., "Characterization of water-soluble organic matter isolated from atmospheric fine aerosol," *J. Geophys. Res.*, vol. 107, no. D21, p. 8339, 2002.

[114] Kiss, G., Varga, B., Gelencser, A., Krivacsy, Z., Molnar, A., Alsberg, T., Persson, L., Hansson, H. C., and Facchini, M. C., "Characterisation of polar organic compounds in fog water," *Atmos. Environ.*, vol. 35, no. 12, pp. 2193–2200, 2001.

[115] Köhler, H., "The nucleus in and the growth of hygroscopic droplets," *Trans. Faraday Soc.*, vol. 43, pp. 1152–1161, 1936.

[116] Konig, G., Brunda, M., Puxbaum, H., Hewitt, C. N., Duckham, S. C., and Rudolph, J., "Relative contribution of oxygenated hydrocarbons to the total biogenic voc emissions of selected mid-european agricultural and natural plant-species," *Atmos. Environ.*, vol. 29, no. 8, pp. 861–874, 1995.

[117] Kostenidou, E., Pathak, R. K., and Pandis, S. N., "An algorithm for the calculation of secondary organic aerosol density combining ams and smps data," *Aerosol Sci. Technol.*, vol. 41, no. 11, pp. 1002 – 1010, 2007.

[118] Krivacsy, Z., Gelencser, A., Kiss, G., Meszaros, E., Molnar, A., Hoffer, A., Meszaros, T., Sarvari, Z., Temesi, D., Varga, B., Baltensperger, U., Nyeki, S., and Weingartner, E., "Study on the chemical character of water soluble organic compounds in fine atmospheric aerosol at the jungfraujoch," *J. Atmos. Chem.*, vol. 39, no. 3, pp. 235–259, 2001.

[119] Krivacsy, Z., Kiss, G., Varga, B., Galambos, I., Sarvari, Z., Gelencser, A., Molnar, A., Fuzzi, S., Facchini, M. C., Zappoli, S., Andracchio, A., Alsberg, T., Hansson, H. C., and Persson, L., "Study of humic-like substances in fog and interstitial aerosol by size-exclusion chromatography and capillary electrophoresis," *Atmos. Environ.*, vol. 34, no. 25, pp. 4273–4281, 2000.

[120] Kroll, J. H., Ng, N. L., Murphy, S. M., Flagan, R. C., and Seinfeld, J. H., "Secondary organic aerosol formation from isoprene photooxidation," *Environ. Sci. Technol.*, vol. 40, no. 6, pp. 1869–1877, 2006.

[121] Laaksonen, A., Korhonen, P., Kulmala, M., and Charlson, R. J., "Modification of the kuhler equation to include soluble trace gases and slightly soluble substances," *J. Aerosol Sci.*, vol. 55, no. 5, pp. 853–862, 1998.

[122] Lance, S., Medina, J., Smith, J. N., and Nenes, A., "Mapping the operation of the dmt continuous flow ccn counter," *Aerosol Sci. Technol.*, vol. 40, no. 4, pp. 242–254, 2006.

[123] Lance, S., Nenes, A., and Rissman, T. A., "Chemical and dynamical effects on cloud droplet number: Implications for estimates of the aerosol indirect effect," *J. Geophys. Res.*, vol. 109, no. D22, 2004. D22208.

[124] Langmuir, I., "The constitution and fundamental properties of solids and liquids. ii. liquids," *J. Am. Chem. Soc.*, vol. 39, pp. 1848–1906, 1917.

[125] Lee, A., Goldstein, A. H., Keywood, M. D., Gao, S., Varutbangkul, V., Bahreini, R., Ng, N. L., Flagan, R. C., and Seinfeld, J. H., "Gas-phase products and secondary aerosol yields from the ozonolysis of ten different terpenes," *J. Geophys. Res.*, vol. 111, no. D7, 2006. D07302.

[126] Lee, S., Baumann, K., Schauer, J. J., Sheesley, R. J., Naeher, L. P., Meinardi, S., Blake, D. R., Edgerton, E. S., Russell, A. G., and Clements, M., "Gaseous and particulate emissions from prescribed burning in georgia," *Environ. Sci. Technol.*, vol. 39, no. 23, pp. 9049–9056, 2005.

[127] Li, Z. D., Williams, A. L., and Rood, M. J., "Influence of soluble surfactant properties on the activation of aerosol particles containing inorganic solute," *J. Aerosol Sci.*, vol. 55, no. 10, pp. 1859–1866, 1998.

[128] Lim, H. J., Carlton, A. G., and Turpin, B. J., "Isoprene forms secondary organic aerosol through cloud processing: Model simulations," *Environ. Sci. Technol.*, vol. 39, no. 12, pp. 4441–4446, 2005.

[129] Limbeck, A., Kulmala, M., and Puxbaum, H., "Secondary organic aerosol formation in the atmosphere via heterogeneous reaction of gaseous isoprene on acidic particles," *Geophys. Res. Lett.*, vol. 30, no. 19, p. 1996, 2003. 1996.

[130] Lohmann, U. and Feichter, J., "Global indirect aerosol effects: a review," *Atmos. Chem. Phys.*, vol. 5, pp. 715–737, 2005.

[131] Lu, M. L., Conant, W. C., Jonsson, H. H., Varutbangkul, V., Flagan, R. C., and Seinfeld, J. H., "The marine stratus/stratocumulus experiment (mase): Aerosol-cloud relationships in marine stratocumulus," *J. Geophys. Res.*, vol. 112, no. D10, 2007.

[132] Markowski, G. R., "Improving twomey algorithm for inversion of aerosol measurement data," *Aerosol Sci. Technol.*, vol. 7, no. 2, pp. 127–141, 1987.

[133] Marple, V. A. and Chien, C. M., "Virtual impactors - a theoretical-study," *Environ. Sci. Technol.*, vol. 14, no. 8, pp. 976–985, 1980.

[134] Mayol-Bracero, O., Guyon, P., Graham, B., Andreae, M., Decesari, S., Facchini, M., Fuzzi, S., and Artaxo, P., "Black carbon, organic carbon and water-soluble organic compounds in biomass smoke particles over the amazon basin," *J. Geophys. Res.*

[135] McFiggans, G., Artaxo, P., Baltensperger, U., Coe, H., Facchini, M. C., Feingold, G., Fuzzi, S., Gysel, M., Laaksonen, A., Lohmann, U., Mentel, T. F., Murphy, D. M., O'Dowd, C. D., Snider, J. R., and Weingartner, E., "The effect of physical and chemical aerosol properties on warm cloud droplet activation.," *Atmos. Chem. Phys.*, vol. 6, pp. 2593–2649, 2006.

[136] Medina, J. and Nenes, A., "Cloud condensation nuclei closure during the international consortium for atmospheric research on transport and transformation 2004 campaign: Effects of size-resolved composition," *J. Geophys. Res.*, vol. 112, no. D10, 2007. D10S31.

[137] Meskhidze, N., Chameides, W. L., and Nenes, A., "Dust and pollution: A recipe for enhanced ocean fertilization?," *J. Geophys. Res.*, vol. 110, no. D3, 2005. D03301.

[138] Mircea, M., Facchini, M. C., Decesari, S., Fuzzi, S., and Charlson, R. J., "The influence of the organic aerosol component on ccn supersaturation spectra for different aerosol types," *Tellus B*, vol. 54, no. 1, pp. 74–81, 2002.

[139] Moore, R. H., Ingall, E. D., Sorooshian, A., and Nenes, A., "Molar mass sureface tension and roplet growth kinetics of marine organic ccn; molar mas ssurface tension of marine organics from measurment of ccn activity," *Geophys. Res. Lett.*, in review.

[140] Nenes, A., Charlson, R. J., Facchini, M. C., Kulmala, M., Laaksonen, A., and Seinfeld, J. H., "Can chemical effects on cloud droplet number rival the first indirect effect?," *Geophys. Res. Lett.*, vol. 29, no. 17, p. 1848, 2002. 1848.

[141] Nenes, A., Chuang, P. Y., Flagan, R. C., and Seinfeld, J. H., "A theoretical analysis of cloud condensation nucleus (ccn) instruments," *J. Geophys. Res.*, vol. 106, no. D4, pp. 3449–3474, 2001.

[142] Nenes, A. and Medina, J., "Scanning mobility ccn analysis - a method for fast measurements of size resolved ccn activity and growth kinetics," *Aerosol Sci. Technol.*, in review.

[143] Nenes, A., Pandis, S. N., and Pilinis, C., "Isorropia: A new thermodynamic equilibrium model for multiphase multicomponent inorganic aerosols," *Aqua. Geochem.*, vol. 4, no. 1, pp. 123–152, 1998.

[144] Noone, K. J., Ogren, J. A., Heintzenberg, J., Charlson, R. J., and Covert, D. S., "Design and calibration of a counterflow virtual impactor for sampling of atmospheric fog and cloud droplets," *Aerosol Sci. Technol.*, vol. 8, no. 3, pp. 235–244, 1988.

[145] Novakov, T. and Penner, J. E., "Large contribution of organic aerosols to cloud-condensation-nuclei concentrations," *Nature*, vol. 365, no. 6449, pp. 823–826, 1993.

[146] O'Dowd, C. D. and De Leeuw, G., "Marine aerosol production: a review of the current knowledge," *Philosophical Transactions of the Royal Society a-Mathematical Physical and Engineering Sciences*, vol. 365, no. 1856, pp. 1753–1774, 2007.

[147] O'Dowd, C. D., Facchini, M. C., Cavalli, F., Ceburnis, D., Mircea, M., Decesari, S., Fuzzi, S., Yoon, Y. J., and Putaud, J. P., "Biogenically driven organic contribution to marine aerosol," *Nature*, vol. 431, no. 7009, pp. 676–680, 2004.

[148] Odum, J. R., Hoffmann, T., Bowman, F., Collins, D., Flagan, R. C., and Seinfeld, J. H., "Gas/particle partitioning and secondary organic aerosol yields," *Environ. Sci. Technol.*, vol. 30, no. 8, pp. 2580–2585, 1996.

[149] Oppo, C., Bellandi, S., degli Innocenti, N., Stortini, A. M., Loglio, G., Schiavuta, E., and R., C., "Surfactant components of marine organic matter as agents for biogeochemical fractionation and pollutant transport via marine aerosols," vol. 63, pp. 235–253, 1999.

[150] Padró, L., Asa-Awuku, A., Morisson, R., and Nenes, A., "Inferring thermodynamic properties from ccn activation experiments: single-component and binary aerosols," *Atmos. Chem. Phys.*, vol. 7, pp. 5263–5274, 2007.

[151] Pankow, J. F., "An absorption-model of gas-particle partitioning of organic-compounds in the atmosphere," *Atmos. Environ.*, vol. 28, no. 2, pp. 185–188, 1994.

[152] Pathak, R. K., Presto, A. A., Lane, T. E., Stanier, C. O., Donahue, N. M., and Pandis, S. N., "Ozonolysis of alpha-pinene: parameterization of secondary organic aerosol mass fraction," *Atmos. Chem. Phys.*, vol. 7, no. 14, pp. 3811–3821, 2007.

[153] Perry, R. H., Green, D. W., and Maloney, J. O., *Perry's Chemical Engineers' Handbook.* New York: McGraw-Hill, 7th ed. ed., 1997.

[154] Petters, M. D. and Kreidenweis, S. M., "A single parameter representation of hygroscopic growth and cloud condensation nucleus activity," *Atmos. Chem. Phys.*, vol. 7, no. 8, pp. 1961–1971, 2007.

[155] Prenni, A. J., Petters, M. D., Kreidenweis, S. M., DeMott, P. J., and Ziemann, P. J., "Cloud droplet activation of secondary organic aerosol," *J. Geophys. Res.*, vol. 112, no. D10, 2007. D10223.

[156] Presto, A. A., Hartz, K. E. H., and Donahue, N. M., "Secondary organic aerosol production from terpene ozonolysis. 1. effect of uv radiation," *Environ. Sci. Technol.*, vol. 39, pp. 7036–4045, 2005.

[157] Presto, A. A., Hartz, K. E. H., and Donahue, N. M., "Secondary organic aerosol production from terpene ozonolysis. 2. effect of nox concentration," *Environ. Sci. Technol.*, vol. 39, no. 18, pp. 7046–7054, 2005.

[158] Ramanathan, V., Crutzen, P. J., Kiehl, J. T., and Rosenfeld, D., "Atmosphere - aerosols, climate, and the hydrological cycle," *Science*, vol. 294, no. 5549, pp. 2119–2124, 2001.

[159] Raymond, T. and Pandis, S. N., "Cloud activation of single-component organic aerosol particles," *J. Geophys. Res.*, vol. 107, no. D24, p. 4787, 2002.

[160] Reynolds, J. C., Last, D. J., McGillen, M., Nijs, A., Horn, A. B., Percival, C., Carpenter, L. J., and Lewis, A. C., "Structural analysis of oligomeric molecules formed from the reaction products of oleic acid ozonolysis," *Environ. Sci. Technol.*, vol. 40, no. 21, pp. 6674–6681, 2006.

[161] Rissler, J., Swietlicki, E., Zhou, J., Roberts, G., , Andreae, M. O., Gatti, L., and Artaxo, P., "Physical properties of the sub-micrometer aerosol over the amazon rain forest during the wet-to-dry season transition - comparison of modeled and measured ccn concentrations," *Atmos. Chem. Phys.*, vol. 4, pp. 2119–2143, 2004.

[162] Rissler, J., Vestin, A., Swietlicki, E., Fisch, G., Zhou, J., Artaxo, P., and Andreae, M. O., "Size distribution and hygroscopic properties of aerosol particles from dry-season biomass burning in amazonia," *Atmos. Chem. Phys.*, vol. 6, pp. 471–491, 2006.

[163] Roberts, G., Mauger, G., Hadley, O., and Ramanathan, V., "North american and asian aerosols over the eastern pacific ocean and their role in regulating cloud condensation nuclei," *J. Geophys. Res.*, vol. 111, no. D13, 2006.

[164] Roberts, G. C. and Nenes, A., "A continuous-flow streamwise thermal-gradient ccn chamber for atmospheric measurements," *Aerosol Sci. Technol.*, vol. 39, no. 3, pp. 206–221, 2005.

[165] Roberts, G. C., Nenes, A., Seinfeld, J. H., and Andreae, M. O., "Impact of biomass burning on cloud properties in the amazon basin," *J. Geophys. Res.*, vol. 108, no. D2, 2003. 4062.

[166] Robinson, A. L., Donahue, N. M., Shrivastava, M. K., Weitkamp, E. A., Sage, A. M., Grieshop, A. P., Lane, T. E., Pierce, J. R., and Pandis, S. N., "Rethinking organic aerosols: Semivolatile emissions and photochemical aging," *Science*, vol. 315, no. 5816, pp. 1259–1262, 2007.

[167] Rogge, W. F., Mazurek, M. A., Hildemann, L. M., Cass, G. R., and Simoneit, B. R. T., "Quantification of urban organic aerosols at a molecular-level - identification, abundance and seasonal-variation," *Atmos. Environ.*, vol. 27, no. 8, pp. 1309–1330, 1993.

[168] Rose, D., Frank, G. P., Dusek, U., Gunthe, S. S., Andreae, M. O., and Pöschl, U., "Calibration and measurement uncertainties of a continuous-flow cloud condensation nuclei counter (dmt-ccnc): Ccn activation of ammonium sulfate and sodium chloride aerosol particles in theory and experiment," *Atmos. Chem. Phys.*, vol. 7, no. 2, pp. 8193–8260, 2007.

[169] Rudich, Y., "Laboratory perspectives on the chemical transformations of organic matter in atmospheric particles," *Chem. Rev.*, vol. 103, no. 12, pp. 5097–5124, 2003.

[170] Ruehl, C., Nenes, A., and Chuang, P., "How quickly do cloud droplets form on atmospheric particles?," *Atmos. Chem. Phys.*, vol. 8, pp. 1043–1055, 2008.

[171] Russell, L. M., Noone, K. J., Ferek, R. J., Pockalny, R. A., Flagan, R. C., and Seinfeld, J. H., "Combustion organic aerosol as cloud condensation nuclei in ship tracks," *J. Aerosol Sci.*, vol. 57, no. 16, pp. 2591–2606, 2000.

[172] Saathoff, H., Naumann, K. H., Schnaiter, M., Schock, W., Mohler, O., Schurath, U., Weingartner, E., Gysel, M., and Baltensperger, U., "Coating of soot and $(nh_4)_2so_4$ particles by ozonolysis products of alpha-pinene," *J. Aerosol Sci.*, vol. 34, no. 10, pp. 1297–1321, 2003.

[173] Salma, I., Ocskay, R., Varga, I., and Maenhaut, W., "Surface tension of atmospheric humic-like substances in connection with relaxation, dilution, and solution ph," *J. Geophys. Res.*, vol. 111, no. D23, p. D23205, 2006. D23205.

[174] Sannigrahi, P., Sullivan, A. P., Weber, R. J., and Ingall, E. D., "Characterization of water-soluble organic carbon in urban atmospheric aerosols using solid-state c-13 nmr spectroscopy," *Environ. Sci. Technol.*, vol. 40, no. 3, pp. 666–672, 2006.

[175] Saxena, P. and Hildemann, L. M., "Water-soluble organics in atmospheric particles: A critical review of the literature and application of thermodynamics to identify candidate compounds," *J. Atmos. Chem.*, vol. 24, no. 1, pp. 57–109, 1996.

[176] Saxena, P., Hildemann, L. M., McMurry, P. H., and Seinfeld, J. H., "Organics alter hygroscopic behavior of atmospheric particles," *J. Geophys. Res.*, vol. 100, no. D9, pp. 18755–18770, 1995.

[177] Schneider, J., Borrmann, S., Wollny, A. G., Blasner, M., Mihalopoulos, N., Oikonomou, K., Sciare, J., Teller, A., Levin, Z., and Worsnop, D. R., "Online mass spectrometric aerosol measurements during the minos campaign (crete, august 2001)," *Atmos. Chem. Phys.*, vol. 4, pp. 65–80, 2004.

[178] Schwarz, J. P., Gao, R. S., Fahey, D. W., Thomson, D. S., Watts, L. A., Wilson, J. C., Reeves, J. M., Darbeheshti, M., Baumgardner, D. G., Kok, G. L., Chung, S. H., Schulz, M., Hendricks, J., Lauer, A., Karcher, B., Slowik, J. G., Rosenlof, K. H., Thompson, T. L., Langford, A. O., Loewenstein, M., and Aikin, K. C., "Single-particle measurements of midlatitude black carbon and light-scattering aerosols from the boundary layer to the lower stratosphere," *J. Geophys. Res.*, vol. 111, no. D16, 2006. D16207.

[179] Seinfeld, J. H. and Pandis, S. N., *Atmospheric Chemistry & Physics: From Air Pollution to Climate Change*. John Wiley & Sons, 1998.

[180] Seinfeld, J. H. and Pankow, J. F., "Organic atmospheric particulate material," *Annu. Rev. Phys. Chem.*, vol. 54, pp. 121–140, 2003.

[181] Shantz, N. C., Leaitch, W. R., and Caffrey, P. F., "Effect of organics of low solubility on the growth rate of cloud droplets," *J. Geophys. Res.*, vol. 108, no. D5, 2003. 4168.

[182] Shilling, J. E., King, S. M., Mochida, M., and Martin, S. T., "Mass spectral evidence that small changes in composition caused by oxidative aging processes alter aerosol ccn properties," *J. Phys. Chem.*, vol. 111, no. 17, pp. 3358–3368, 2007.

[183] Shu, Y. G. and Atkinson, R., "Rate constants for the gas-phase reactions of o3 with a series of terpenes and oh radical formation from the o3 reactions with sesquiterpenes at 296+/-2-k," *J. Chem. Kinetics*, vol. 26, no. 12, pp. 1193–1205, 1994.

[184] Shulman, M. L., Jacobson, M. C., Carlson, R. J., Synovec, R. E., and Young, T. E., "Dissolution behavior and surface tension effects of organic compounds in nucleating cloud droplets," *Geophys. Res. Lett.*, vol. 23, no. 3, pp. 277–280, 1996.

[185] Snider, J. R. and Brenguier, J. L., "Cloud condensation nuclei and cloud droplet measurements during ace-2," *Tellus B*, vol. 52, no. 2, pp. 828–842, 2000.

[186] Snider, J. R., Guibert, S., Brenguier, J. L., and Putaud, J. P., "Aerosol activation in marine stratocumulus clouds: 2. kohler and parcel theory closure studies," *J. Geophys. Res.*, vol. 108, no. D15, 2003.

[187] Sorjamaa, R. and Laaksonen, A., "The influence of surfactant properties on critical supersaturations of cloud condensation nuclei," *J. Aerosol Sci.*, vol. 37, no. 12, pp. 1730–1736, 2006.

[188] Sorjamaa, R., Svenningsson, B., Raatikainen, T., Henning, S., Bilde, M., and Laaksonen, A., "The role of surfactants in kohler theory reconsidered," *Atmos. Chem. Phys.*, vol. 4, pp. 2107–2117, 2004.

[189] Sorooshian, A., Brechtel, F. J., Ma, Y. L., Weber, R. J., Corless, A., Flagan, R. C., and Seinfeld, J. H., "Modeling and characterization of a particle-into-liquid sampler (pils)," *Aerosol Sci. Technol.*, vol. 40, no. 6, pp. 396–409, 2006.

[190] Sorooshian, A., Ng, N. L., Chan, A. W. H., Feingold, G., Flagan, R. C., and Seinfeld, J. H., "Particulate organic acids and overall water-soluble aerosol composition measurements from the 2006 gulf of mexico atmospheric composition and climate study (gomaccs)," *J. Geophys. Res.*, vol. 112, no. D13. D13201.

[191] Sorooshian, A., Ng, N. L., Chan, A. W. H., Feingold, G., Flagan, R. C., and Seinfeld, J. H., "Particulate organic acids and overall water-soluble aerosol composition measurements from the 2006 gulf of mexico atmospheric composition and climate study (gomaccs)," *J. Geophys. Res.*, vol. 112, no. D13. D13201.

[192] Sorooshian, A., Varutbangkul, V., Brechtel, F. J., Ervens, B., Feingold, G., Bahreini, R., Murphy, S. M., Holloway, J. S., Atlas, E. L., Buzorius, G., Jonsson, H., Flagan, R. C., and Seinfeld, J. H., "Oxalic acid in clear and cloudy atmospheres: Analysis of data from international consortium for atmospheric research on transport and transformation 2004," *J. Geophys. Res.*, vol. 111, no. D23, 2006. D23S45.

[193] Sotiropoulou, R. E. P., Medina, J., and Nenes, A., "Ccn predictions: Is theory sufficient for assessments of the indirect effect?," *Geophys. Res. Lett.*, vol. 33, no. 5, 2006. L05816.

[194] Stanier, C. O., Pathak, R. K., and Pandis, S. N., "Measurements of the volatility of aerosols from alpha-piniene ozonolysis," *Environ. Sci. Technol.*, vol. 41, no. 8, pp. 2756–2763, 2007.

[195] Stephens, M., Turner, N., and Sandberg, J., "Particle identification by laser-induced incandescence in a solid-state laser cavity," *Appl. Opt.*, vol. 42, no. 19, pp. 3726–3736, 2003.

[196] Stroud, C. A., Nenes, A., Jimenez, J. L., DeCarlo, P. F., Huffman, J. A., Bruintjes, R., Nemitz, E., Delia, A. E., Toohey, D. W., Guenther, A. B., and Nandi, S., "Cloud activating properties of aerosol observed during celtic," *J. Aerosol Sci.*, vol. 64, no. 2, pp. 441–459, 2007.

[197] Sullivan, A. P., Peltier, R. E., Brock, C. A., de Gouw, J. A., Holloway, J. S., Warneke, C., Wollny, A. G., and Weber, R. J., "Airborne measurements of carbonaceous aerosol soluble in water over northeastern united states: Method development and an investigation into water-soluble organic carbon sources," *J. Geophys. Res.*, vol. 111, no. D23, p. D23S46, 2006. D23S46.

[198] Sullivan, A. P. and Weber, R. J., "Chemical characterization of the ambient organic aerosol soluble in water: 1. isolation of hydrophobic and hydrophilic fractions with a xad-8 resin," *J. Geophys. Res.*, vol. 111, no. D5, p. D05314, 2006. D05314.

[199] Sullivan, A. P. and Weber, R. J., "Chemical characterization of the ambient organic aerosol soluble in water: 1. isolation of hydrophobic and hydrophilic fractions with a xad-8 resin," *J. Geophys. Res.*, vol. 111, no. D5, p. D05314, 2006. D05314.

[200] Sullivan, A. P. and Weber, R. J., "Chemical characterization of the ambient organic aerosol soluble in water: 2. isolation of acid, neutral, and basic fractions by modified size-exclusion chromatography," *J. Geophys. Res.*, vol. 111, no. D5, p. D05315, 2006. D05315.

[201] Sullivan, A. P., Weber, R. J., Clements, A. L., Turner, J. R., Bae, M. S., and Schauer, J. J., "A method for on-line measurement of water-soluble organic carbon in ambient aerosol particles: Results from an urban site," *Geophys. Res. Lett.*, vol. 31, no. 13, 2004. L13105.

[202] Taraniuk, I., Graber, E., Kostinski, A., and Rudich, Y., "Surfactant properties of atmospheric and model humic-like substances (hulis)," *Geophys. Res. Lett.*, vol. 34, p. L16807, 2007.

[203] Tomlinson, J. M., Li, R. J., and Collins, D. R., "Physical and chemical properties of the aerosol within the southeastern pacific marine boundary layer," *J. Geophys. Res.*, vol. 112, no. D12, 2007. D12211.

[204] Turpin, B. J. and Lim, H. J., "Species contributions to pm2.5 mass concentrations: Revisiting common assumptions for estimating organic mass," *Aerosol Sci. Technol.*, vol. 35, no. 1, pp. 602–610, 2001.

[205] Twohy, C. H., Anderson, J. R., and Crozier, P. A., "Nitrogenated organic aerosols as cloud condensation nuclei," *Geophys. Res. Lett.*, vol. 32, no. 19, 2005. L19805.

[206] VanReken, T. M., Ng, N. L., Flagan, R. C., and Seinfeld, J. H., "Cloud condensation nucleus activation properties of biogenic secondary organic aerosol," *J. Geophys. Res.*, vol. 110, no. D7, 2005. D07206.

[207] VanReken, T., T.A., R., G.C., R., Varutbangkul, V., Jonsson, H. H., Flagan, R. C., and Seinfeld, J. H., "Toward aerosol/cloud condensation nuclei (ccn) closure during crystal-face," *J. Geophys. Res.*, vol. 108, no. D20.

[208] Varutbangkul, V., Brechtel, F. J., Bahreini, R., Ng, N. L., Keywood, M. D., Kroll, J. H., Flagan, R. C., Seinfeld, J. H., Lee, A., and Goldstein, A. H., "Hygroscopicity of secondary organic aerosols formed by oxidation of cycloalkenes, monoterpenes, sesquiterpenes, and related compounds," *Atmos. Chem. Phys.*, vol. 6, pp. 2367–2388, 2006.

[209] Vestin, A., Rissler, J., Swietlicki, E., Frank, G. P., and Andreae, M. O., "Cloud-nucleating properties of the amazonian biomass burning aerosol: Cloud condensation nuclei measurements and modeling," *J. Geophys. Res.*, vol. 112, no. D14, 2007. D14201.

[210] Virkkula, A., Van Dingenen, R., Raes, F., and Hjorth, J., "Hygroscopic properties of aerosol formed by oxidation of limonene, alpha-pinene, and beta-pinene," *J. Geophys. Res.*, vol. 104, no. D3, pp. 3569–3579, 1999.

[211] Volkamer, R., Jimenez, J. L., San Martini, F., Dzepina, K., Zhang, Q., Salcedo, D., Molina, L. T., Worsnop, D. R., and Molina, M. J., "Secondary organic aerosol formation from anthropogenic air pollution: Rapid and higher than expected," *Geophys. Res. Lett.*, vol. 33, no. 17, 2006. L17811.

[212] Wex, H., Hennig, T., Salma, I., Ocskay, R., Kiselev, A., Henning, S., Massling, A., Wiedensohler, A., and Stratmann, F., "Hygroscopic growth and measured and modeled critical super-saturations of an atmospheric hulis sample," *Geophys. Res. Lett.*, vol. 34, no. 2, 2007. L02818.

[213] Wilson, J. C., Lafleur, B. G., Hilbert, H., Seebaugh, W. R., Fox, J., Gesler, D. W., Brock, C. A., Huebert, B. J., and Mullen, J., "Function and performance of a low turbulence inlet for sampling supermicron particles from aircraft platforms," *Aerosol Sci. Technol.*, vol. 38, no. 8, pp. 790–802, 2004.

[214] Yamasoe, M. A., Artaxo, P., Miguel, A. H., and Allen, A. G., "Chemical composition of aerosol particles from direct emissions of vegetation fires in the amazon basin: water-soluble species and trace elements," *Atmos. Environ.*, vol. 34, no. 10, pp. 1641–1653, 2000.

[215] Yaws, C. L., "Chemical properties handbook : physical, thermodynamic, environmental, transport, safety, and health related properties for organic and inorganic chemicals / carl l. yaws.," 1999.

[216] Yoon, Y. J., Ceburnis, D., Cavalli, F., Jourdan, O., Putaud, J. P., Facchini, M. C., Decesari, S., Fuzzi, S., Sellegri, K., Jennings, S. G., and O'Dowd, C. D., "Seasonal characteristics of the physicochemical properties of north atlantic marine atmospheric aerosols," *J. Geophys. Res.*, vol. 112, no. D4, 2007. D04206.

[217] Yum, S. S., Roberts, G., Kim, J. H., Song, K., and Kim, D., "Submicron aerosol size distributions and cloud condensation nuclei concentrations measured at gosan, korea, during the atmospheric brown cloudseast asian regional experiment 2005," *J. Geophys. Res.*, vol. 112, no. D22, 2006. D22S32.

[218] Zappoli, S., Andracchio, A., Fuzzi, S., Facchini, M. C., Gelencser, A., Kiss, G., Krivacsy, Z., Molnar, A., Meszaros, E., Hansson, H. C., Rosman, K., and Zebuhr, Y., "Inorganic, organic and macromolecular components of fine aerosol in different areas of europe in relation to their water solubility," *Atmos. Environ.*, vol. 33, no. 17, pp. 2733–2743, 1999.

[219] Zhang, Q. H., Birgersson, G., Zhu, J. W., Lofstedt, C., Lofqvist, J., and Schlyter, F., "Leaf volatiles from nonhost deciduous trees: Variation by tree species, season and temperature, and electrophysiological activity in ipstypographus," *J. Chem. Ecol.*, vol. 25, no. 8, pp. 1923–1943, 1999.

[220] Zhao, C. S., Ishizaka, Y., and Peng, D. Y., "Numerical study on impacts of multi-component aerosols on marine cloud microphysical properties," *J. of the Meteorological Soc. of Japan*, vol. 83, no. 6, pp. 977–986, 2005.